Coordination of the *Arabidopsis thaliana* circadian clock

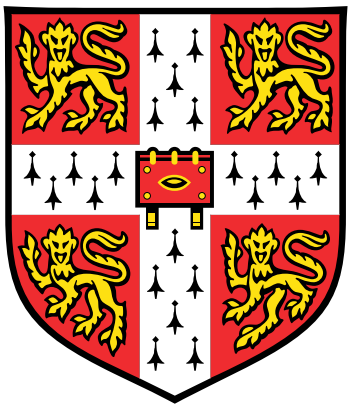

Mark Greenwood

Department of Biochemistry
University of Cambridge

This dissertation is submitted for the degree of
Doctor of Philosophy

Darwin College

September 2019

Declaration

I hereby declare that except where specific reference is made to the work of others, the contents of this dissertation are original and have not been submitted in whole or in part for consideration for any other degree or qualification in this, or any other university. This dissertation is my own work and contains nothing which is the outcome of work done in collaboration with others, except as specified in the text and Acknowledgements. This dissertation contains fewer than 60,000 words including appendices, bibliography, footnotes, tables and equations and has fewer than 150 figures.

Mark Greenwood
September 2019

Coordination of the *Arabidopsis thaliana* circadian clock

Mark Greenwood

Individual plant cells have a genetic circuit, the circadian clock, that times key processes to the day-night cycle. These clocks are aligned to the day-night cycle by multiple environmental signals that vary across the plant. Thus, the clock may be set separately in cells creating discrepancies in timing. However, cells and tissues often must act in unison in order to time biological events appropriately. How does the plant integrate clock rhythms, both within and between organs, to ensure coordinated timing?

To address this question, we developed an imaging method capable of monitoring the clock at the sub-tissue level across entire *Arabidopsis thaliana* seedlings. Consistent with previous tissue-level studies, our results showed that the clock runs at different speeds (periods) in each organ, which causes the clock to peak at different times across the plant in both constant environmental conditions and light-dark cycles. Closer examination revealed that spatial waves of clock gene expression propagate both within and between organs. A combination of modelling and experiment revealed that these spatial waves are the result of the period differences between organs and local coupling, rather than long-distance signalling.

With further imaging experiments we showed that the endogenous period differences, and thus the spatial waves, can be generated by the organ specificity of inputs into the clock. We demonstrated this by modulating periods using light and metabolic signals, as well as with genetic perturbations.

Finally, in the field, clocks entrain to complex environmental cycles. To begin to understand how clock's respond to more natural light-dark cycles, we developed methods for imaging seedlings under more realistic light conditions. Preliminary results suggested altered spatial and temporal organisation amongst the core clock genes under more realistic light-dark cycles.

Together, our results suggest that plant clocks can be set locally by environmental inputs, but coordinated via cellular coupling.

Acknowledgements

Firstly, I thank my primary supervisor James Locke. I feel his support in bringing me to Cambridge, and then on his supervision, will prove pivotal in my career. Second, I thank Anthony Hall for his mentorship and positivity from my first day in a lab until today.

The Gatsby Foundation generously provided the funding to conduct my PhD at the Sainsbury Laboratory. It was the people here that made it an enjoyable place to work. I'm particularly grateful to Katie Abley, Hugo Tavares, and Bruno Martins for the reading of drafts and Mana Afsharinafar for the technical help towards the end of my PhD. I also thank the Works and Horticulture departments for their technical help.

I gratefully acknowledge Krishna Kumar (University of Cambridge) for the template used for this thesis and contributors to the Plant Illustrations repository for graphics utilised in the figures.

Much of the research in this thesis has been published within the peer reviewed publications Greenwood et al., 2019 [1], Greenwood et al., 2020 [2], Rees et al., 2019 [3], and Gould et al., 2018 [4]. I thank all of my co-authors for their collaboration. In particular, I wish to thank Mirela Domijan (University of Liverpool) for collaboration on the mathematics and Matthieu Bourdon (University of Cambridge) for collaboration on plasmodesmata experiments. I highlight their specific contributions at the end of each chapter.

Table of contents

List of figures

List of tables

Nomenclature

Acronyms / Abbreviations

G_1 Gap 1

K coupling strength

R order parameter

bZIP63 BASIC LEUCINE ZIPPER63

CALS3 CALLOSE SYNTHASE 3

CCA1 CIRCADIAN CLOCK ASSOCIATED 1

CDC6 CELL DIVISION CONTROL 6

ELF3 EARLY FLOWERING 3

ELF4 EARLY FLOWERING 4

FT FLOWERING LOCUS T

GI GIGANTEA

LHY LATE ELONGATED HYPOCOTYL

LUX LUX ARRYTHMO

PER1 PERIOD 1

PER2 PERIOD 2

PHYB PHYTOCHROME B

PRR1 PSEUDO-RESPONSE REGULATOR 1

PRR3 *PSEUDO-RESPONSE REGULATOR 3*

PRR7 *PSEUDO-RESPONSE REGULATOR 7*

PRR9 *PSEUDO-RESPONSE REGULATOR 9*

SUC2 *SUCROSE-PROTON SYMPORTER 2*

TOC1 *TIMING OF CAB EXPRESSION 1*

YFP *YELLOW FLUORESCENT PROTEIN*

ZTL *ZEITLUPE*

CCD charge-coupled device

DCMU 3-(3,4-dichlorophenyl)-1,1-dimethylurea

DD constant darkness

DMSO Dimethyl sulfoxide

EC EVENING COMPLEX

FFT-NLLS fast Fourier transform nonlinear least squares

GUS β-glucuronidase

h hour

LD light-dark

LEDs light emitting diodes

LUC LUCIFERASE

MS Murashige and Skoog

ODE ordinary differential equation

PAP 3′-phosphoadenosine 5′-phosphate

PIF PYTOCHROME INTERACTING FACTOR

PRR PSEUDO-RESPONSE REGULATOR

RB red and blue light

ROI region of interest

RT root tip

RVE REVEILLE

S DNA Synthesis

SD standard deviation

UV ultra violet

UVR8 UV RESISTANCE LOCUS 8

WT wild-type

Chapter 1

Introduction

1.1 Introduction to circadian systems

1.1.1 What are circadian clocks?

In response to the Earth's predictable light-dark (LD) cycles, many organisms have evolved a genetic circuit known as the circadian clock [5]. A common design principle is a central oscillator that receives input from multiple environmental signals and uses them to predict the time of day. This timing information is used to coordinate processes, matching them to the optimum time of day or year. The advantage gained from doing this is substantial, and perhaps best demonstrated in plants; individuals with a functional clock matching the day-night cycle fix more carbon, grow, and survive better than those without [6, 7].

1.1.2 Conceptual model of a circadian system

Circadian systems have evolved independently multiple times in different kingdoms [8]. Despite this, some common characteristics are clear, leading to what is now considered the classical model of a circadian system (Figure 1.1). At the centre is a network of interacting genes that form feedback loops (Figure 1.1, centre). This is what is often referred to as the clock itself. These genes interact at the transcriptional, post-transcriptional and post-translational levels to generate oscillating levels of proteins [9]. Although very simple networks are capable of creating oscillations in this way, nature has favoured more complex networks with multiple interacting feedback loops [5]. This complexity enables differential phasing of proteins, increased robustness, seasonality, and multiple environmental inputs [10–13]. We discuss the molecular details of the clock network in plants in section 1.2.

The input pathways (Figure 1.1, left) align the central clock network to day-night cycles. This process is known as entrainment. Light is the best-studied input pathway but non-photic cues are also capable of entraining the clock. Entrainment works by promoting or repressing the expression of proteins of the central oscillator. This change in expression of clock proteins causes a shift in phase, aligning the oscillator with the day-night cycle [14]. We discuss the molecular details of entrainment in section 1.3.

Completing the system, the output pathways connect the clock to the organism's physiology. A well-entrained clock activates or represses genes across the day-night cycle, matching expression to the optimum time of day (Figure 1.1, right). These outputs are usually widespread, with as much as half of the transcriptome controlled by the clock in some eukaryotes [15, 16]. The result of this large-scale temporal control is that the organism's physiology is well coordinated with the environment. We discuss the details of some of the physiological outputs in plants in **??**.

This simple conceptual model is a useful starting point to begin to understand how clocks function. However, in actual fact the picture is more complex and the distinctions between different parts of the system less defined. For example, in some organisms (including plants), light signalling components can act in an input pathway, form part of the central oscillator, and be regulated as an output [17–19].

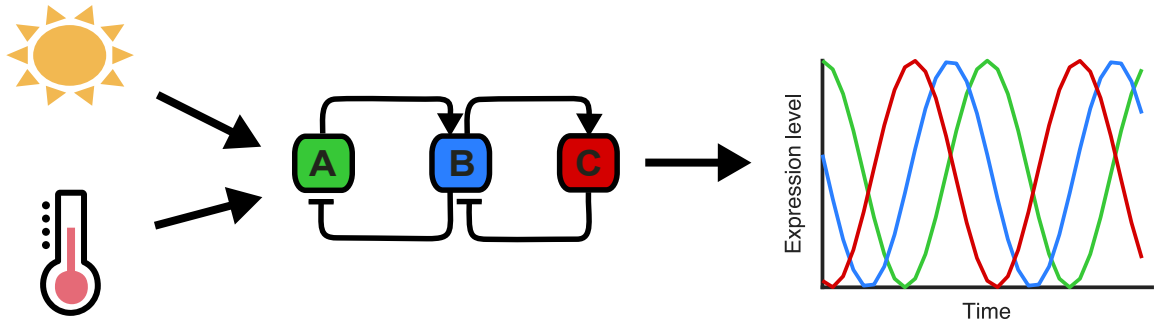

Fig. 1.1 A simple conceptual model of a circadian system. A central network of genes and proteins (centre) uses environmental inputs to align to the day-night cycle (left) and times oscillations of output genes (right).

1.1.3 Interpreting circadian rhythms

It is useful when studying circadian rhythms to consider a few key properties. Period and phase are most commonly used to describe rhythms. The period of a rhythm is how long it takes for one oscillation to complete (Figure 1.2). The phase is a measure of position within the oscillation. This must be in relation to a chosen reference point in the rhythm. Commonly,

dawn is used, and the time elapsed since dawn to a peaks of expression quoted. Alternatively, a position within each cycle of an oscillation can be used as a reference. In this case, often angular units are used so that the phase value is independent of the period and elapsed time (Figure 1.2) [20].

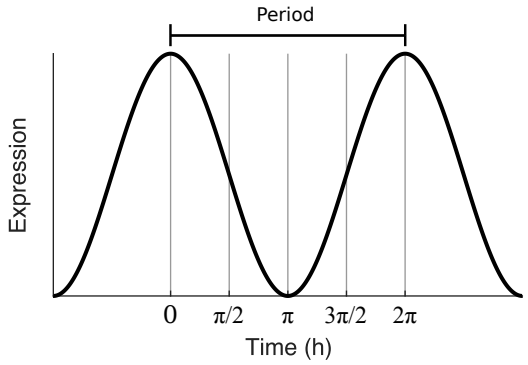

Fig. 1.2 Circadian rhythms can be characterised by period and phase.

Measures of period and phase become useful when comparing multiple rhythms. Rhythms are said to be synchronised when they oscillate with the same phase. Desynchronisation can occur when rhythms have different periods, causing divergence in phase [20]. This property of phase synchrony may be crucial for circadian rhythms, which we discuss later in detail (section 1.4).

1.2 The core clock network in *Arabidopsis thaliana*

Using *Arabidopsis thaliana* as a model organism, the development of molecular methods and transgenic imaging has led to the identification of many components of the central oscillator. In tandem with mathematical modelling, this has led to a good understanding of how the clock generates oscillations of gene expression (Figure 1.3).

1.2.1 Interlocked genetic feedback loops generate oscillations of proteins

At dawn, the transcription factors CIRCADIAN CLOCK ASSOCIATED 1 (CCA1) and LATE ELONGATED HYPOCOTYL (LHY) are induced by light [21, 22]. *CCA1* and *LHY* have largely redundant function in the clock and are often considered as the same component in models [23].

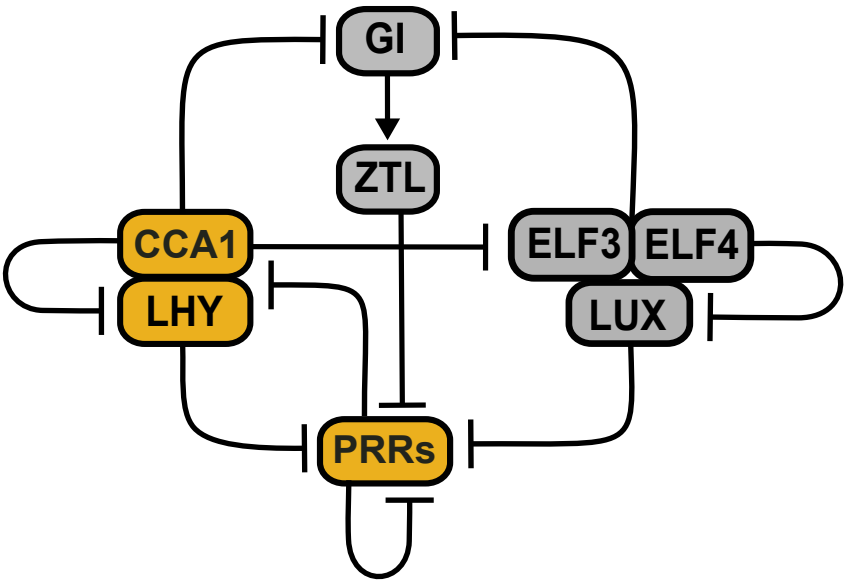

Fig. 1.3 The *Arabidopsis* central circadian clock network. Network diagram representing the major genetic interactions at the core of the *Arabidopsis* circadian clock. Note, for the sake of clarity the network and interactions are not comprehensive. Omissions of particular interest include the RVEs, which activate *PRR9*, *GI*, *TOC1*, and *ELF4* and are repressed by PRR5, PRR7, and PRR9. Pointed arrows show activation and "T" arrows repression.

Later in the day, the PSEUDO-RESPONSE REGULATOR (PRR) family are expressed. The PRR family includes *PRR9*, *PRR7*, *PRR3*, and *TIMING OF CAB EXPRESSION 1 TOC1* (also known as *PRR1*). Their expression are staggered from morning to dusk in this order [24]. Light can also induce the morning expressed *PRR9*, similar to *CCA1* and *LHY* [25]. The PRRs form feedback loops with *CCA1* and *LHY*, reciprocally regulating each other's expression [26–29].

In the evening, *GIGANTEA* (*GI*) is required for correct circadian timing [30, 31]. Before dusk, GI forms a stable complex with the blue light photoreceptor ZEITLUPE (ZTL). Only after dusk, when blue light is lost, does the complex dissociate, allowing GI and ZTL to bind to their targets [18]. ZTL binds the PRRs, targeting them for degradation in the night-time [32]. GI activates *CCA1*/*LHY*, although this interaction may not be direct [31]. CCA1/LHY in-turn repress *GI*, forming another feedback loop.

Also at dusk, *EARLY FLOWERING 3* (*ELF3*), *EARLY FLOWERING 4* (*ELF4*), and *LUX ARRHYTHMO* (*LUX*) form the Evening Complex (EC) [33]. The EC integrates light and temperature signals into the clock, through light and temperature regulation of the EC components themselves [34, 35], and modulation of EC binding to its targets [36]. These targets include transcriptionally repressing *PRR9* and *PRR7* [37]. The individual components

of the EC can also function individually, independently of the complex. ELF3 targets GI for degradation [38], and ELF4 sequesters GI to the cytoplasm, away from its favoured partner, ZTL [39]. To complete the feedback loops, *ELF3*, *ELF4*, and *LUX* are repressed by CCA1/LHY. ELF4 and LUX are additionally repressed by TOC1 and the EC itself [40–42].

1.2.2 Our understanding of the complexity within the clock is increasing

The continued discovery of novel genes and interactions adds to the complexity of the oscillator. A recent example are the *REVEILLE* family, whom are relatives of *CCA1/LHY* and transcriptionally activate day and evening expressed clock genes [43–45]. In turn, the RVEs are repressed transcriptionally by *PRR5*, *PRR7*, and *PRR9* [46, 47, 43–45]. The complexity is further increased by levels of regulation beyond the transcription and protein level. For example, *CCA1* mRNA instability in light contributes to entrainment [48], and alternative splicing of transcripts in response to environmental stress is common [49]. Yet more regulation occurs outside of the central-dogma, with chromatin structure [50] and post-translational modifications [51] also influencing the network.

Despite our increasing appreciation of the complexity in regulation, modelling studies have shown that simplified loop structures are capable of describing most features of the clock [52–54]. It is likely that these additional levels of regulation enable the more sophisticated properties observed in vivo, such as high robustness, temperature compensation, and response to environmental changes [11, 55, 50].

1.3 Entrainment of the *Arabidopsis* circadian clock

1.3.1 Mechanisms of entrainment

To be an effective timekeeper, the circadian clock must be synchronised with the diurnal environment. The process by which a clock aligns with the environment is known as entrainment. In entrainment, environmental signals alter the level of components of the core clock network. This adjusts the phase of the clock oscillations, helping align it with the day-night cycle.

Much of our understanding of the mechanisms behind entrainment comes from light pulse experiments. Pulses of bright light applied to plants under constant darkness causes jumps in phase [56, 57]. The size and direction (advance or delay) of the change depends on the timing of the light pulse. For example, a pulse of light late in the subjective night causes

a phase advance, in an attempt to catch up with dawn, whereas a pulse early in the night causes a phase delay (Figure 1.4). This phenomenon is known as 'gating' [58]. These gated adjustments to phase are sufficient in mathematical models to predict experiments under LD cycles [14].

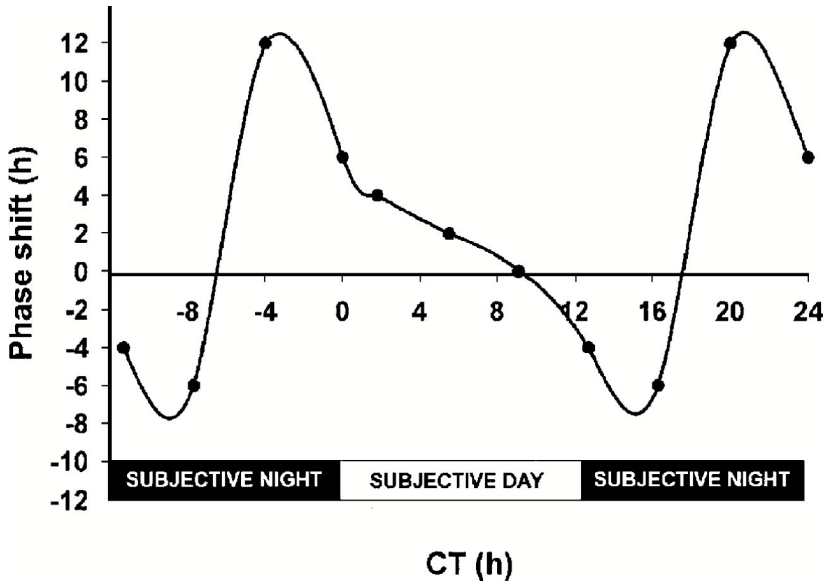

Fig. 1.4 The response of the *Arabidopsis* circadian clock to bright pulses of light. Batches of seedlings were entrained and transferred to constant low level red light. At 4 h intervals after transfer to constant light successive batches of seedlings were exposed to 3 h of bright red light. The phase shift caused by the pulse was compared to control seedlings for each circadian time (CT) [56]. Reprinted with permission from [56].

.

Although light pulse experiments have been crucial for understanding how entrainment works, in the field exposure to light is more prolonged, occurring throughout the day. The effect of light on the clock is therefore the net effect of the phase advances and delays that occur throughout the day. Rather than jumps in phase, this continuous adjustment creates what appears as an acceleration or deceleration of the oscillator, matching it to the LD cycle.

Light signals are arguably the most important, and the signal most often used for the study of entrainment. However, there are a number of exogenous and endogenous cues that can adjust period or phase in plants (Table 1.1). We review the details of these signalling pathways, including light, in the following sub-sections.

1.3.2 Light perception for entrainment

Light is an important cue for entrainment. However, for light to be useful, it must first be converted into a biochemical signal. This signal can then be used to adjust the core clock network.

Plants have at least five families of photoreceptors for this purpose: (1) phytochromes, (2) cryptochromes, (3) the ZTL family, (4) phototropins, and (5) UV RESISTANCE LOCUS 8 (UVR8). Each photoreceptor family has distinct, but overlapping, sensitivities to wavelengths of light. The phytochromes detect red, the cryptochromes blue-green, the phototropins and ZTL family blue, and UVR8 the UV portion of the light spectrum. Each photoreceptor contains a region that when excited by photons triggers a conformational change, creating a biochemical signal that can be interpreted within the cell [59].

Circadian studies combined with forward genetic approaches have implicated each family in circadian entrainment [17, 60–63]. For example, mutations in phytochrome genes cause a decrease in the effect of red light on circadian period [17], whereas overexpression causes fast periods under all red light intensities [60, 61]. Similar observations were made for cryptochrome and ZTL family mutants under blue light [17, 62], and *UVR8* mutants under UV light [63]. Exceptionally, the phototropins do not appear to transmit light information to the nuclear clock [64, 65], but may be required for circadian responses to blue light in chloroplasts [64].

The photoreceptors themselves are also tightly regulated, controlling the level of light input to the clock. There is evidence that transcription of phytochromes and cryptochromes are regulated by the clock, causing them to oscillate [66, 19, 67]. However, oscillations in protein levels are weak [68], and it is unclear whether they have physiological function. There is also regulation of the photoreceptors at the spatial level. The phytochromes and cryptochromes have a spatial pattern across seedlings, with higher expression at the tips of organs [69, 70, 66, 19, 71]. Sub-cellularly there are spatial dynamics also. When activated by light, phytochromes move to the nucleus and form subnuclear foci termed photobodies [72, 73]. These photobodies are critical for phytochrome controlled physiological processes [74].

1.3.3 Light transmission to the core clock network

Once perceived, the light derived signal must be transmitted to the clock network, and alter protein levels. Although a molecular understanding of these pathways lags behind that of the clock network, considerable progress has been made in recent years. The most direct mechanism involves protein-protein interactions between photoreceptors and clock proteins. The first of such interaction identified was between ELF3 and PHYB [75]. Some years later, further experiments showed PHYB also interacts with CCA1, LHY, GI, TOC1, and LUX [76]. Further, an unbiased screen for ELF3 and ELF4 binding partners identified associations with all five phytochromes and related signalling proteins [77].

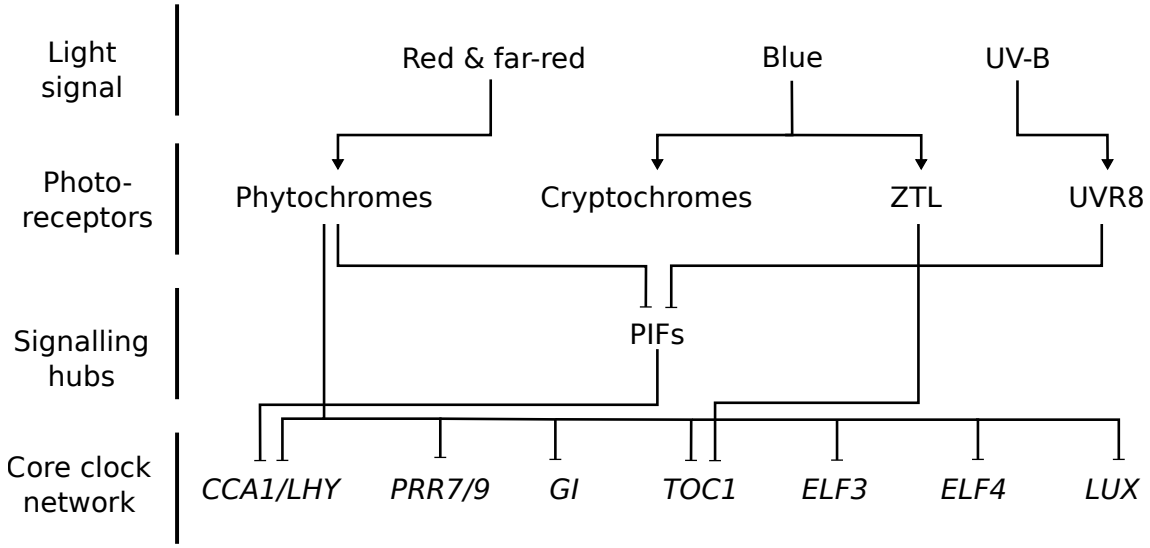

Fig. 1.5 Light is perceived by and transmitted to the clock network by multiple overlapping pathways. Light signals are perceived by photoreceptors with sensitivities to different wavelengths and converted to a biochemical signal. This signal is transduced to the clock network, either directly or indirectly, through various molecular interactions. Pointed arrows show genetic activation, “T" arrows repression. Note that not all molecular interactions are shown. Adapted with permission from [59]

.

Photoreceptors may also influence the clock network by altering transcription of genes. This can be directly at the promoters of clock genes; PHYB can bind and repress at the promoters of *GI* and *PRR9* [78]. Alternatively, it may also be indirect, through signalling hubs. For example, the PHYTOCHROME INTERACTING FACTOR family of transcription factors (PIFs) are central regulators of growth, and integrate light, temperature, and hormone pathways to do so. As part of the control of growth, several clock genes can bind and repress PIF expression, suppressing growth until the evening [2]. It is therefore tempting to speculate that the PIFs also influence expression of the clock genes. Although the evidence for this is so-far limited, it was recently shown that PIF3 can bind to and repress expression of *CCA1*, influencing the speed of the clock [79]. Thus, light signals can reach the clock at multiple nodes of the clock network. However, in all of these examples, there exists a missing part in our understanding: how are the clock proteins altered once bound?

One interaction in which this question has been unravelled comes from the ZTL family. In addition to a light sensing domain, proteins of the ZTL family have an F-box domain. When active, this domain enables proteins to function within the Skp–Cullin–F-box (SCF) ubiquitin ligase complex and trigger the degradation of protein targets [80–82]. However, under blue rich light, ZTL instead binds with GI [18]. GI and ZTL help stabilise one-another causing accumulation of ZTL towards the end of the day [18, 83]. After dusk, the GI-ZTL complex dissociates freeing ZTL to form the SCF complex. This complex marks PRR5 and TOC1 with ubiquitin leading to degradation by the proteasome [32, 84]. Thus, the clock phase is altered.

1.3.4 Other exogenous inputs to the clock

Although light is by far the best-studied example, there are a number of exogenous signals capable of entraining the clock. Temperature is one such example. On the one hand, all biochemical reactions are sensitive to temperature, so the clock must be compensated in order to maintain its period within a narrow range. On the other, within that narrow range the clock can adjust its period and phase to entrain to cycles of only a few degrees [85]. It is emerging that some of the proteins that sense light can also sense temperature [78, 86]. However, there appears to be some genetic differences in how this signal is transmitted to the clock [87]. Clocks can respond to temperature through a number of transcriptional, alternative splicing and post-translational mechanisms [88, 55, 89, 90]. Further work will be required to understand whether there is overlap between temperature compensation, temperature entrainment, and light entrainment pathways.

Recently it was also shown that daily rhythms in atmospheric humidity can also entrain the plant clock. This may occur through the up-regulation of *CCA1* [91], although the proteins that sense humidity and transmit the information to *CCA1* have not been elucidated.

1.3.5 Metabolic inputs to the clock

The clock is sensitive to a number of signals that are not part of the external environment but exist within the cell. It may be that these signals act as secondary entrainment cues in order to fine-tune the clock to the external environment. The metabolic status of the cell represents one important internal time cue.

The evidence that metabolic cues can entrain the clock is compelling. The clock regulates key transcripts involved in photosynthesis [67], and in turn photosynthetic sugars can adjust the period and phase of the clock [92]. Sugar signals are sensed by specialised sugar sensing kinases, which activates the transcription factor *BASIC LEUCINE ZIPPER63* (*bZIP63*). *bZIP63* alters the expression of core clock genes through protein-DNA and protein-protein interactions [93].

In addition to sugars, some secondary metabolites are also known to regulate the clock. 3′-phosphoadenosine 5′-phosphate (PAP), which accumulates in response to metabolic stress, can lengthen circadian period [94]. Fe^{3+} ions and nitrogen, both of which have roles in photosynthesis and metabolism, can also adjust the clock [95, 96].

Additionally, the metabolic status of the plant can adjust the clock indirectly, through more general growth pathways. As discussed in relation to light signalling (subsection 1.3.3), the PIFs can bind to clock genes and influence the speed of the clock [79]. Intriguingly, another study demonstrated that sugars enhance the binding ability, and influence the speed of the clock [97]. Thus, the PIFs together with sugars communicate the general metabolic status of the cell to the clock.

1.3.6 Other endogenous inputs to the clock

Other endogenous signals not obviously associated with metabolism can also entrain the clock. Hormones are small signalling molecules that impact diverse physiological processes, from germination to response to pests. Auxin, cytokinin, brassinosteroids, abscisic acid, and ethylene have all been shown to modify the period or phase of least one clock gene [98–100]. Mutants in some of these hormonal pathways also display clock phenotypes [99].

A final interesting example of entrainment to endogenous signals is calcium. Ca^{2+} ions are a common secondary messenger in plants and oscillate with a period of approximately 24 h [101]. Ca^{2+} ions also feed-back into the clock, decreasing free running period length [102].

Imposed rhythms of Ca^{2+} can also entrain the clock alone [102]. Further, nicotinamide, an antagonist of Ca^{2+} release, lengthens free running periods [103]. This results in plants that entrain less well under LD cycles [104].

Thus, endogenous processes can entrain the clock at multiple levels of physiology, from biochemical outputs, to upstream genetic coordinators, and the cellular messengers (Table 1.1).

Table 1.1 Exogenous and endogenous signals adjust the clock

	Signal	Effect on free running period
Exogenous	Light intensity	shorten
	Temperature	shorten
	Humidity	none[a]
Endogenous	Sugars	shorten
	PAP	lengthen
	Fe^{3+}	lengthen
	nitrogen	lengthen
	auxin	lengthen[b]
	cytokinin	shorten
	homobrassinolide	shorten
	abscisic acid	shorten/lengthen[c]
	ethylene	shorten[d]
	Ca^{2+}	shorten[e]
	nicotinamide	lengthen
	copper	none[f]

[a] An effect on free running period has yet to be demonstrated.
[b] Acute exogenous auxin application causes a modest lengthening effect.
[c] Shortening and lengthening reported under different experimental conditions [99, 105].
[d] Conditional on sucrose.
[e] Disruption of Ca^{2+} signalling lengthens period.
[f] Phase but not period effect demonstrated [106].
PAP, 3′-phosphoadenosine 5′-phosphate.

1.3.7 Natural versus artificial entrainment cycles

In the laboratory, plants are usually studied under simplified environmental conditions. For the study of entrainment, plants are usually grown and assayed inside of plant growth chambers with the lights switched fully on at dawn and fully off at dusk in order to simulate

the outdoor LD cycle (Figure 1.6, left). However, in the field, environmental conditions are more gradual. Due to the steady rotation of the Earth the natural light cycle ramps up in light intensity at dawn to a peak at noon and then back down to dusk (Figure 1.6, right).

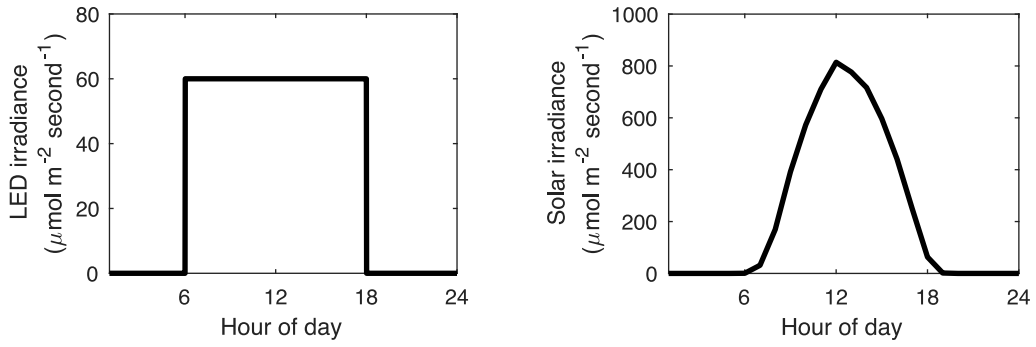

Fig. 1.6 Laboratory LD conditions approximate natural LD cycles. The typical 12h-light 12-h dark on-off type LD cycle used in the laboratory (left) differs from the natural graded LD cycle (right). Natural LD data is the mean solar irradiance for March 2015 in Rothamsted, UK [107]. See subsection 2.2.4 for details.

As discussed previously (subsection 1.3.2), light is an important entrainment cue, which acts by activating and repressing multiple clock genes. A more gradual on-off light cycle would likely alter the activation and/or degradation rates of the clock proteins, which may alter their phasing. Quantification of clock gene mRNA's extracted from *Arabidopsis* plants grown in the field revealed some potential differences in amplitude and phase of expression [108, 109]. However, these experiments were limited in resolution making phase estimation difficult.

1.3.8 Spatial discordance of entrainment cues

Unlike mammals, individual organs of the plant can be entrained directly [110, 111]. However, plants and their individual organs are exposed to very different environments. For example, clocks in cells of the root will be exposed to different light levels, temperatures, and nutrients in comparison to the aerial parts of the plant. Additionally, the phase between the signals can also differ. For example, the temperature rhythm in the soil lags air temperature, because the soil takes longer to absorb the heat from the sun (Figure 1.7) [112, 113]. In experiments with *Drosophila melangosta*, small phase conflict between light and temperature altered rhythms of locomotion and larger shifts of over 6 hours caused arrhythmia [114]. This could also potentially further complicate entrainment for plants.

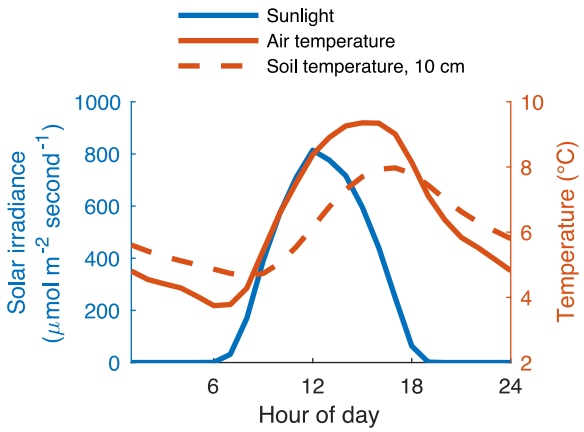

Fig. 1.7 Diurnal temperature rhythms lag the LD cycle. Air temperature typically peaks 2-3 h after noon and the soil later in the afternoon, dependent on the depth. Data an analysis of data from [107]. See subsection 2.2.4 for details.

1.4 Internal coordination of the *Arabidopsis* circadian system

1.4.1 Specificity in the circadian system

Most of our understanding of the circadian clock, and its entrainment, has been built from whole-plant experimental assays. However, this assumes that the clock is identical across the entire plant. This may lead to misinterpretations of experimental data. For example, whole-plant experimental data often display damped rhythms under constant conditions (Figure 1.8A). However, this could be due to desynchronisation of rhythms (Figure 1.8B, top), rather than true damping of the oscillation (Figure 1.8B, bottom).

That there are differences in clock rhythms within the plant is now well established. This was first demonstrated in bean plants, where the clock-controlled movement of leaves runs at a different period to rhythms of photosynthesis and stomatal conductance under constant conditions [115]. Later, a number of higher-resolution transgenic studies reported that different tissues of the plant could generate circadian oscillations with different periods [116–119], extending to the cellular level [120, 4, 121, 122]. We term this tissue or cell specificity in the clock system.

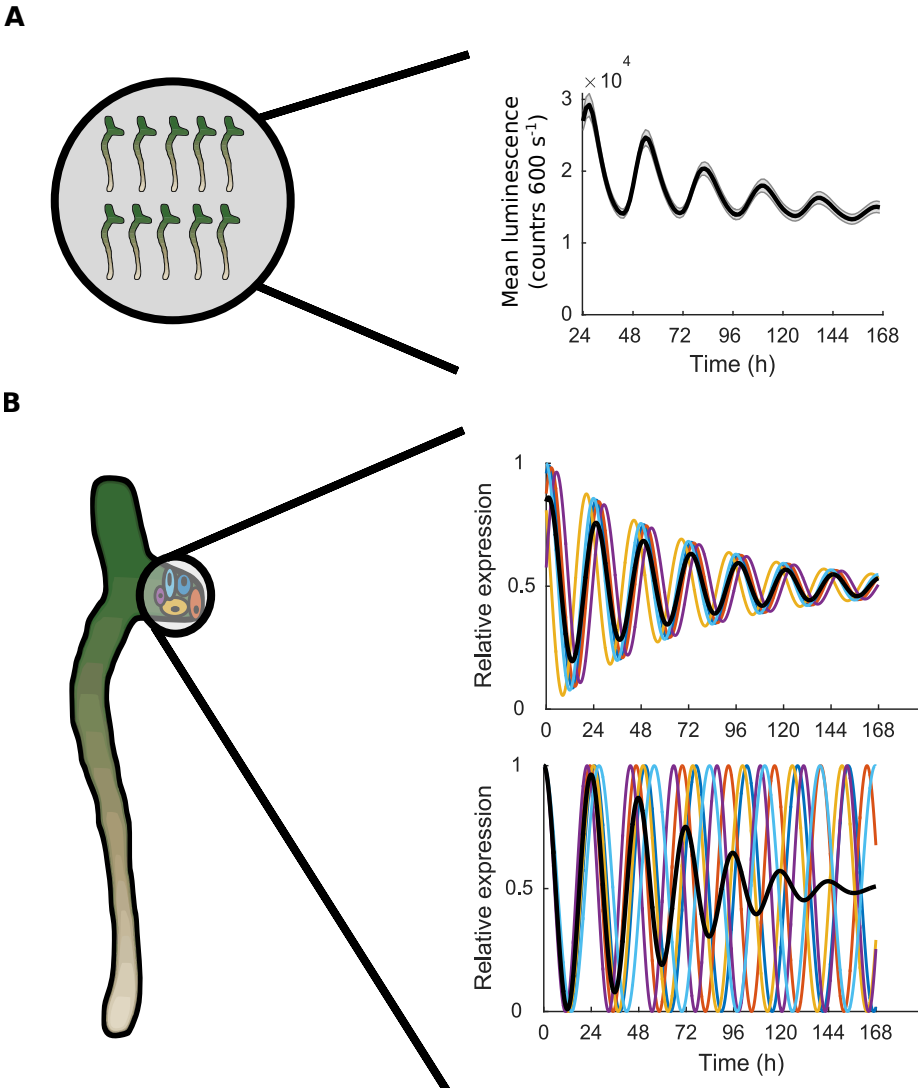

Fig. 1.8 Whole-plant assays mask the true circadian dynamics. (A) *CCA1*::*LUC* expression averaged over multiple seedlings shows damping oscillations. (B) The reason for damping could be due to damping rhythms in individual cells (top) or desynchronisation between cells (bottom). From [4].

1.4.2 Clocks in individual tissues regulate distinct developmental outputs

If the clock's network is cell and tissue specific, is also the function? Previous work has revealed that the clock can regulate distinct sets of targets in different tissues to bring about appropriate changes in physiology. By isolating the individual tissues of the cotyledon enzymatically, it was shown that the clock in the vasculature oscillates with an earlier phase and greater robustness than the mesophyll clock (Figure 1.9A) [123–125]. The clock also binds distinct regulatory targets [125]. As a consequence, the vasculature clock, but not the mesophyll clock, regulates the accumulation of *FLOWERING LOCUS T* (*FT*) and the initiation of flowering under long days (Figure 1.9B, top) [125, 123]. Similarly, the epidermis clock controls hypocotyl elongation through the regulation of PHYTOCHROME INTERACTING FACTOR 4 (PIF4; Figure 1.9B, middle) [123, 126]. It remains to be seen whether this specificity of output control extends to other cell types (Figure 1.9B, bottom). The specificity may be provided by tissue specific co-actors that are required for the binding of clock genes to targets, as is the case in *Drosophila* [127]. In support of this, vasculature specific *cis* elements have been identified in clock target genes [125]. Although further work is required to understand the mechanisms, it is clear that clocks in different tissues are able to regulate distinct developmental processes. This specificity may enable the clock to have such diverse roles in development.

1.4.3 Spatial structure of the circadian system

Rather than a disordered collection of cells, plants have a clear spatial structure to their circadian system. This was perhaps best demonstrated in our own recent study by monitoring expression of the core clock protein *CCA1* at single cell resolution *in vivo* [4]. Crucially, cells were imaged across all regions of the same seedling. Having such resolution, and coverage, allowed us to observe how rhythms are structured spatially. Plotting the position of the individual cells revealed a clear spatial structure to the periods of rhythms (Figure 1.10). In the cotyledon and hypocotyl, cells oscillated with a period close to 24 h, as typically observed in whole-plant assays under similar conditions [128]. In the middle region of the root we observed slower periods, as reported by others for the entirety of the root [129, 111]. Surprisingly, in the root tip we observed a dramatic increase in the speed of rhythms. Amplitudes showed a qualitatively similar pattern across the seedling. Thus, the clock has a clear spatial structure across the seedling.

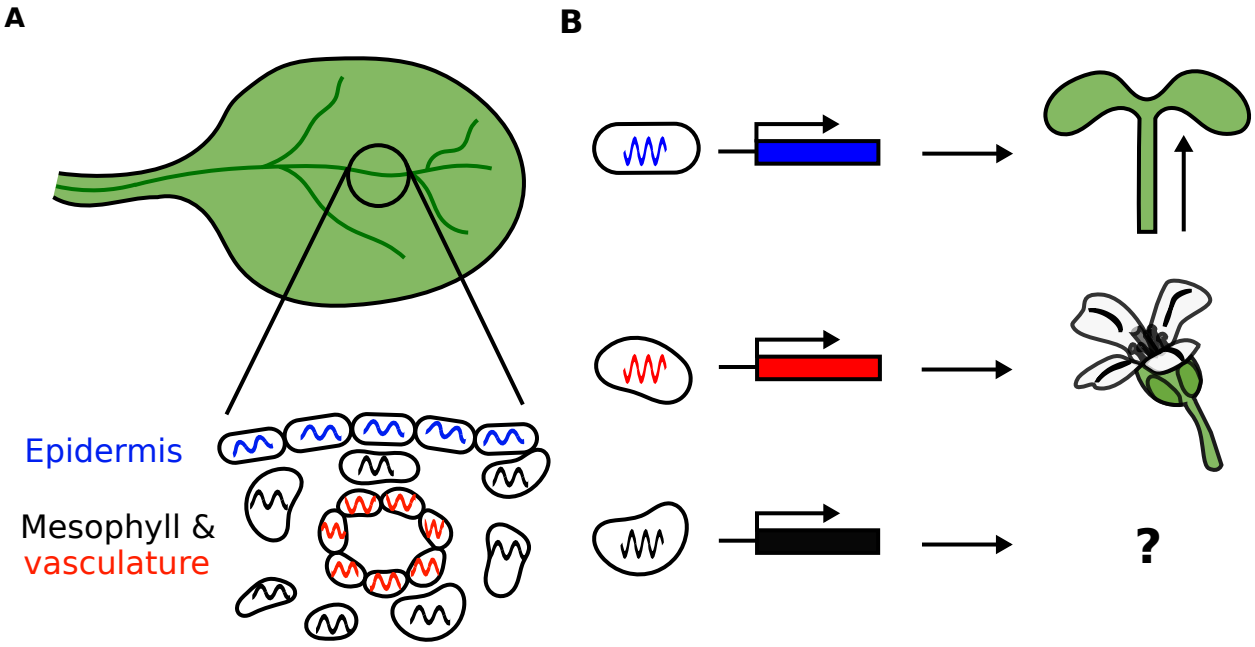

Fig. 1.9 Tissue specific clocks regulate distinct developmental outputs. (A) Circadian clocks in different tissues within the leaf oscillate with distinct properties. (B) Clocks in the epidermis and vasculature regulate different sets of target genes leading to control of hypocotyl elongation and photoperiodic flowering time respectively.

1.4.4 What causes specificity in the circadian system?

Two hypotheses can be envisaged as to the cause of cell and tissue specificity of rhythms. First, if the clock network is wired differently in distinct parts of the plant, it may cause them to oscillate out of synchrony. There is some evidence that the network has some tissue specificity. Previous work has shown that although most clock genes are expressed in most cell types [130, 4, 131, 111], some core clock genes may have a tissue enriched expression pattern [130, 132, 133, 125]. For example, β-glucuronidase (GUS) staining experiments suggest that *GI*, *PRR9*, and *PRR3* are enriched in the vasculature [130, 132]. However, a caveat of GUS staining is that the apparent signal levels are dependent on cell size and density, as demonstrated by vasculature enriched stains in *35S*::*LUC* lines [134, 135]. Indeed, in experiments with *PRR3*::PRR3-YFP reporter lines, expression can be detected at similar levels in other tissues [136].

If clock genes are differentially expressed within plants, it could be predicted that mutations would have differential effects on tissues. Indeed, mutations to *GI* were reported to have differential effects on the root and shoot [133]. However, in this study rhythms were weak in the wild-type root, making comparisons challenging. The effect of tissue specific clock networks therefore remains inconclusive.

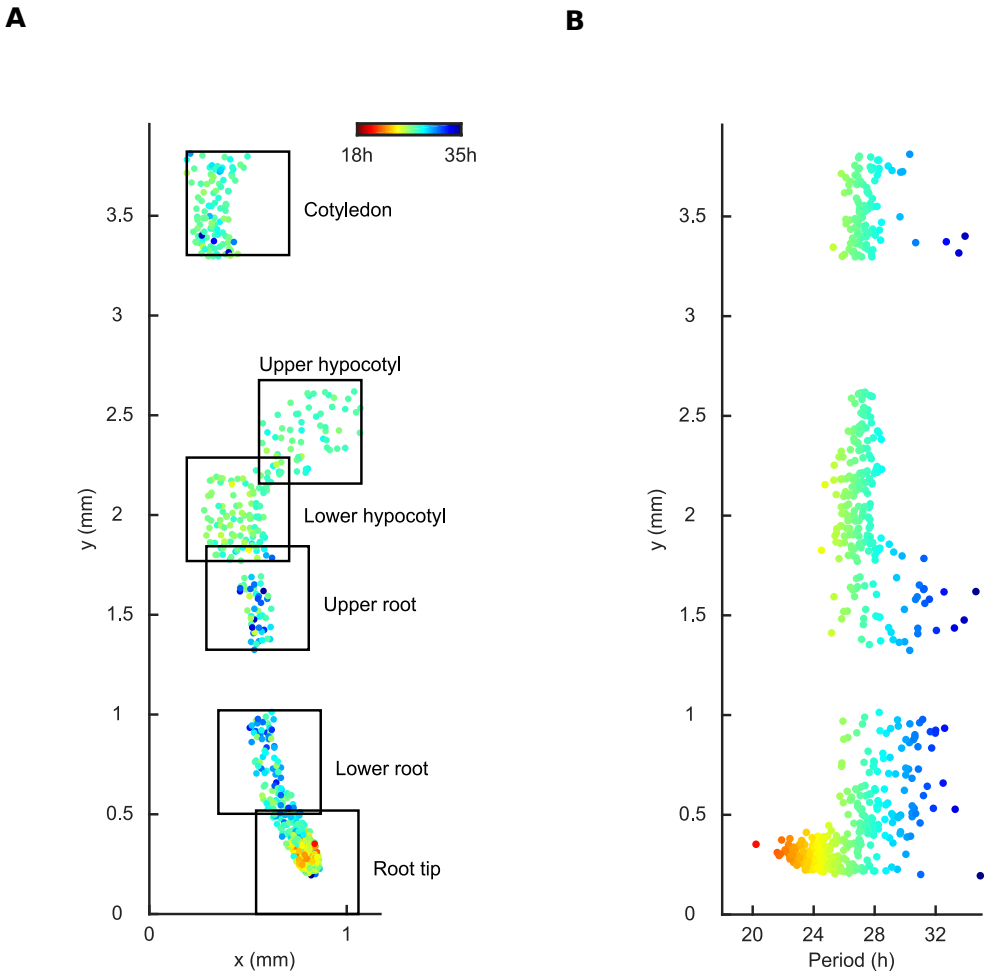

Fig. 1.10 Single cell period differences have a spatial structure in the seedling. (A) The *x*,-*y* position of single cells across a seedling are plotted. The colour indicates the period of the individual cellular CCA1-YFP oscillations. (B) Longitudinal position of cells plotted against the period of the individual cell. The colour legend is as in A. From [4].

A second possibility would be that rather than the central network, the sensitivity of environmental inputs varies across the plant. There is evidence for this hypothesis too. It has been shown that clocks in different cell types respond preferentially to temperature or light inputs. For example, the clock in the epidermis specifically senses temperature information [123, 124, 137]. Tissues also vary quantitatively in their sensitivity to inputs. For example, although both the shoot and root clock can be entrained by light, the root is more sensitive, entraining to lower levels of light [111].

It remains to be seen how whole-plant timing is affected by tissue level differences in the clock network, or differences in sensitivity to clock inputs.

1.4.5 Spatial coordination of the circadian system

In complex organisms, many physiological processes, including those under control of the clock, require coordinated timing across tissues. It is therefore likely that the individual oscillations need to be coordinated in order to control physiology. In many eukaryotes, cell-to-cell communication maintains clock coherence across the organism. For example, in mammals, clock cells located in the suprachiasmatic nucleus (SCN) drive rhythms in peripheral tissues across the body via neural and humoral signals [5, 138]. However, early experiments in plants showed that clocks in different tissues can be entrained to, and will maintain different phases, suggesting they are more independent of one another [110].

Later higher resolution studies suggested that there may be a degree of communication between individual clocks. Fluorescence imaging at the cellular level and luciferase imaging at the sub-tissue level revealed the presence of spatial-temporal phase patterns within tissues [4, 139–141]. For example, within the leaves of *Arabidopsis*, Wenden et al. observed spatial waves in the phase of *CCA1*::*LUC* [139]. These patterns were changeable, rather than fixed. In some leaves waves propagated from the base to the tip whereas in other leaves waves propagated from the centre outward radially. Although experiments to test the mechanisms have not been completed, the coherent patterns are indicative of communication acting between clocks.

Perhaps the ‘cleanest’ experimental test for circadian communication came from the use of tissue specific perturbations. Endo et al., induced arrhythmia specifically in the vasculature tissue by overexpressing *CCA1* with the vasculature specific *SUCROSE-PROTON SYMPORTER 2* (*SUC2*) promoter (*SUC2*::*CCA1*). They found that the clock was not only perturbed in the vasculature cells but also in the mesophyll, indicating communication between the clocks of the two tissues [125]. Finally, further evidence for communication between clocks comes from grafting experiments. By grafting WT clock shoots to clock

mutant roots, it was shown that the shoot clock can restore rhythms in the root, indicating communication between them [142].

1.4.6 Hierarchy of organisation in the circadian system

The presence of communication between clocks raises the question of hierarchy. In a hierarchical network some parts dominate over others, providing organisation. The plant clock does appear to have some hierarchy, rather than being a distributed (or hierarchy-less) network (Figure 1.11, right). This is evidenced by the dominance of the vasculature clock over the mesophyll clock within the leaf (subsection 1.4.5) [125]. However, the overall hierarchy structure across the plant, including whether it is centralised (Figure 1.11, left) or decentralised (Figure 1.11, centre), is less clear.

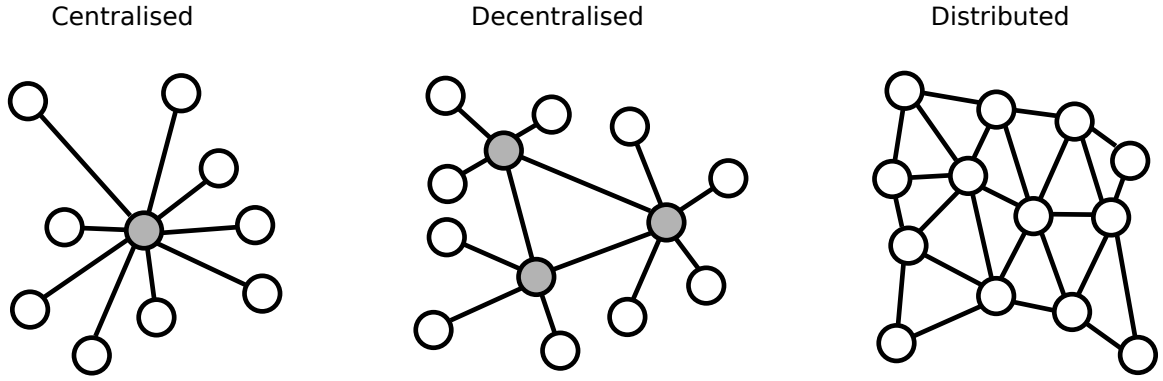

Fig. 1.11 Potential spatial structures for a circadian system. The *Arabidopsis* clock is considered either centralised or decentralised due to the presence of asymmetric coupling.

The mammalian circadian system has a centralised hierarchy (Figure 1.11, left), with the SCN acting as the 'master' and driving oscillations in peripheral tissues [5, 138]. It has been proposed that the plant circadian system is also controlled centrally, with the shoot clock acting as the 'master' [142, 133]. This conclusion was largely based on a series of grafting experiments which demonstrated that WT clock shoots can restore rhythms in mutant clock roots, but the opposite was not true, as WT clock roots did not restore rhythms in mutant shoots [142].

Further studies have delivered results inconsistent with a centralised structure. For example, detached roots can oscillate without the shoot for at least a week under constant light, and can be entrained directly to LD cycles [111, 143]. Additionally, fast cells in the root tip [4], as well as striped phase patterns in the root [140], suggest they are not driven from the shoot. Finally, by inducing arrhythmia specifically in the shoot apex with tissue specific promoters, it was shown that rhythms persist elsewhere. This suggests the shoot apex

may not be a centralised coordinator, as has been proposed [142]. A decentralised structure, with multiple points of coordination across the plant (Figure 1.11, centre), could potentially explain more of these results.

1.4.7 Local cell-to-cell mechanisms of coordination

Experimental methods for the direct study of local cell-to-cell communication are lacking in plants. Instead, evidence for local communication is usually inferred from studies of synchronisation. By studying how synchronised a set of oscillators are, or the way in which they desynchronise, the presence of local coupling can be inferred. This is often done by comparison to simple, locally coupled models [144]. In plants, analysis of the local synchrony in single cell rhythms across seedlings indicated a level of synchrony under LL that indicates the presence of local coupling [4]. Comparison to models allowed estimation of the strength of this coupling. Estimates varied across the plant, with the strongest effects in the cell densest regions, such as the root tip. This is consistent with other estimates in plants, where a considerably higher coupling strength was estimated in the cell dense shoot apex, in comparison to the leaf [142]. It remains to be seen, however, whether other intracellular signals that feature strongly here, such as the cell cycle, also effect synchrony.

A second way by which the presence of coupling can be inferred is from the spatial patterns of clock gene expression at the tissue level. The local interactions between cells creates ordered patterns, which can be predicted by locally coupled models. In plants, linear, spiral, and striped spatial wave patterns of clock gene expression have been observed within tissues [139–141, 145–147, 4]. These often intricate patterns can be predicted well by locally coupled models [4, 140, 141]. In mammals this approach has been extended to make estimates of the strength of coupling in the SCN by comparing spatial patterns between experiment and model [148].

Although it appears that plant clocks do couple locally (Figure 1.12), little progress has been made pertaining to the mechanism. Plant cells can communicate locally with their neighbours via the movement of molecules through the cell wall, or via microscopic channels called plasmodesmata [149]. Cell membrane receptors which allow coupling of clocks through the cell wall have not been identified. There are however, a number of molecules known to influence the clock that can move through plasmodesmata [150–154]. This makes plasmodesmata mediated coupling of clocks a likely mechanism.

Movement through plasmodesmata is mediated by the deposition of the polysaccharide callose, which forms the physical pore between neighbouring cells [155]. Mutations to the callose biosynthesis gene *CALLOSE SYNTHASE 3* (*CALS3*) can cause gain of function and over-deposition of callose at the pore. This results in a reduced aperture size, decreasing

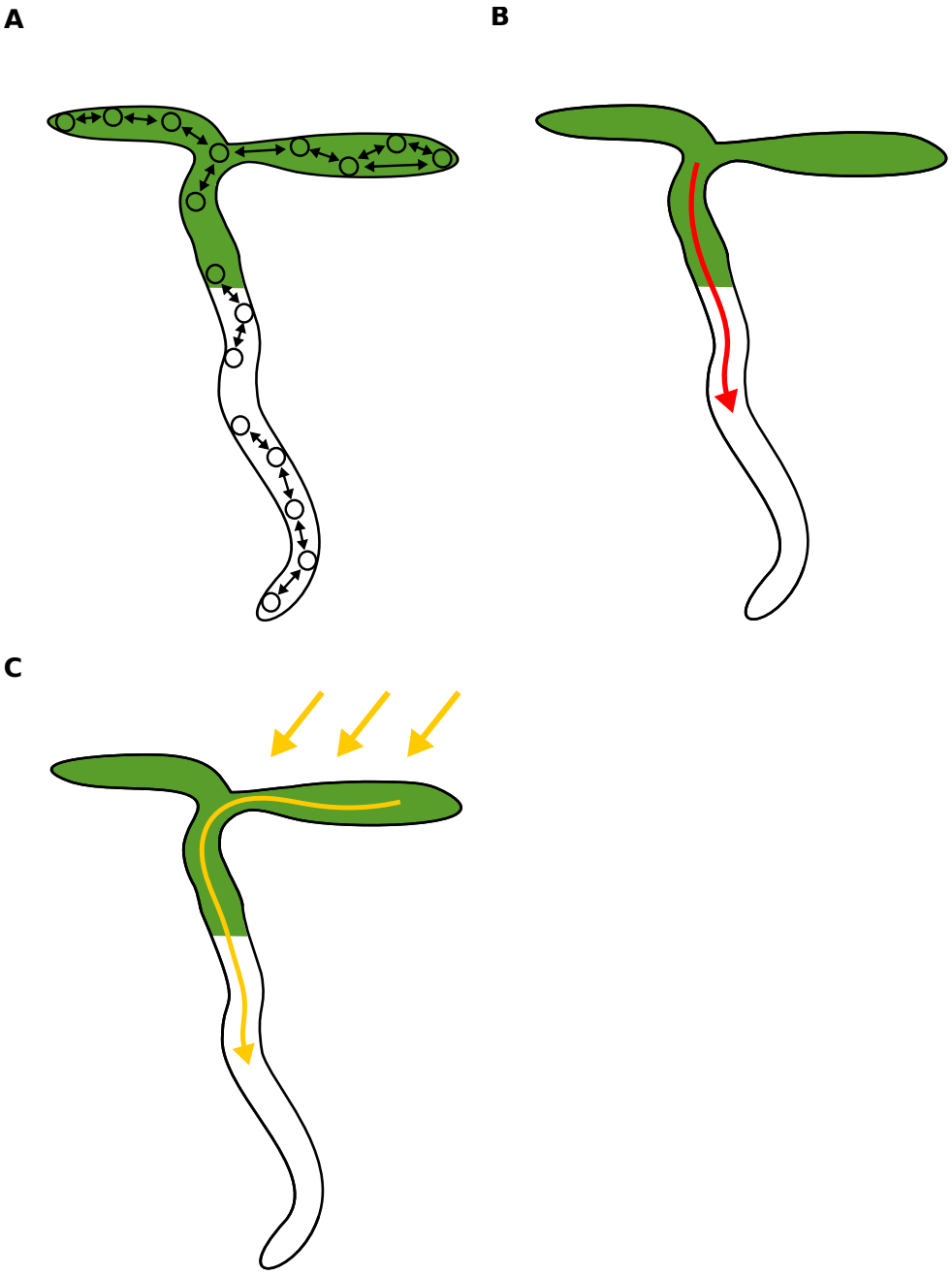

Fig. 1.12 Individual clocks coordinate within and between tissues. (A) Local cell-to-cell coupling coordinates rhythms within and between organs in seedlings. (B) Molecular long-distance signals in the shoot can drive rhythms in the root. (C) Light piped from the shoot can entrain rhythms in the root.

transport of molecules between cells [155]. Gain of function mutations in *CALS3* such as the *cals3-1d* allele can be utilised for the study of cell-to-cell coupling of clocks. Seedlings carrying the *cals3-1d* mutation showed a loss of rhythms of *CCA1* and *TOC1* expression measured across the entire root, although rhythms persisted in the shoot [142]. However, it was not clear whether this resulted from a loss of synchrony at the cellular level as would be expected if circadian coupling was perturbed. Experiments using the *cals3* system at higher resolution will be required to test the role of plasmodesmata in local cell-to-cell coupling of clocks.

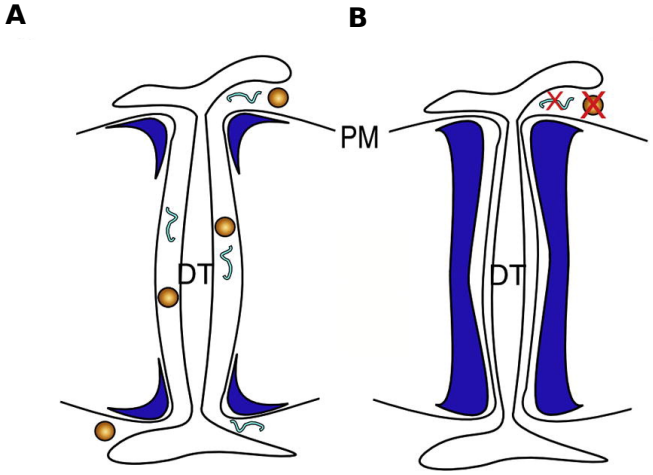

Fig. 1.13 Callose biosynthesis at the neck of the plasmodesmata pore controls cell-to-cell movement. (A) Controlled callose biosynthesis (blue) creates an opening allowing the controlled movement of molecules such as proteins and mRNA. (B) Over-deposition of callose constricts the opening restricting movement of molecules cell-to-cell. DT, desmotubule; PM, plasma membrane. Circles represent proteins and squiggled lines mRNA. Reprinted with permission from [155].

1.4.8 Long distance mechanisms of coordination

Plants can also communicate longer distances through molecules being selectively loaded into the phloem translocation stream. Long distance signals could potentially be useful for coupling between physically separated organs. A series of grafting experiments revealed that the shoot of a wild-type plant can recover the clock in the roots of arrhythmic clock mutants. However, wild type roots could not recover rhythms in mutant shoots, indicating there is a molecular signal coupling clocks from the shoot to root (Figure 1.12B) [142]. This hypothesis is seemingly supported by the observation that the root clock lags in phase, and is less robust than the shoot clock under constant light [129, 133]. However, it appears that a

mobile signal is secondary to direct entrainment of the root. When the shoot and root are entrained in anti-phase, the root maintains its phase, indicating the effect of a mobile signal is weak [111]. The molecular mechanism behind long distance coupling, or the mobile signal, has yet to be found.

A plausible long distance mechanism has also been proposed for light. Exposure of the top of roots to light affects the period of the whole root [143]. Since in plants light can be piped through shoots to roots [156–158], and trigger phytochrome responses in the root [105], light could potentially directly couple clocks between organs (Figure 1.12C) [143]. In future work it will be interesting to decipher how coupling mechanisms interact, in order to coordinate clocks across the plant during development.

1.4.9 Mobile signals in coordination

Excepting the light-piping hypothesis described above (subsection 1.4.8), both local and distance coupling mechanisms are dependent on a signal that is cell-to-cell mobile. As discussed (subsection 1.4.7), movement through plasmodesmata is the most likely mechanism of local cell-to-cell coupling. A selection of hormones, sugars, mRNAs, proteins, and ions have been shown to be both mobile between cells and capable of influencing the clock [150–154]. It will be important to investigate whether one, some, or all of these mobile signals act to couple the clock. Of particular interest is the transcription factor *ELONGATED HYPOCOTYL 5* [159], which can move cell-to-cell, is activated by stem-piped light [105], and can influence the circadian clock [160–162]. As many components can move between cells, with, for example, thousands of mobile mRNA elements [151], single cell "omics" methods [163, 164] will become increasingly important tools.

A long distance coupling signal must move locally towards the phloem, and then selectively be loaded into the phloem. The number of molecules that are transported long distances is therefore shorter than those that exclusively move locally. That said, the list of molecules that can move long distances still includes an array of hormones, sugars, mRNAs, proteins, and ions [150–154]. It has been proposed that sucrose acts as a long distance coupling signal from shoot to root. This hypothesis is appealing because sucrose is known to move from shoot to root [165], and can have a strong effect on the clock in whole-plant assays [92]. Organ resolution experiments showed that sucrose can selectively perturb the clock in the root [129], and inhibition of photosynthesis in the shoot caused damping of rhythms in the root [142]. However, it is unclear whether the damping was a result of a break in communication, or a metabolic effect. Further, in other studies differences in period between the shoot and root persisted with exposure of both to sucrose [111]. A mix of time-lapse

imaging and molecular perturbations will eventually decipher the signals behind the coupling of clocks.

1.5 Outline of thesis

Understanding how circadian clocks remain coordinated, both between one another and with the external environment, will prove critical if they are to be manipulated for use in the field. Mechanisms for external entrainment and internal coordination have been proposed, however, they currently fail to explain all of the complexities observed in experimental studies.

To address these questions, higher-resolution methods than those that have been typically used to study plant clocks were required. We developed a near-cellular luciferase imaging assay, and spatial-temporal data analysis methods for this purpose. We detail these methods in Chapter 2.

In Chapter 3, we apply our methods to monitor the clock at the sub-tissue level across entire *Arabidopsis* seedlings. We observed period and phase differences under both constant environmental conditions and LD cycles. Spatial waves of clock gene expression also propagated both within and between organs. We combined modelling and experiment to show that these patterns arise from the period differences together with local cell-to-cell communication, rather than long-distance signals.

In Chapter 4, we investigate the underlying cause of the organ-level period differences. We do this using light and metabolic signals, as well as with genetic perturbations. Our results reveal that period differences can be set by the specificity and sensitivity to environmental inputs. Manipulation of the periods drives the spatial waves of clock gene expression, as predicted by our model.

Finally in Chapter 5, we begin to investigate how circadian clocks coordinate under more realistic light-dark cycles. Our results suggest altered spatial and temporal organisation amongst the core clock genes.

Acknowledgements / disclosures

Parts of section 1.4 are published as part of a review paper, Greenwood & Locke 2020 [2].

Chapter 2

Materials and Methods

2.1 Plant materials and growth conditions

2.1.1 Plant materials

We utilised luciferase reporter constructs to monitor clock gene expression. The constructs consisted of the promoter regions of *GI*, *PRR9*, *TOC1*, or *ELF4* fused to the *LUC* reporter gene. The WT *GI*::*LUC*, *PRR9*::*LUC*, and *TOC1*::*LUC* lines are in the Col-0 background and as described previously [166, 167]. The *ELF4*::*LUC* line is also in the Col-0 background and was built by Laszlo Kozma-Bognar (Hungarian Academy of Sciences) for this study.

Table 2.1 Genetic lines used throughout the thesis

Line name	Source
GI::*LUC*	[166]
PRR9::*LUC*	[166]
TOC::*LUC*	[167]
ELF4::*LUC*	This thesis, by Laszlo Kozma-Bognar
phyb-9 GI::*LUC*	[166]
cca1-11 GI::*LUC*	This thesis, by Peter Gould
prr9-1 GI::*LUC*	This thesis, by Peter Gould
prr7-3 GI::*LUC*	This thesis, by Peter Gould
toc1-101 GI::*LUC*	This thesis, by Peter Gould
lux-4 GI::*LUC*	This thesis, by MG
G1090-XVE::*cals3m*; *GI*::*LUC*	This thesis, by MG

In addition to the WT clock reporter lines, a number of mutant background lines carrying the *GI*::*LUC* reporter construct were utilised. The *phyb-9 GI*::*LUC* line is in the Col-0

background and as described previously [166]. The *cca1-11 GI*::*LUC* (Ws background back-crossed with Col-0 three times), *prr9-1 GI*::*LUC*, *prr7-3 GI*::*LUC*, *toc1-101 GI*::*LUC* were built for this study by Peter Gould (University of Liverpool). The *GI*::*LUC* construct [166] was transformed into each mutant background by *Agrobacterium*-mediated transfection [168]. The *lux-4 GI*::*LUC* line was produced in this study by crossing the WT *GI*::*LUC* line with the *lux-4* mutant allele [41]. Homozygous third generation lines were used for experiments.

The *G1090-XVE*::*cals3m* line is controlled by the ubiquitous *G10-90* promoter with a estradiol inducible XVE domain [169]. This promoter has previously been combined with the *cals3m* construct, a hyper-active synthetic version of the callose biosythesis gene *CALLOSE SYNTHASE 3* (*CALS3*). Induction of this construct causes an increase in callose, which physically decreases the aperture of plasmodemata [155]. We crossed this line with our wild-type *GI*::*LUC* line to create a *G1090-XVE*::*cals3m*; *GI*::*LUC* line which allowed imaging of circadian dynamics during induction of plasmodesmata blockage.

2.1.2 Growth conditions prior to imaging

Seeds were surface sterilized and placed in the dark at 4 °C for 3 d. Seeds were sown at dawn of the fourth day on full-strength Murashige and Skoog (MS), 2% agar, pH 5.7 media, without sucrose unless otherwise specified. Seeds were then grown inside of plant growth incubators (MLR-352; Panasonic, Japan) for 4 d under 80 $\mu mol\,m^{-2}\,s$ cool white light at a constant temperature of 22 °C. Seedlings were grown under 12-h light–12-h dark cycles unless otherwise specified. Plates were orientated vertically during growth.

For experiments in which roots were grown in the dark (Figure 4.4), seedlings were grown in an optimised hydroponic growth system described previously [170]. In brief, lids of black 1.5 ml micro-centrifuge tubes (Thermo-Fisher Scientific, USA) were filled with MS, 2% agar media. A pore was created in the middle of each lid using a 19G hypodermic needle (Becton Dickinson, USA) and a single seed sown into the pore. Lids were placed in a 24 well floater rack (Scientific Specialities, USA) containing liquid MS media and transferred to growth cabinets. This design meant that the root grew downwards into the liquid medium, shielded from light, whereas the shoot grew upwards whilst exposed to light. After 4 d of growth, working under green light only, seedlings were transferred to square MS 2% agar plates and moved to imaging cabinets.

2.2 Luciferase imaging

2.2.1 Luciferase macro-imaging

At dusk of the fourth day of growth, seedlings were sprayed with a 5 mM D-Luciferin (Promega, USA), 0.01% Triton X-100 solution (Sigma-Aldrich, St. Louis, Missouri). At dawn of the fifth day, 6–8 seedlings were transferred into a 3- by 3-cm area of the media plate in order to fit inside of the camera's field of view. Plates were orientated vertically during imaging.

For experiments in Chapter 3 and 4, imaging was performed inside of growth incubators (MIR-154; Panasonic, Japan) at a constant temperature of 22 °C and under an equal mix of red and blue (RB) light–emitting diodes (LEDs; 40 µmol m^{-2} s total; Figure 2.1), unless specified as red light only (40 µmol m^{-2} s red) or blue light only (40 µmol m^{-2} s blue). Images were taken every 90 min for 6 d, with an exposure time of 20 min. Images were taken using a LUMO charge-coupled device (CCD) camera (QImaging, Canada) controlled using Micro-Manager (V2.0; Open Imaging) as previously described [64, 3]. The camera lens (Xenon 25 mm f/0.95; Schneider, Germany) was modified with a 5-mm optical spacer (Cosmicar, Japan) to increase the focal length and decrease the working distance.

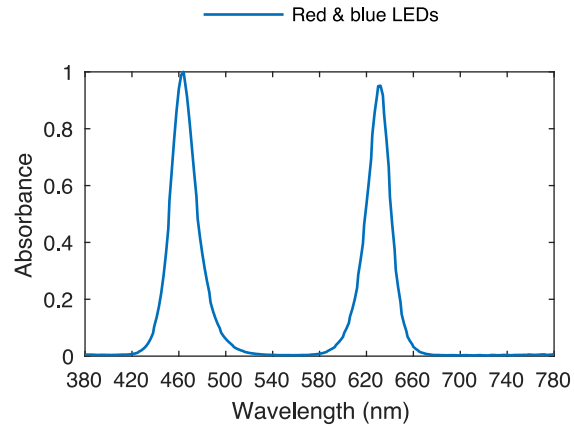

Fig. 2.1 Visible light emission spectrum under red and blue LEDs

2.2.2 Cuts and treatments

For cut experiments, seedlings were cut approximately 3 h after dawn of the fifth day of growth, immediately prior to the commencement of imaging. For "hypocotyl cut" experiments (Figure 3.6B, E, I), seedlings were cut in the root as close to the hypocotyl junction

as discernible by eye; for "root tip cut" experiments (Figure 3.6C, F and J), seedlings were cut approximately 100–200 μm from the root cap. Cuts were made with a pair of Vanna's type microdissection scissors (Agar Scientific, UK). Following all excisions, the organs were gently separated with a pair of forceps to ensure no physical contact.

3-(3,4-dichlorophenyl)-1,1-dimethylurea (DCMU; Sigma-Aldrich, USA) was added to the media at a final concentration of 20 mM. Seedlings were transferred to the DCMU-containing media at dusk of the fourth day of growth. For sugar application experiments (Figure 4.11 and Figure 4.13), media was added in 8-well rectangular dishes (NUNC; Thermo-Fisher Scientific, USA) so that one well contains media supplemented with MS and sugar whilst the adjoining well contains media supplemented with MS only. Wells were filled with equal volumes to the brim of the wells so that the two agar pads form a continual flat surface but do not touch. Sucrose or mannitol (Sigma-Aldrich, USA) was added at a final concentration of 90 mM (3 % w/v). Seedlings were cut at the hypocotyl junction (as described above) and laid across the adjoining agar pads so that approximately the top 1 mm of the excised root rests on the sugar-supplemented media, and the remainder of the root rests on the non-sugar-supplemented media. Seedlings were cut and transferred to the media at dawn of the fifth day of growth, immediately prior to the commencement of imaging.

For callose induction experiments (Figure 3.10 and Figure 3.11), seedlings were transferred to media supplemented with estradiol or Dimethyl sulfoxide (DMSO) at dawn of the fifth day of growth. Seedlings were kept on the supplemented media for the full 6 d of imaging. β-estradiol (Sigma-Aldrich, USA) or DMSO (Sigma-Aldrich, USA) was added to half-strength MS agar at a final concentration of 10 μM.

2.2.3 Aniline blue staining and confocal microscopy

To validate our inducible callose constructs, aniline blue staining was performed on seedlings. Staining was performed after completion of the first imaging experiment, in-which roots were induced by estradiol containing media for 6 days (Figure 3.9). Staining was performed as described previously [171]. A 0.1 mg/ml stock solution of aniline blue fluorochrome (Bisupplies Australia Pty. Ltd., Australia) in H_20 was diluted in a 1:3 ratio with 67 mM K_3PO_4, pH 9.5. Seedlings were incubated in this solution at room temperature for 2 h. Finally, to counter-stain root cells, seedlings were soaked in a 10 μg/ml propidium iodide (Sigma-Aldrich, USA) solution for 2 minutes.

Following staining, seedlings were mounted in a drop of anti-fading medium (Citiflour, USA). Imaging was performed using a upright confocal microscope (LSM700; Zeiss, Germany). Fluorescence was excited using a 405 nm and 555 nm laser and detected with a 490 nm short-pass and 560 nm long-pass filter respectively.

2.2.4 Environmental data analysis

In Figure 1.6 and Figure 1.7 we plotted a dataset of meteorological data to demonstrate the complexity of real environmental cycles. We plot the mean irradiance, air temperature (dry bulb), and soil temperature (at 10 cm soil depth) for March 2015, collected from a weather station in Rothamsted, U.K. [107]. Note that the values in this dataset are hourly summaries of recordings made at 5 second intervals. Higher frequency noise is therefore not visible but present [172].

2.2.5 Luciferase imaging under LD cycles

In Chapter 3, we imaged luciferase reporter expression in seedings under LD cycles (subsection 3.1.2). Seedlings were imaged under an equal mix of red and blue light (RB) as for constant light experiments (subsection 2.2.1). To simulate LD cycles lights were switched on to full intensity at dawn (40 $\mu mol\,m^{-2}\,s$ total) and completely off at dusk. In Chapter 5, we refer to this condition as 'RB on-off' for comparison to the altered LD conditions described below.

In Chapter 5 we imaged the clock under more realistic LD cycles by modifying our luciferase imaging protocol (subsection 2.2.1). Seedlings were grown and prepared for imaging as before. Imaging was performed inside of growth chambers (BDR16; Conviron, UK) at a constant temperature of 22 °C. Broad spectrum white light was provided by specialised LEDs (DYNA; Heliospectra, Sweden) retrofitted to the chamber (Figure 2.2).

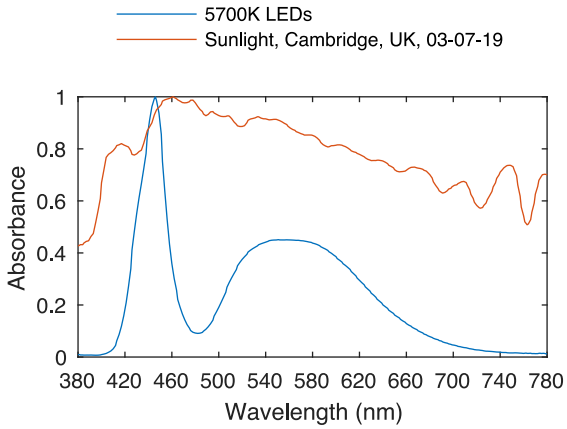

Fig. 2.2 Imaging cabinet LEDs approximate the visible wavelengths of sunlight.

In this setup, two different LD conditions were tested. In the first, broad spectrum white light was switched fully on at dawn (60 $\mu mol\,m^{-2}\,s$) and off at dusk (Figure 2.3, left). We

refer to this condition as 'white on-off'. In the second, broad spectrum white light was ramped up from dawn to a peak at noon, before declining towards dusk (Figure 2.3, right). The light levels for the two conditions were set such that the total flux of light received during the day period was equal (2592 mmol m^{-2} d). This was equivalent to a light intensity of 60 µmol m^{-2} s under on-off LD cycles. The camera acquisition and LED intensity were controlled programmatically using custom Python scripts. The program allowed for near continuous updating of light intensity during the experiment. The natural daily solar cycle was approximated, as previously [173], using the function

$$I(t) = \begin{cases} I_{max} sin\left(\frac{2\pi mod(t_{exp}-12,24)}{2T_L}\right) & \text{if } 0 <= mod(t_{exp}-12,24) <= T_L, \\ 0 & \text{otherwise} \end{cases}$$

where *mod* is the modulo operator, T_L is the day length (12 h), and t_{exp} is the time relative to the beginning of the experiment. $I_{max} = 12A\pi/2T_L$ where A is the light level under control experiments where the lights are switched fully on at dawn and off at dusk. In these experiments $A = 60$ µmol m^{-2} s, so $I_{max} = 94.25$ µmol m^{-2} s. Images were taken every 60 minutes using a LUMO CCD camera (QImaging, Canada) modified for high-resolution imaging as described in subsection 2.2.1.

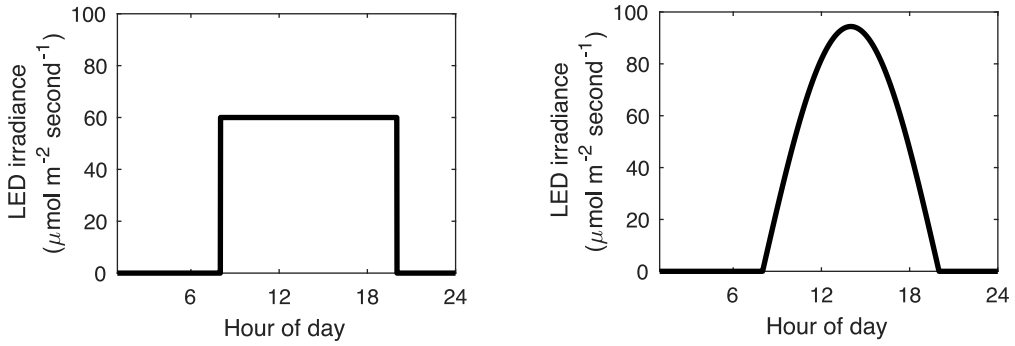

Fig. 2.3 On-off LD versus our graded approximation of natural LD conditions. On-off LD cycle commonly used in the laboratory (left) and our graded approximation of natural LD conditions (right).

2.3 Organ-level analysis of period and phase

2.3.1 Image analysis

For the organ-level analysis of the period and phase, organs were first tracked manually in Imaris (BitPlane, Switzerland) using the "Spots" functionality. We use a circular region of interest (ROI) of approximately 315-µm diameter and track the centre of a single cotyledon, hypocotyl, root, and the root tip from each seedling. As the root grows, we maintain the root ROI a fixed distance from the hypocotyl junction. A small number of cotyledons and hypocotyls were not trackable due to their orientation or their overlap with each other. These organs were excluded from the analysis. The median of the ROI was extracted to give the time series.

2.3.2 Period and phase analysis

Prior to the analysis of period and phase, the time series were first background subtracted. Very low expression rhythms with a minimum intensity value of less than zero after background subtraction were then removed. All time series were inspected by eye after preprocessing steps and prior to analysis.

Period analysis was conducted in BioDare2, a data server for the analysis of circadian data (biodare2.ed.ac.uk) [174]. All period estimates were performed on time series between 24–144 h from dawn of the day imaging began using the fast Fourier transform nonlinear least squares (FFT-NLLS) algorithm [175, 176]. Data were first detrended by subtraction of a polynomial of degree three from the data. Oscillations were classed as rhythmic if the FFT-NLLS algorithm returned a period in the range of 18–36 h with a confidence level (as defined in [174]) below 0.6.

For the analysis of the times of peaks of expression, peaks were identified using the MATLAB (MathWorks, UK) "findpeaks" function. This was done after the application of a third-order Butterworth filter to remove high-frequency noise. Only peaks in which all organs complete the full cycle within 24–144 h from dawn of the day imaging are used. Additionally, peaks were discarded if they are closer than 18 h or further than 36 h apart.

2.3.3 Phase analysis under LD cycles

In Chapter 5, we observe complex waveforms of circadian clock genes under LD conditions. The peak detection algorithms we applied to LL data proved ineffective for this data. We therefore applied the mFourfit algorithm, which was previously developed for estimating

phase from complex waveforms [12]. Briefly, for a range of test periods, mFourfit fits a 5th order Fourier series to the data. The Fourier series with the best fit gives the theoretical time series representing the data. Peaks are identified from the derivative of this theoretical data.

mFourfit identifies the peaks within the first 24 h cycle of the time-series, assuming a stable phase relationship. However, we observed potential changes in the waveform over time (e.g. Figure 5.6). We therefore apply the algorithm over 24 h windows in our data. We take the largest of the peaks in each 24 h window as the phase of expression for that time period, and define the smaller peaks as 'shoulders'. In the case of *GI*::*LUC* and *TOC1*::*LUC*, we sometimes observed a second strong peak at dawn. We therefore excluded the first 4 h from the analysis window for these markers.

2.3.4 Statistical analyses

In all figures, data points, measure of error, statistical test used, N, and the range of n are reported in the figure legend. When values are described in the text, they are quoted as mean ± standard deviation of the mean. For the comparisons of period estimates, one-way ANOVA (with Tukey post hoc method) was used for comparisons of more than two groups, and the t test (with Welch correction) for comparison of two groups. For comparison of times of peaks of expression, the distribution is often skewed, therefore the Kruskal-Wallis one-way ANOVA (with Dunn post hoc method) was used for multiple comparisons and the Wilcoxon rank-sum test for comparison of two groups. An alpha level of 0.05 was used for all ANOVA tests.

2.4 Sub-tissue phase analysis

To analyse spatial patterns within the organ, we first created space-time intensity plots of the luciferase images before obtaining a phase representation of the plots using a wavelet transform (henceforth called "phase plots"). These phase plots allowed interpretation of the space-time dynamics of the signal across the length of the organ independent of amplitude fluctuations.

Space-time intensity plots of the luciferase data were created as described previously [4], although with some modifications—most importantly of which, we include a modification that allowed us to better section curved roots. The method including modifications is outlined here in its entirety. Unless otherwise specified, steps are implemented via custom-developed MATLAB scripts.

2.4.1 Image preprocessing

A number of image processing steps were applied prior to the extraction of oscillations:

1. Each seedling was cropped into individual image stacks using ImageJ (NIH) in order to facilitate the further analysis.

2. A rectangle ROI encompassing the whole of the organ of interest plus the surrounding background was defined. When multiple organs were plotted together (Figure 3.5), the regions are defined so that there are neither longitudinal gaps nor overlap between them. The ROI was manually checked for signal from neighbouring organs or seedlings. These pixels were removed using ImageJ.

3. A 3-by-3 median filter was applied to the images to deal with background intensity spikes supposedly from cosmic rays and camera sensor imperfections.

4. The luminescent signal from the organ was segmented from background pixels by applying a threshold to each image individually. The mean of the intensity counts across the ROI was used as the threshold value.

5. Small objects remaining in the image that are not connected to the organ were removed by applying a morphological opening algorithm. Connected objects less than 50 pixels are removed.

2.4.2 Intensity space-time plots

To create the space-time plot, we averaged the signal across longitudinal sections of the organ. However, because plant organs naturally curve during growth, we took our longitudinal sections to be perpendicular to the angle of growth. We did this as follows:

1. For an ROI of dimensions m,n (with m representing the horizontal dimension and n the vertical dimension), the grey-level-weighted centroid C across each vertical section n was calculated as

$$C^n(t) = \frac{\sum_{m=1}^{Np} m \cdot W_{m,n}(t)}{\sum_{m=1}^{Np} W_{m,n}(t)},$$

where W represents the pixel intensity value and Np the width of the plant, as the number of segmented pixels.

2. A polynomial function of seventh degree was fitted to the centroids to give a curve that describes the shape of the hypocotyl and root $\{C(t)\}$ (Figure 2.4A).

3. At each horizontal position of the ROI $\{C^n(t) : n = 1, 2, \dots\}$, the tangent and normal line was calculated (Figure 2.4A).

4. The slope of the normal line was rasterised to give pixel coordinates describing the line (Figure 2.4B). The Bresenham algorithm was utilised for this purpose [177], implemented in MATLAB [178].

5. The rasterised line was limited to 10 pixels, centred around the intersect with the curve fit $\{C(t)\}$. This prevents multiple intersects with the organ.

6. The mean intensity of the pixels corresponding to the coordinates was taken to give the intensity value for section n at time t in the space-time intensity plots (Figure 2.4C).

2.4.3 Phase space-time plots

We used the wavelet transform to obtain phase plots (Figure 2.4D) from intensity space-time plots (Figure 2.4C). The continuous wavelet transform is closely related to the Fourier transform. However, unlike the Fourier transform, the continuous wavelet transform does not assume a stationary signal [179, 180]. This could be relevant to our data, given that an oscillator response to perturbations may be transient or changing. This method has been used previously to analyse dynamic oscillations [181, 182].

Given a time series $V = (V1, \dots, Vn)$, the continuous wavelet transform of V is given by

$$W_s(t) = \frac{1}{\sqrt{s}} \sum_{p=1}^{n} V_p Z^* \left(\frac{p-t}{s} \right),$$

where t represents time, Z is a wave-like function known as the mother wavelet, and s is a dimensionless frequency scale variable. Z^* denotes the complex conjugate of Z. For Z, we chose the Morlet wavelet,

$$Z(u) = \frac{e^{6iu} e^{iu2/2}}{\pi^{1/4}},$$

an oscillatory function that depends on a dimensionless time, like parameter u, and is localized in time with zero mean [180]. The wavelet transform can instead be expressed in terms of its phase θ and magnitude q,

$$W_s(t) = q_s(t) e^{i\phi_s(t)}.$$

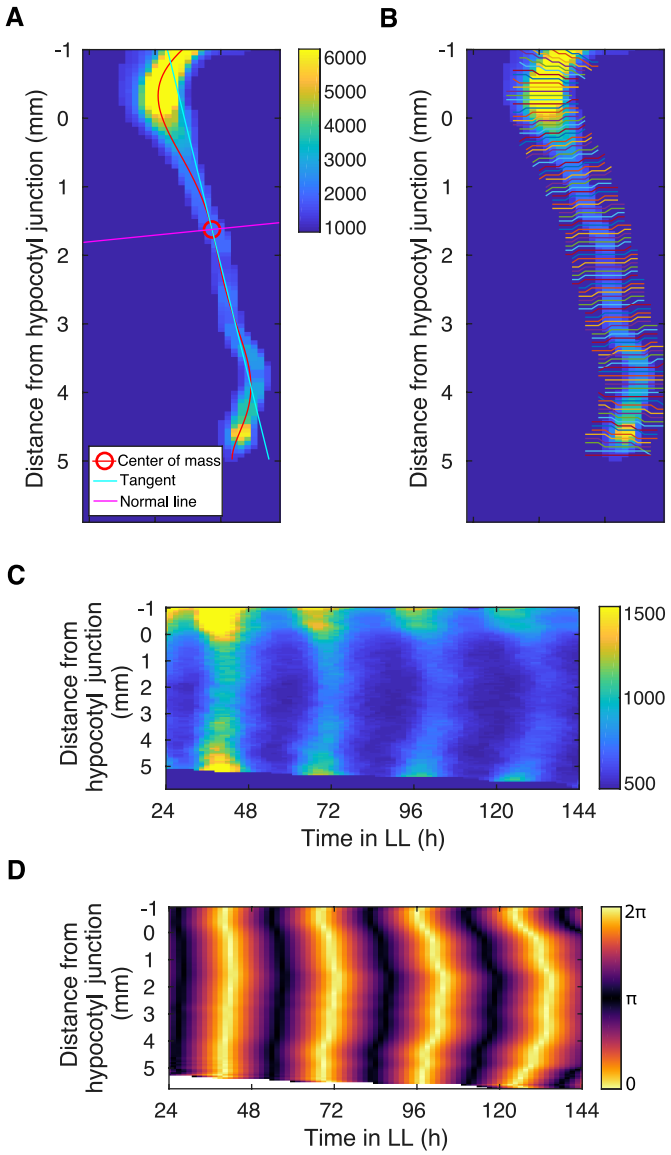

Fig. 2.4 Space-time phase plots from luciferase images. (A) Luciferase images are thresholded and a line fitted through the centre of mass of the organ. At each index on this line, the normal line is taken. (B) Each normal line is rasterized and limited to 5 pixels around the centre of mass to give pixel coordinates for longitudinal sections. (C) The mean value across longitudinal sections is taken at each time point to create a raw intensity space-time plot of a single seedling. (D) The phase of the oscillations is extracted using a wavelet transform to give a space-time map of the phase.

For meaningful interpretation of the phase values, s must be chosen close to the characteristic period of the times series V. However, the resultant phases are robust to small variations of s. We therefore selected a single s for each organ, matching s to the frequency of the rhythms that we observed in the organ under the experimental condition. Carrying out this procedure for every row of the intensity kymographs resulted in a phase plot (Figure 2.4D) corresponding to the intensity plot (Figure 2.4C). For comparison between plots, we plotted the first 16 pixels (approximately 1 mm) of the hypocotyl and the entirety of the root.

2.4.4 Synchrony analysis

By looking at the all-to-all synchrony between pixels within the hypocotyl and root, the synchrony of oscillators in these tissues can be estimated. We excluded the cotyledons from the analysis because their orientation and movement make phase extraction difficult. For each time point, the order parameter [183] R at time t was obtained as

$$R(t) = \frac{1}{N}\sum_{j=1}^{N} e^{i\theta_j(t)},$$

where N is the total number of pixels in the hypocotyl and root combined and θ_j the phase of the j-th pixel. R values range from 0 to 1, with a value of 1 indicating a set of completely synchronised oscillators and a value of 0 a set of completely desynchronised oscillators.

2.5 Phase oscillator models

2.5.1 Local cell-to-cell coupled model

We used the Kuramoto phase oscillator model to describe the dynamics of *GI*::*LUC* in each pixel (here, a pixel represents a set of individual, neighbour cells). We viewed the plant in two dimensions with positions in horizontal and vertical (longitudinal) directions described by index positions i and j, respectively, so that every pixel, $P(i,j)$, have has an associated position, (i,j). The phase at the pixel $P(i,j)$ was represented by $\theta^{(i,j)}$, where its dynamics in time, t, are governed by the following equation

$$\frac{d\theta^{i,j}}{dt} = \omega^{i,j} + K\sum_{m,n} sin(\theta^{m,n} - \theta^{i,j}) - K_{LD} sin(\frac{\pi}{12}t - \theta^{i,j}).$$

Here, the first term is the intrinsic frequency of the pixel, $\omega^{(}(i,j))$. The second term is the coupling contribution from the nearest-neighbour pixels in positions (m,n) that are closest to (i,j), namely, $m = i-1, i, i+1$, while $n = i-1, i, i-1$. We assumed a plant template that is symmetric and resembles the shape of a seedling (Figure 2.5). For the sake of simplicity, we assumed that the coupling constant, K, is the same across all pixels, and set it arbitrarily to $K = 1$ unless otherwise specified. The final term represents the coupling of the oscillator to the external force— in this case, the light force. Here, K_{LD} is the constant for the intensity of the light forcing, where in which all oscillators are subject to 24- h forcing. Note that when the clocks are not entrained to the LD cycles, $K_{LD} = 0$. Since *GI* tends to peak at the onset of dusk in 12- h light-12- h dark cycles and shorter photoperiods [12], we assume that the phase of *GI* will be antiphase to light, hence the negative sign in front of K_{LD}. In our simulations of the LD-to-LD model, we set $K_{LD} = 1$.

Intrinsic periods are different across different sections of the plant. Intrinsic periods of the pixels in each section were taken from normal distributions with means to match the experimental data, with the standard deviation at 10% of the mean value (Figure 2.5A-D).

Initial values of all phases in the LD-to-LL and LD-to-LD simulations were at the time of the start of measurement identical, with first peaks occurring approximately 11 h after the first measurement. In the LL-to-LL model, because we had no information about the initial phases, we set them to be uniformly distributed across a cycle (i.e., random). ODEs were solved using the Euler method and simulations performed in MATLAB.

Because the seedlings in our experiments grow, we introduced growth to the template seedling: we allowed the root to grow by one pixel every 5 h. Every newborn cell (and hence the new pixel) had the same phase as the closest set of cells (pixels) in the template, namely new pixels $P(i,j), P(i+1,j)$, and $P(i+2,j)$ will inherit the phases from $P(i,j-1), P(i+1,j-1)$, and $P(i+2,j-1)$, respectively. Their periods were taken from the normal distribution, with the mean of 26.90 h and the standard deviation 10% of the mean value.

After root growth, the root tip should stay fixed in size (of 5-by-5 pixels), so the previous most upper set of root tip pixels at the root/root tip junction were, from then on, considered as root tissue instead. This means that their periods lengthen and they were taken from a normal distribution with the mean of 28.04 h and the standard deviation 10% of the mean value.

2.5.2 Alternative models without cell-to-cell coupling

An alternative model that could give rise to the LD-to-LL spatial wave behaviours observed is one where there is no coupling but periods increase towards the middle of the root. This means that $K = 0$, and we set periods in the root to increase linearly from 25.41 h at the

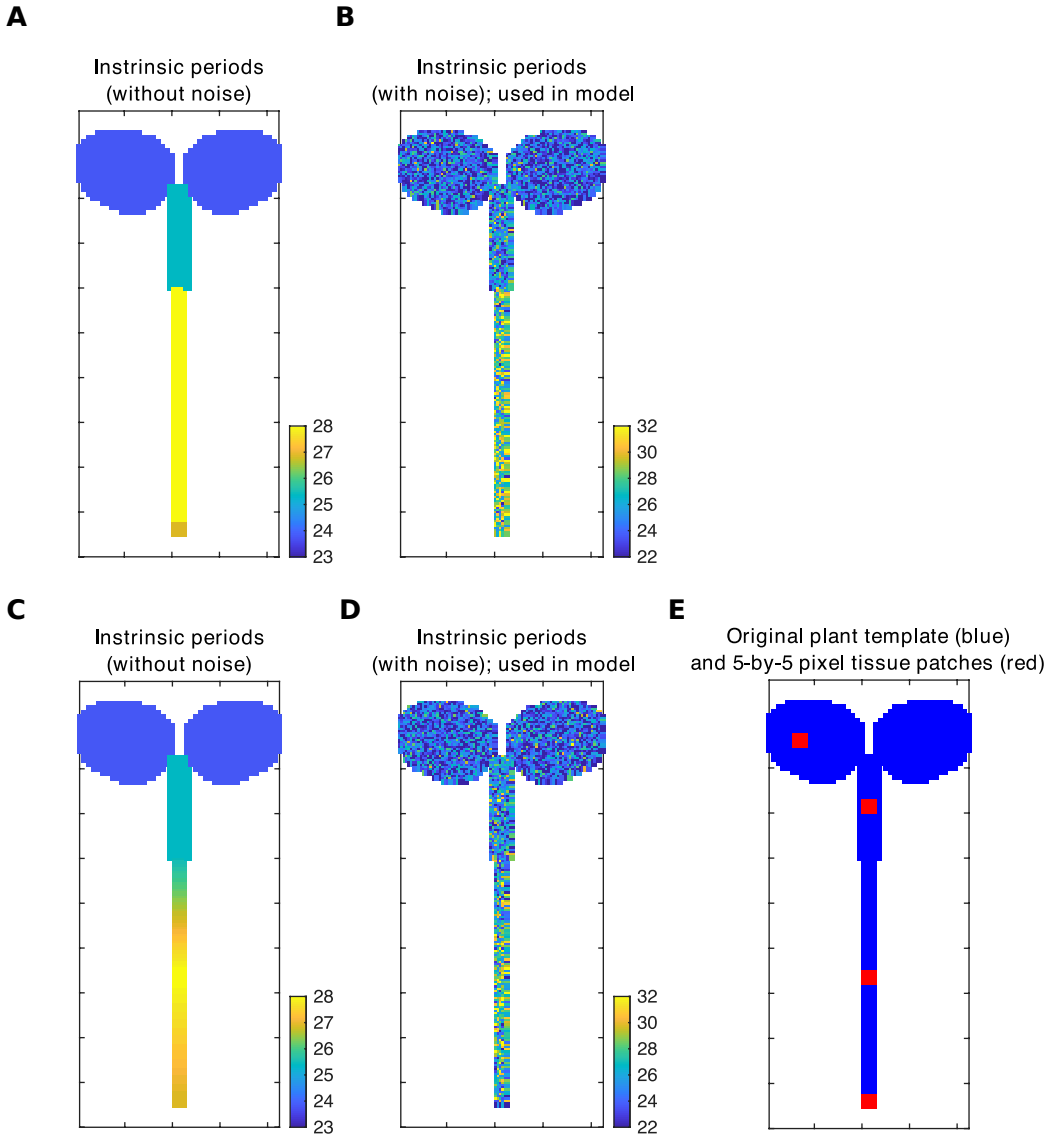

Fig. 2.5 Template for simulations with organ-specific periods and the ROI used for analysis. (A, B) Template for simulations, in which, in A, the periods of the pixels in each tissue are set to the mean periods measured in the LD-to-LL experimental data. In B, a representative set of periods for each region are shown, as drawn from the period distributions described in Materials and methods. (C, D) Template for simulations of the alternative model, in which, in C, periods of the pixels in each tissue are set to the mean periods measured in the LD-to-LL experimental data but with a gradient of periods in the root, as described in Materials and methods. In D, a representative set of seedling periods are shown, drawn from the period distributions and gradient described in Materials and methods. (E) The 5-by-5 pixel ROIs used for phase and period analyses are identified on the template.

hypocotyl/root junction to 28.04 h in the middle of the root, and then decrease linearly again to 26.90 h at the root/root tip junction. All other previous assumptions were adopted.

2.5.3 Model sub-tissue phase analysis

The expression of *GI* for each pixel, $GI^{(i,j)}$, was calculated from the phase model as:

$$GI^{(i,j)}(t) = cos(\theta^{(i,j)}(t)) + 1.$$

It follows that the total sum of the luminescence for every longitudinal position j is

$$GItot^{(j)} = \sum_{i=1}^{n_{(j)}} GI^{(i,j)},$$

where the total number of cells measuring across that section of the plant is n_j. The total luminescence was normalized so the maximum peak of expression in every longitudinal position is 1. The phases were extracted from the luminescence using the wavelet transform, as described above for the experimental data in subsection 2.4.3.

2.5.4 Model organ-level analysis of period and phase

To calculate the periods of the tissues as shown in Figure 3.12A and B, we took regions of 5-by-5 pixels in each tissue (Figure 2.5E) and calculated the median *GI* expression level for each region. Periods were calculated as the mean of the peak-to-peak periods of the median trace. To observe the distributions of periods and phases within a single simulation of a seedling (Figure 3.14 and Figure 3.15), we analysed *GI* expression for all pixels on the plant template individually. Periods were calculated as the mean of the peak-to-peak periods, and phases were taken at $t = 96$ h. Due to growth of the seedling template, there were a small number of pixels with a short time series containing less than two peaks of expression. These pixels were excluded from the analysis.

Acknowledgements / disclosures

The model was formulated by Mirela Domijan (University of Liverpool). Some lines were produced by Laszlo Kozma-Bognar (Hungarian Academy of Sciences) and Peter Gould (University of Liverpool; see Table 2.1 for details). A modified form of the imaging methodology (subsection 2.2.1) is published as part of Rees et al., 2019 [3].

Chapter 3

Local coordination of the *Arabidopsis* circadian clock

A number of studies of the plant circadian clock have reported differences in rhythms between tissues and cells [119]. However, most of these were focused on a single tissue or cell type, so the interactions between them are missed. To begin to address how rhythms coordinate between one-another, we imaged clocks across entire seedlings using a high-resolution luciferase method (subsection 2.2.1). Our approach allowed us to make perturbations to test the mechanisms of coordination, and we capture this understanding with a simple model.

3.1 Organ specific clocks

We monitored promoter activity of the core clock gene *GIGANTEA* (*GI*) [184] fused to the *LUCIFERASE* (*LUC*) reporter gene, for multiple days at near-cellular resolution (subsection 2.2.1). This reporter line was chosen because of its strong expression level across the entire seedling.

3.1.1 Clocks in different organs have different phases and periods under constant light

In order to observe the endogenous component of the rhythms, we first imaged seedlings under LL, having previously grown them under LD cycles (LD-to-LL; Figure 3.1 and subsection 2.1.2). Under the LD-to-LL condition we observed phase differences of *GI*::*LUC* expression between organs (Figure 3.1B, D). The cotyledon and hypocotyl peaked before the root, but the tip of the root peaked before the middle region of the root (Figure 3.1D and Figure 3.2). Furthermore, we observed a decrease in coherence between regions over time,

with a range between the earliest and latest peaking region of 4.92 ± 3.79 h (mean ± standard deviation) in the first and 18.36 ± 5.67 h in the final oscillation. This is due to the emergence of period differences between all regions (Figure 3.1F). The cotyledon maintained a mean period of 23.82 ± 0.60 h, whereas the hypocotyl and root ran at 25.41 ± 0.91 h and 28.04 ± 0.86 h, respectively. However, the root tip ran slightly faster than the middle of the root, with a mean period of 26.90 ± 0.45 h, demonstrating the presence of endogenous period differences across all regions.

We verified that our results were not specific to the *GI*::*LUC* reporter, as we observed similar differences in periods and phases across the plant using luciferase reporters for promoter activity of the core clock genes *PSEUDO-RESPONSE REGULATOR 9* (*PRR9*) [185], *TIMING OF CAB EXPRESSION 1* (*TOC1*) [128], and *EARLY FLOWERING 4* (*ELF4*); Figure 3.3) [40]. These observations are also qualitatively similar to the periods and phases previously observed in isolated organs, where the root as a whole has been reported to lag behind the shoot [111, 142, 129]. Our results also match data at the cellular level, where cells in the root tip run faster than elsewhere in the root (Figure 1.10) [4], thus validating our whole-plant, near-cellular assay for the circadian clock.

3.1.2 Clocks in different organs entrain to LD cycles with different phases

The phase at which a rhythm entrains to the environment can depend on the mismatch between its endogenous period and the period of the entraining signal [14, 186, 187]. We therefore tested the consequence of endogenous period differences between organs on the entrainment of the plant, by monitoring *GI*::*LUC* rhythms under LD cycles (LD-to-LD; Figure 3.1 and subsection 2.1.2). Under the LD-to-LD condition, we observed robust and entrained rhythms (Figure 3.1C). However, closer inspection of the timing of the peaks of the oscillations revealed significant differences in clock phase between organs (Figure 3.1E and Figure 3.4). The cotyledon and hypocotyl peaked earlier than the middle region of the root, but the root tip peaked earlier than the middle of the root (Figure 3.1E and Figure 3.4). This is qualitatively similar to the pattern observed under LL (Figure 3.1D). However, under the LD-to-LD condition, the organs showed a more stable phase relationship than under LL, with a range between the earliest and latest peaking region of 2.08 ± 1.56 h in the first oscillation and 1.10 ± 1.44 h in the final oscillation. This is due to the fact that all organs oscillate with a period of approximately 24 h (Figure 3.1C and G). We note that although small apparent differences can be observed between organs in the period analysis (Figure 3.1G), this is likely due the algorithm being designed for the analysis of rhythms under constant light

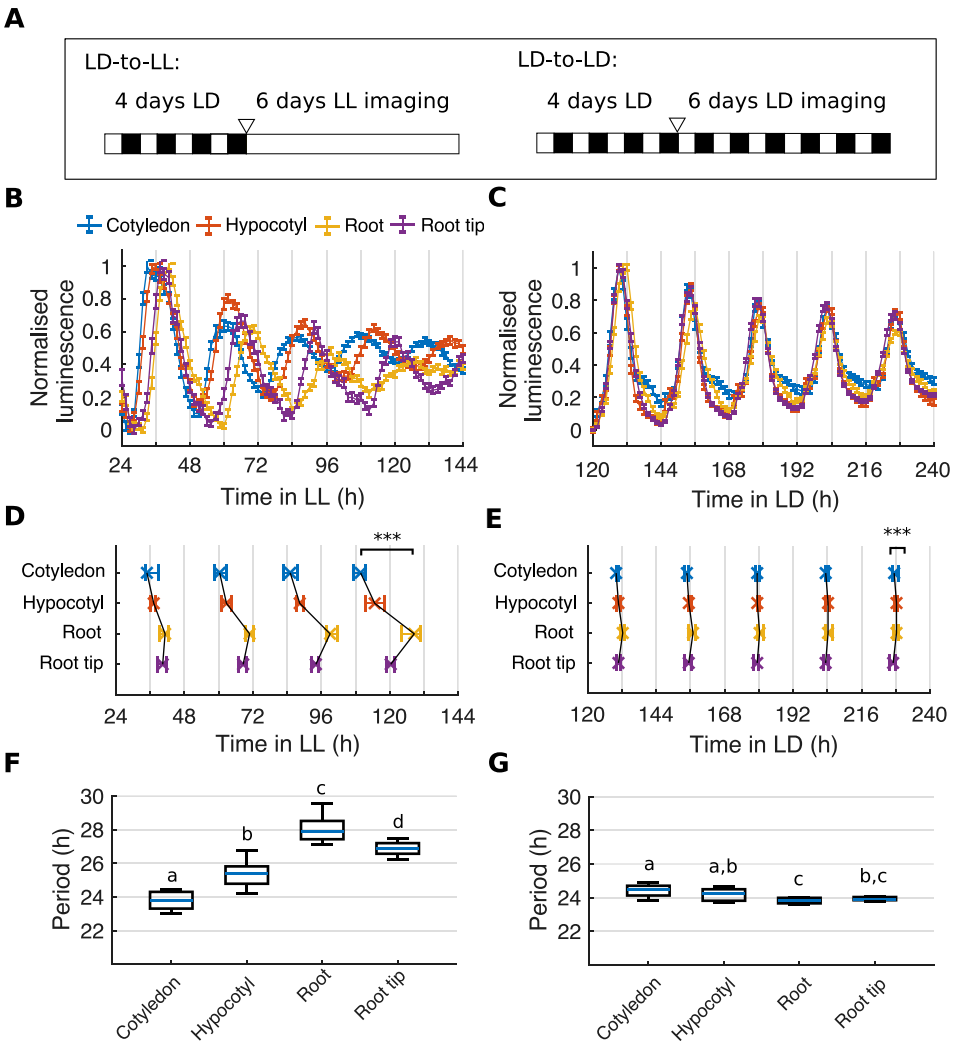

Fig. 3.1 Organ-specific clocks show phase differences under constant environmental conditions and LD cycles. (A) Schematic depicting the experimental conditions used. Seedlings were grown for 4 d under LD cycles and imaged either under constant light (LD-to-LL) or LD (LD-to-LD). The white triangle represents the beginning of imaging. (B, C) Expression of *GI*::*LUC* from different organs imaged under the LD-to-LL (B) or LD-to-LD condition (C). Data represent the mean ± standard error of organs scored as rhythmic. Luminescence counts were normalised to the minimum and maximum values of the time series. (D, E) Times of peaks of *GI*::*LUC* expression in different organs under the LD-to-LL (D) or LD-to-LD condition (E). Plots represent the 25th percentile, median, and the 75th percentile for the peak times of organs scored as rhythmic. Organs show significant phase differences, $***p < 0.001$, by Kruskal-Wallis ANOVA. Pairwise comparisons are shown in Figure 3.2 and Figure 3.4. (F, G) Period estimates of *GI*::*LUC* for different organs imaged under the LD-to-LL (F) or LD-to-LD (G) condition. The means of organs are statistically different ($p < 0.05$, by one-way ANOVA, Tukey post hoc tests) if they do not have a letter in common. Box plots indicate the median and upper and lower quartiles, and whiskers the 9th and 91st percentiles of organs scored as rhythmic. For LD-to-LL data, $N = 4$; LD-to-LD, $N = 3$; for both, $n = 26$–35. N represents the number of independent experiments and n the total number of organs tracked.

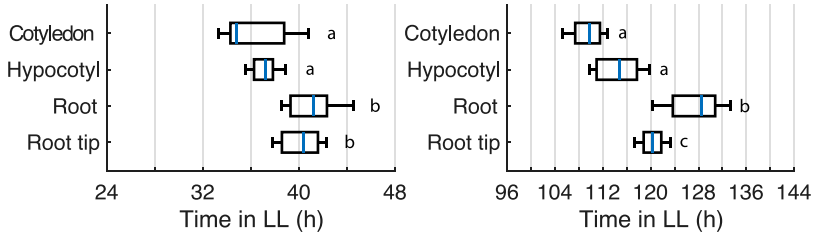

Fig. 3.2 Organs show phase differences under constant environmental conditions from the first to the final oscillation. Times of peaks of *GI*::*LUC* expression in different organs during the first (left) and final (right) observed oscillations under the LD-to-LL condition. Means are statistically different ($p < 0.05$, one-way ANOVA, Tukey post hoc tests) if they do not have a letter in common. Box plots indicate the median and upper and lower quartiles, and whiskers the 9th and 91st percentiles of organs scored as rhythmic. *N* and *n* are as presented in Figure 3.2.

subsection 2.3.2. The similarity of periods can instead be most easily observed in the mean traces (Figure 3.1C).

3.2 Spatial waves of clock gene expression propagate within and between tissues

Spatial waves of clock gene expression have been previously reported in plant leaves [139, 140, 146, 145] and roots [4, 141, 146] under LL. However, their relation to one another and the relevance under LD cycles remained unclear. We analysed our LD-to-LL and LD-to-LD data set of whole, intact seedlings at the sub-tissue level in order to address these questions. We extracted the phase of the luminescence signal across longitudinal sections of seedlings (Figure 2.4, section 2.4) and present phase plots (Figure 3.5) and time lapse videos (S1 and S2 Videos, available from https://gitlab.com/slcu/teamJL/greenwood_etal_2019) of single seedlings representative for each light condition. The clearest waves of expression could be observed in the LD-to-LL condition, as phase differences increased with time. In the cotyledon, a wave of *GI*::*LUC* expression propagated from the tip to the base (Figure 3.5A, top), and downwards into the hypocotyl (Figure 3.5A, middle). In the hypocotyl, we observed a second wave travelling from the root junction upwards into the hypocotyl (Figure 3.5A, middle). Finally, within the root we observed two waves: one propagating down from the hypocotyl junction and the second from the root tip upwards into the root, as we have reported previously (Figure 3.5A, bottom) [4]. Evidence of waves of clock gene expression could also be observed under the LD-to-LD condition. Although they are less pronounced, small phase waves could be discerned within the cotyledon (Figure 3.5B, top), hypocotyl (Figure 3.5B,

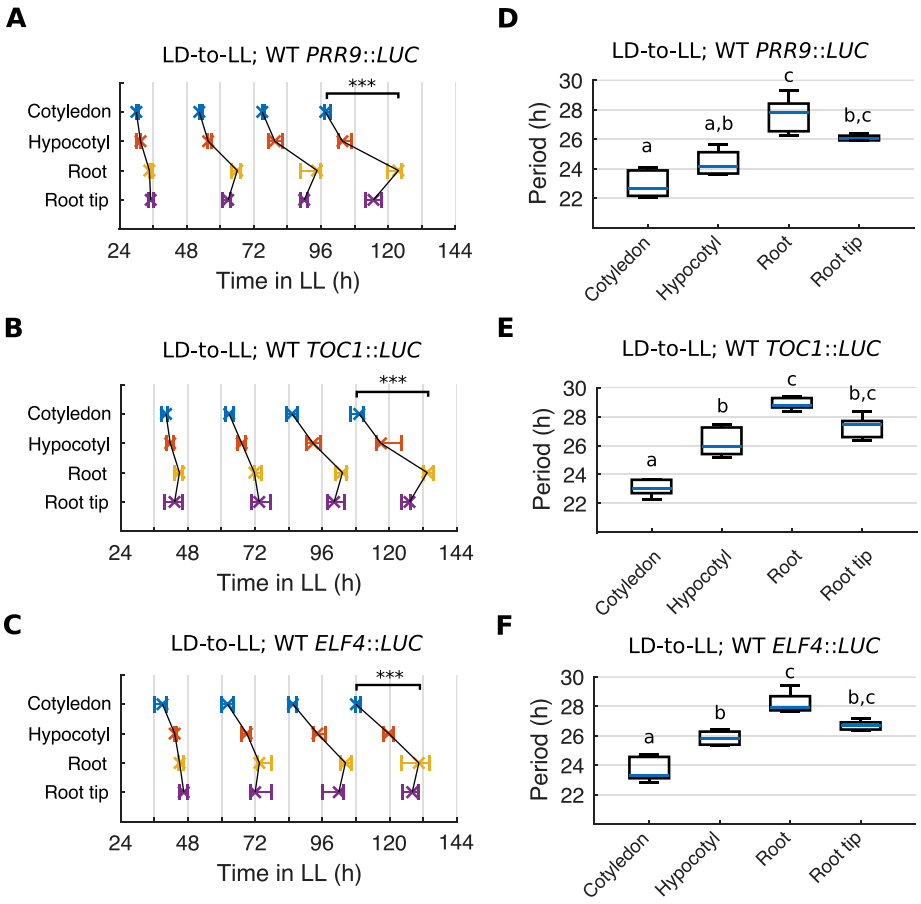

Fig. 3.3 Organs show similar clock phase and period differences under constant environmental conditions in multiple clock reporter lines. (A–C) Times of peaks of expression of *PRR9*::*LUC* (A), *TOC1*::*LUC* (B), or *ELF4*::*LUC* (C) in different organs under the LD-to-LL condition. Plots represent the 25th percentile, median, and the 75th percentile for the peak times of organs scored as rhythmic. ***$p < 0.001$, Kruskal-Wallis ANOVA. (D–F) Period estimates of *PRR9*::*LUC* (D), *TOC1*::*LUC* (E), or *ELF4*::*LUC* (F) expression for different organs imaged under the LD-to-LL condition. Box plots indicate the median and upper and lower quartiles, and whiskers the 9th and 91st percentiles of organs scored as rhythmic. For *PRR9*::*LUC*, N = 3; *TOC1*::*LUC*, $N = 3$; *ELF4*::*LUC*, $N = 3$. For all, $n = 11$–18. N represents the number of independent experiments and n the total number of organs tracked.

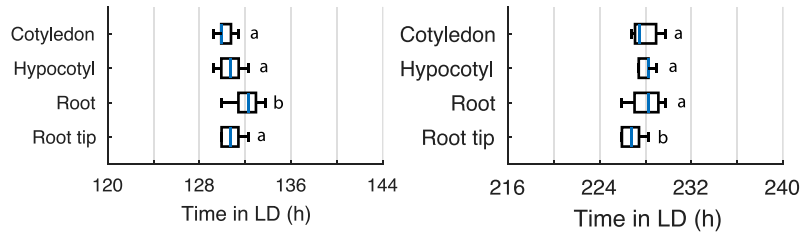

Fig. 3.4 Organs show clock phase differences under LD cycles from the first to the final oscillation. Times of peaks of *GI*::*LUC* expression in different organs during the first (left) and final (right) observed oscillations under the LD-to-LD condition. Means are statistically different ($p < 0.05$, one-way ANOVA, Tukey post hoc tests) if they do not have a letter in common. *N* and *n* are as presented in Figure 3.1. *N* represents the number of independent experiments and *n* the total number of organs tracked. Box plots indicate the median and upper and lower quartiles, and whiskers the 9th and 91st percentiles of organs scored as rhythmic.

middle), and root (Figure 3.5B, bottom) of the phase plots and time lapse videos (S2 Video, available from https://gitlab.com/slcu/teamJL/greenwood_etal_2019).

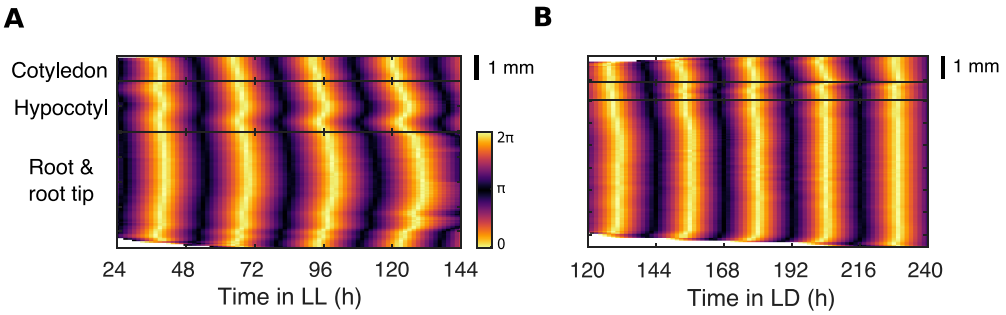

Fig. 3.5 Spatial waves of clock gene expression propagate within and between tissues. (A, B) Representative phase plot of *GI*::*LUC* expression across longitudinal sections of the cotyledon (top), hypocotyl (middle), and root (bottom) of a single seedling under LD-to-LL (A) and LD-to-LD (B) conditions. Colour bars are as in A. *N* and *n* are as in Figure 3.1. *N* represents the number of independent experiments and *n* the total number of organs tracked. Box plots indicate the median and upper and lower quartiles, and whiskers the 9th and 91st percentiles of organs scored as rhythmic.

3.3 The clock system in seedlings is organ autonomous

3.3.1 Phase and period differences between organs persist in the absence of long-distance communication

The period and phase of clocks in individual organs may be set locally, in isolation from the rest of the plant. We define this as organ-autonomous. Alternatively, clocks may be set by signals moving long distance from other organs. To investigate whether rhythms and spatial waves are driven by long-distance, interorgan communication, we blocked signal transmission between organs by cutting the seedling into sections. We cut the root at either the hypocotyl junction, the root tip, or both the hypocotyl junction and the root tip, and then monitored the rhythms under LL (Figure 3.6A). We found that sectioning the plant did not substantially affect the phase of the rhythms (Figure 3.6B–D). Some minor phase differences were observed between cut and uncut controls after cutting, but these were no longer apparent after 6 d (Figure 3.7). Period differences across the plant also persisted after cutting (Figure 3.6E–G). Our results show that rhythms are organ autonomous and not dependent on a long distance signal from another organ.

3.3.2 Spatial waves of clock gene expression persist in the absence of long-distance communication

Although rhythms can persist within organs without a long-distance signal, the presence of spatial waves suggests there is some communication. Previous work has proposed that spatial waves of clock gene expression are driven by local cell-to-cell coupling [4, 139, 141, 140]. However, plants can also communicate through long-distance, interorgan pathways [149], and the root clock has been proposed to be driven by long-range signals from the shoot [142, 129, 133]. We therefore tested whether waves are lost following cuts to the seedling. We analysed seedlings at the sub-tissue level following cuts at the hypocotyl junction, root tip, and both the hypocotyl junction and root tip, as before. We focused our analysis to within the hypocotyl and root, where the simple geometry means the wave patterns can be most easily observed. Strikingly, after all cuts we observed the persistence of waves propagating both from the hypocotyl down into the root and from the root tip upwards in phase plots (Figure 3.8A–D) and time lapse videos (S3 Video, available from https://gitlab.com/slcu/teamJL/greenwood_etal_2019). Our results show that the spatial waves that travel within and between organs are not dependent on a long-distance signal.

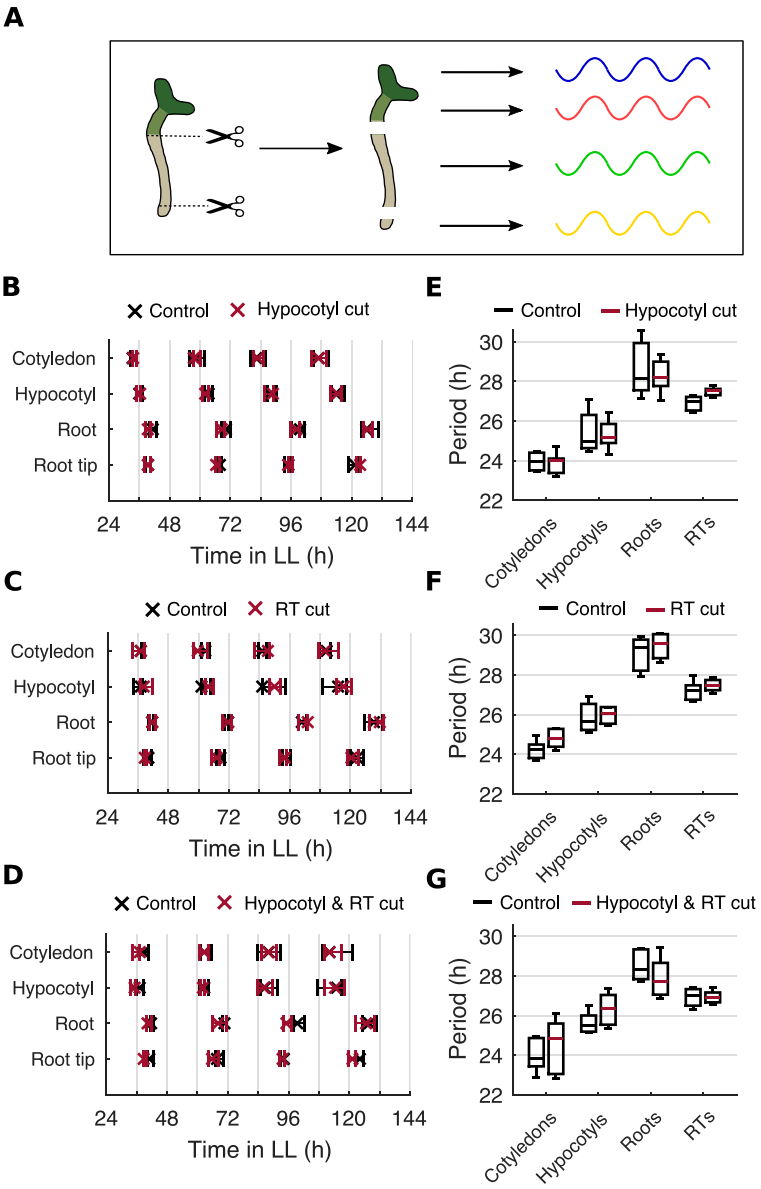

Fig. 3.6 Organ-level rhythms persist in the absence of long-distance signals. (A) Schematic depicting the experimental design. Seedlings were cut at the hypocotyl junction, root tip (RT), or at both the hypocotyl junction and the RT. The rhythm of both the excised organs and the remaining intact organs were subsequently analysed. (B–D) Times of peaks of *GI*::*LUC* expression in different organs following a cut at the hypocotyl junction (B), RT (C), or both the hypocotyl junction and RT (D). Plots represent the 25th percentile, median, and the 75th percentile for the peak times of organs scored as rhythmic. (E–G) Period estimates of *GI*::*LUC* for different organs following a cut at the hypocotyl junction (E), RT (F), and both the hypocotyl junction and RT (G). All comparisons of means are not significantly different, $p > 0.05$, by two-tailed t test, Welch correction. Box plots indicate the median and upper and lower quartiles, and whiskers the 9th and 91st percentiles of organs scored as rhythmic. For hypocotyl cut experiments, $N = 4$; RT cut, $N = 3$; hypocotyl and RT cut, $N = 3$. For all, $n = 9$–17. N represents the number of independent experiments and n the total number of organs tracked.

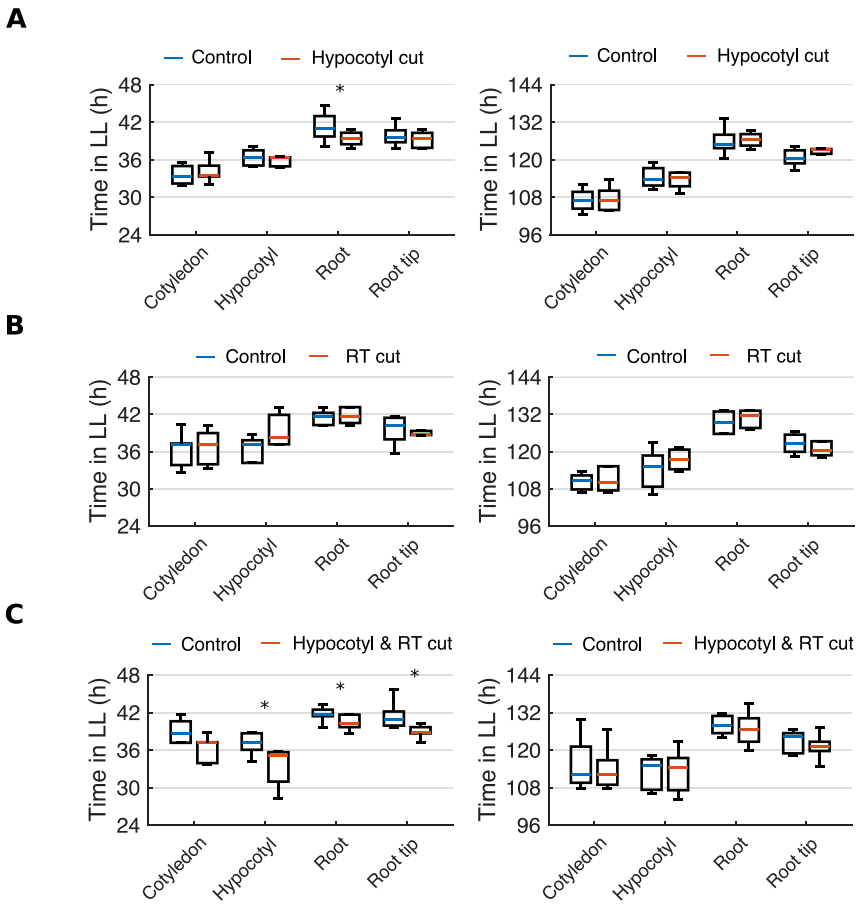

Fig. 3.7 Phase differences between organs following cuts is comparable to controls. (A-C) Times of peaks of *GI*::*LUC* expression in different organs for the first (left) and final (right) observed oscillations following a cut at the hypocotyl junction (A), root tip (B), or both the hypocotyl junction and root tip (C) conditions. $p < 0.05$, Wilcoxon rank-sum test. N and n are as in Figure 3.6. N represents the number of independent experiments and n the total number of organs tracked. Box plots indicate the median and upper and lower quartiles, and whiskers the 9th and 91st percentiles of organs scored as rhythmic.

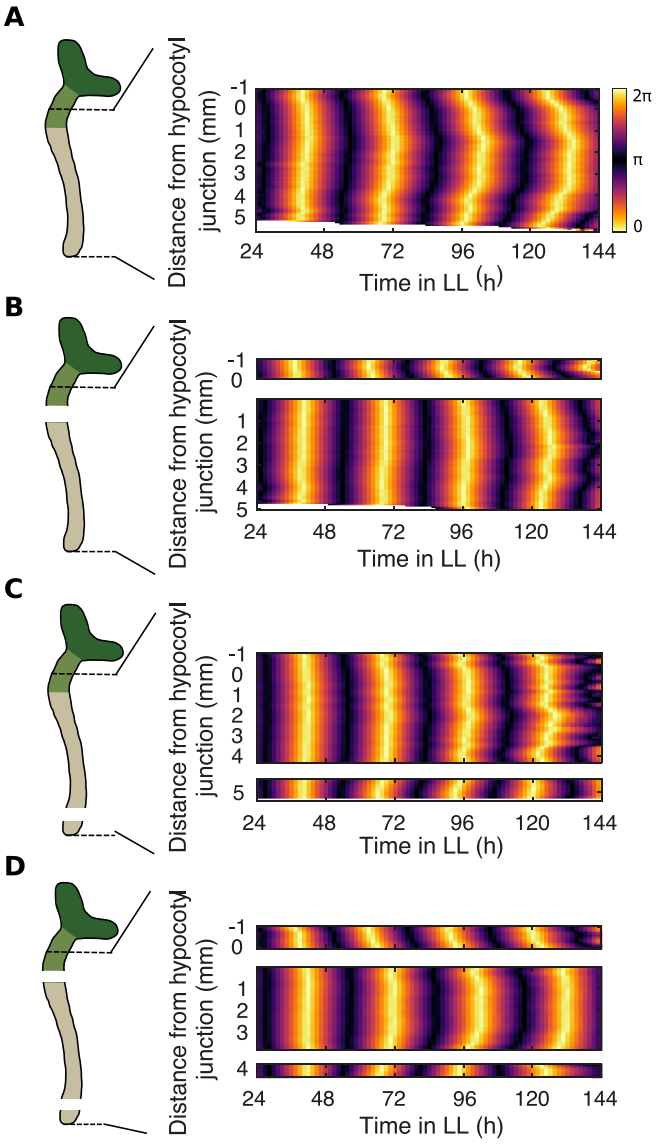

Fig. 3.8 Spatial waves of clock gene expression persist after cuts. (A–D) Representative phase plot of *GI*::*LUC* expression across longitudinal sections of the hypocotyl and root of a single seedling without a cut (A) or with a cut at either the hypocotyl junction (B), RT (C), or both the hypocotyl junction and RT (D). Schematic shows the approximate cut position and the region analysed. Colour maps are as in A. *N* and *n* are as in Figure 3.6. *N* represents the number of independent experiments and *n* the total number of organs tracked.

3.4 Local plasmodesmata mobile signals in the spatial coordination of rhythms

3.4.1 The *cals3m* system for restricting local cell-to-cell communication

Our results suggest that local rather than long-distance signals may be more important for the coordination of rhythms in seedlings. We therefore investigated whether plasmodesmata mobile signals are involved in the local coordination of rhythms. To do this, we took advantage of the *cals3m* gene, a hyper-active synthetic version of the callose biosynthesis gene *CALLOSE SYNTHASE 3* (*CALS3*). The *cals3m* gene is driven by a promoter that can be induced by estradiol [169]. Induction of the *G10-90-XVE*::*cals3m* construct causes an increase in callose, which physically restricts the aperture of the plasmodesmata and partially blocks the trafficking of molecules [155]. We crossed this line with our WT *GI*::*LUC* line, allowing us to observe circadian dynamics during induction of plasmodesmata blockage. By staining the callose with aniline blue, we validated that induction of our *G10-90-XVE*::*cals3m*; *GI*::*LUC* line caused an increase in callose production in the cotyledons (Figure 3.9A) and root (Figure 3.9C) relative to un-induced controls (Figure 3.9B, D). Both the aniline blue and cell wall stain was absorbed poorly in the hypocotyl meaning visualisation of callose was not possible.

Although from the staining it was clear that callose production was induced in our lines, we observed variable levels of deposition within the seedling. In the cotyledon, upon induction callose deposition was high in the guard cells but lower in other cell types (Figure 3.9A). In the root, we observed highest deposition at the most distal region of the root tip (Figure 3.9C). Levels of callose were substantially lower in the elongation and differentiation zone (Figure 3.9C). The variable callose induction may be caused by spatial variation in the *G1090* promoter, which we intended to be ubiquitous (Matthieu Bourdon, personal communication). Despite this complication, we take forward our line as a proof of concept, to demonstrate the potential of such an approach for investigations of coupling.

3.4.2 Induction of callose deposition weakens rhythms in the cotyledon and hypocotyl

We monitored *GI*::*LUC* in our line under LL during induction of the *G10-90-XVE*::*cals3m* construct and found organ-conditional effects on rhythms. In the cotyledon, we observed a decrease in the amplitude of rhythms, and a near complete loss of rhythmicity in the

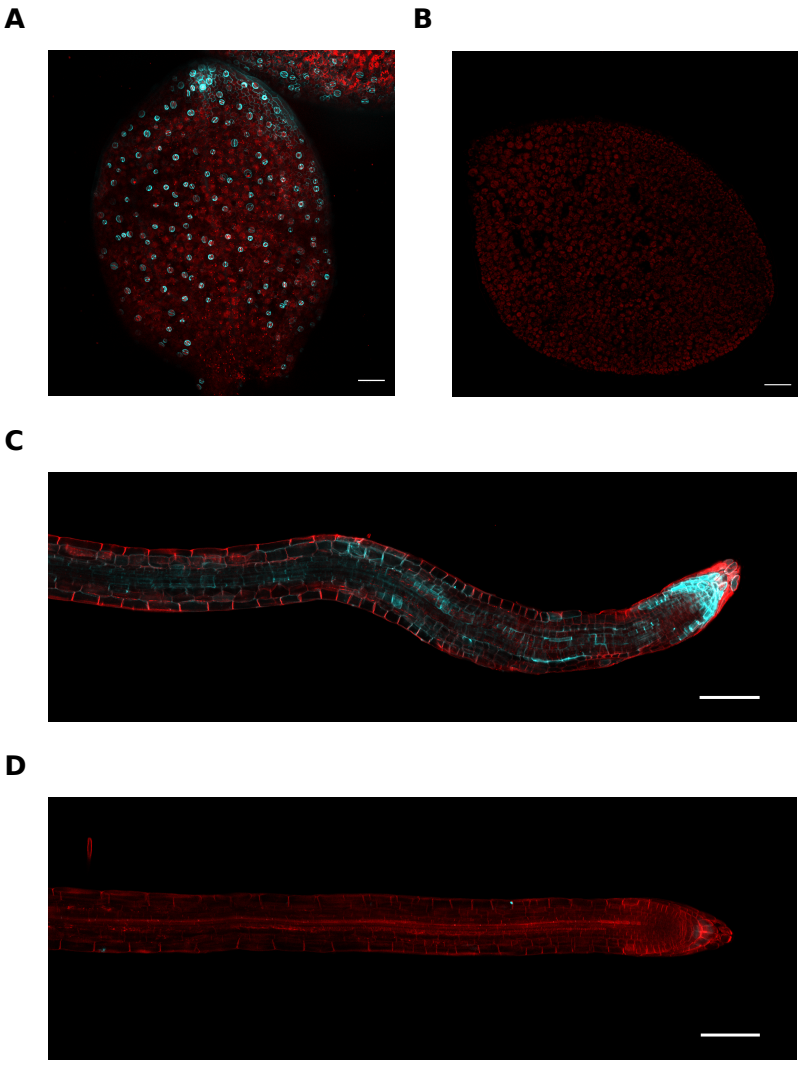

Fig. 3.9 Induction of callose biosynthesis using the *cals3m* system. (A, B) Aniline blue stained cotyledon of the *G1090-XVE*::*icals3m*; *GI*::*LUC* line after 6 days of estradiol (A) or mock DMSO induction (B). (C, D) Aniline blue stained primary root of the *G1090-XVE*::*icals3m*; *GI*::*LUC* line after 6 days of estradiol (C) or mock DMSO induction (D). Staining was repeated on 3 seedlings with similar results. Blue channel shows aniline blue stain, red channel shows cell wall counter-stain, and scale bars show 100 μm.

hypocotyl (Figure 3.10). In the root regions, we observed little effect on robustness, although there may be a slightly earlier phase of expression (Figure 3.10).

The effect on rhythms appears to be partly correlated with the level of callose induction. The effect on the cotyledons was substantial (Figure 3.10), where the induction was strong (Figure 3.9A). The effect on rhythms in the middle region of the root was weaker (Figure 3.10), where the induction was also weaker (Figure 3.9C). In the tip of the root, the effect on rhythms was more ambiguous (Figure 3.10), despite stronger induction than in the middle region of the root (Figure 3.9C). This may be because the region of interest used for the analysis of the root tip captures both cells that are induced strongly and weakly (see subsection 2.3.1).

3.4.3 Induction of callose deposition may influence spatial waves of clock gene expression

At the sub-tissue level we observed some disruption to spatial organisation. After 3 days under LL, rhythms in the cotyledon and hypocotyl appeared less synchronous. Although waves may still be present, they were less distinct and lacked consistent direction (Figure 3.11, top and Figure 3.11, middle). Similarly, in the root, waves became less distinct after 3 days (Figure 3.11, bottom). Thus, the restriction of plasmodesmata aperture, albeit variably, partially disrupted spatial waves of clock gene expression.

3.5 A local cell-to-cell coupled model captures dynamics under LD and LL

3.5.1 A local cell-to-cell coupled circadian clock model

The persistence of rhythms and spatial waves in the absence of long-distance communication suggests clocks may instead be coupled through local interactions. We therefore utilised the Kuramoto mathematical framework to investigate whether local coupling can explain the entrainment behaviours that we observe under LD and LL. In this framework each individual oscillator in a set of oscillators is described by its intrinsic period and phase, and is coupled weakly to its neighbours [144]. We designed our model so that each pixel (which in fact represents multiple cells) on a seedling template is an individual oscillator with an intrinsic period and is weakly coupled to its nearest neighbours (Figure 2.5). The intrinsic period of each pixel was set according to its location in the seedling. Pixels from the cotyledon, hypocotyl, root, and root tip were drawn from distributions centred around

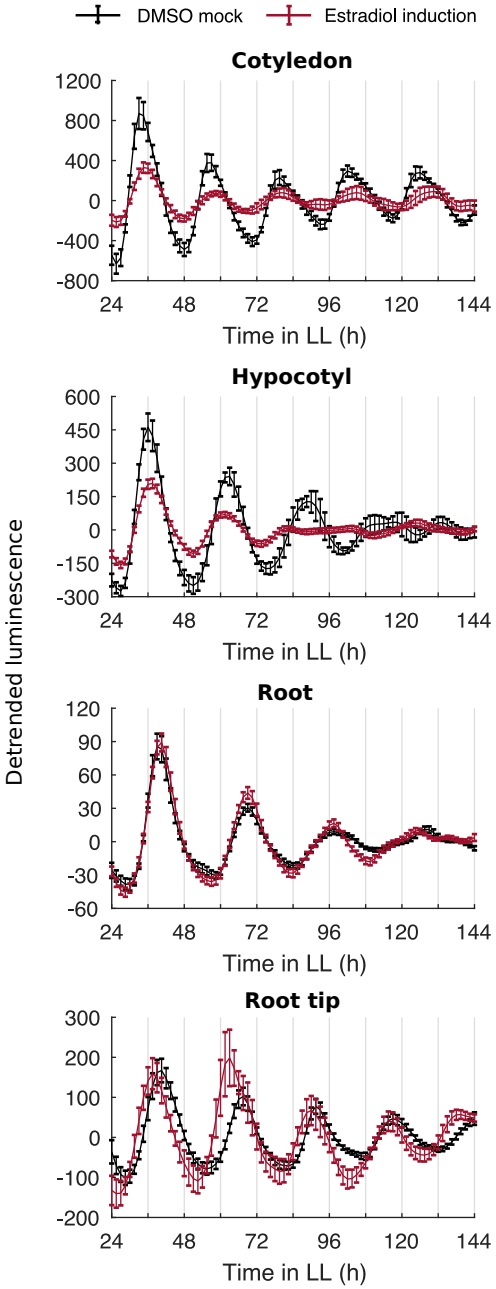

Fig. 3.10 Local plasmodesmata mobile signals signals influence rhythms in the cotyledon and hypocotyl. Expression of *GI*::*LUC* from different organs during induction of the callose biosynthesis (*G1090*::*icals3m*). Data represent the mean ± standard error of tracked organs. $N = 3$, $n = 14$–15. N represents the number of independent experiments and n the total number of organs tracked.

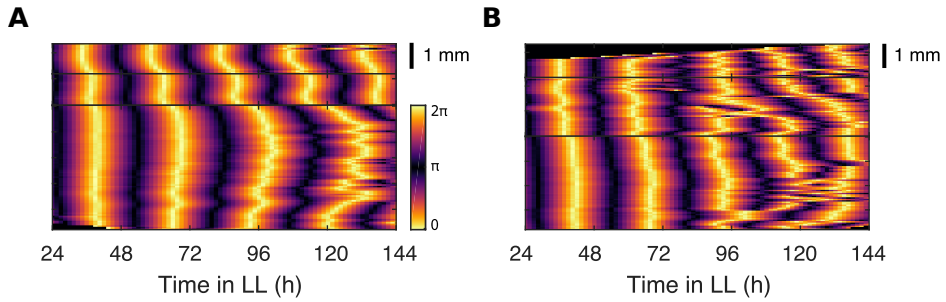

Fig. 3.11 Local plasmodesmata mobile signals influence spatial waves of clock gene expression. (A, B) Representative phase plot of *GI*::*LUC* expression across longitudinal sections of the cotyledon (top), hypocotyl (middle), and root (bottom) of a single seedling during mock DMSO treatment (A) or estradiol induction of the callose biosynthesis (*G1090*::*icals3m*) (B). Colour maps are as in A. *N* and *n* are as in Figure 3.10. *N* represents the number of independent experiments and *n* the total number of organs tracked.

the mean periods that we observed experimentally in each region under LL (Figure 3.12A, Figure 2.5, subsection 2.5.1). These period estimates were made from in vivo experiments and therefore include the effects of coupling. They are, however, as good an estimation of the cell autonomous periods as possible in a physiologically relevant context.

3.5.2 Spatial waves of clock gene expression propagate within and between organs in simulations under LL

In our LD-to-LL simulations, because of the differences in intrinsic periods we saw increasing phase shifts between organs under LL (Figure 3.12C). The size of the phase shifts matched those observed in experiments, demonstrating that the loss of synchrony is caused by period differences between regions. At the sub-tissue level, due to the presence of coupling, two increasingly large waves propagated up and down the root (Figure 3.12E). These waves were visually similar to those observed in experiments under LD-to-LL condition (Figure 3.12G), suggesting they are driven by cell-to-cell coupling.

3.5.3 Spatial waves emerge under a range of realistic coupling strengths

In our model, we arbitrarily set the strength of coupling, K, to equal 1. It is not possible to directly measure coupling strength in experiments, and inferences from data in *Arabidopsis* vary depending on the organ analysed and methods [4, 139, 142, 141]. We therefore simulated our model for a range of K, to test how realistic the emergence of spatial waves is in a biological context. We observed spatial waves of clock gene expression in simulations under

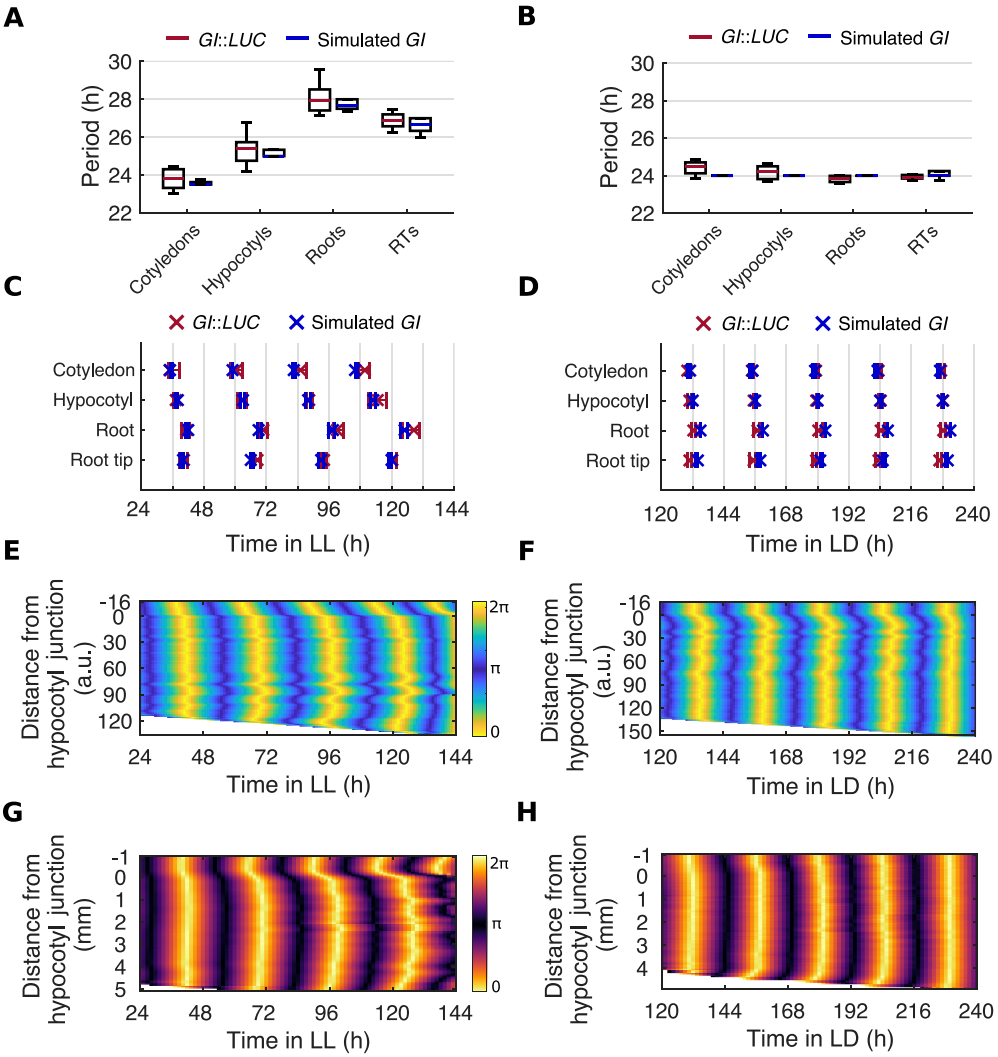

Fig. 3.12 Period differences and local coupling can explain spatial waves of clock gene expression. (A, B) Period estimates of *GI*::*LUC* and simulated *GI* for different organs imaged under LD-to-LL (A) and LD-to-LD (B) conditions. Box plots indicate the median and upper and lower quartiles, and whiskers the 9th and 91st percentiles of organs scored as rhythmic. (C, D) Times of peaks of expression of *GI*::*LUC* and simulated *GI* in different organs under LD-to-LL (C) or LD-to-LD (D) conditions. Plots represent the 25th percentile, median, and the 75th percentile for the peak times of the oscillations of organs scored as rhythmic. (E, F) Representative phase plot of simulated *GI* expression across longitudinal sections of the hypocotyl and root of a single seedling under LD-to-LL (E) or LD-to-LD (F) conditions. Colour maps are as in E. (G, H). Representative phase plot of *GI*::*LUC* expression across longitudinal sections of the hypocotyl and root of a single seedling under LD-to-LL (G) and LD-to-LD (H) conditions. Colour maps are as in G. For experimental data, N and n are as in Figure 3.1. For *GI* simulations, $n = 24$. N represents the number of independent experiments and n the total number of organs tracked.

a range of K (Figure 3.13). Our simulations show that, given the presence of coupling, the emergence of spatial waves is likely under a range of coupling strengths.

3.5.4 Increased coupling strength decreases the variation in period and phase

Coupling is known to decrease the variation in period and phases of connected oscillators [20]. Indeed in our simulations, as the coupling strength was increased, the distribution of periods (Figure 3.14) and phases (Figure 3.15) of the oscillations within a template of a single seedling became tighter. We therefore reasoned that the distribution of periods and phases may be a good indicator of the strength of coupling [188].

To take advantage of this correlation, we analysed the periods and phases from individual pixels within single seedlings of our *GI*::*LUC* data set, and compared the distributions to the simulations. This allowed us to estimate the strength of coupling within seedlings. The distribution of periods within a single seedling approximated the shape of simulations with, but not without, coupling (Figure 3.16A). The distribution had a standard deviation of 1.56, most closely matching simulations with $K = 1$.

We next analysed the phases within single seedlings. The distribution of the phases of *GI*::*LUC* expression was multimodal, approximating the shape of simulations with K greater than 0.4. (Figure 3.16B). Further numerical comparison by means of the standard deviation was not possible due to the complex shapes of the phase distributions. However, alternative statistical methods may improve estimates. Considering both the comparison of period and phase distributions, we estimate the coupling strength, K, to be within the range of 0.4–2 for this modelling framework.

3.5.5 Phase differences between organs under LD can arise due to a mismatch between the clock and the LD cycle

To simulate LD entrainment, we adjust the phase of each oscillator with an entraining cycle. The amount that each oscillator phase is shifted is set by the mismatch of its intrinsic period and the period of this entraining rhythm [14, 186, 187]. This prediction is supported by experimental evidence in various organisms, including plants [189], although dawn can also reset the phase of some clock genes in bulk *Arabidopsis* experiments [190, 12]. We tested whether the phase differences that we observed between organs in *Arabidopsis* under our LD conditions can be reproduced in our model by this mismatch with the entraining rhythm. In our simulations, organs were forced to oscillate with a period of approximately 24 h, due

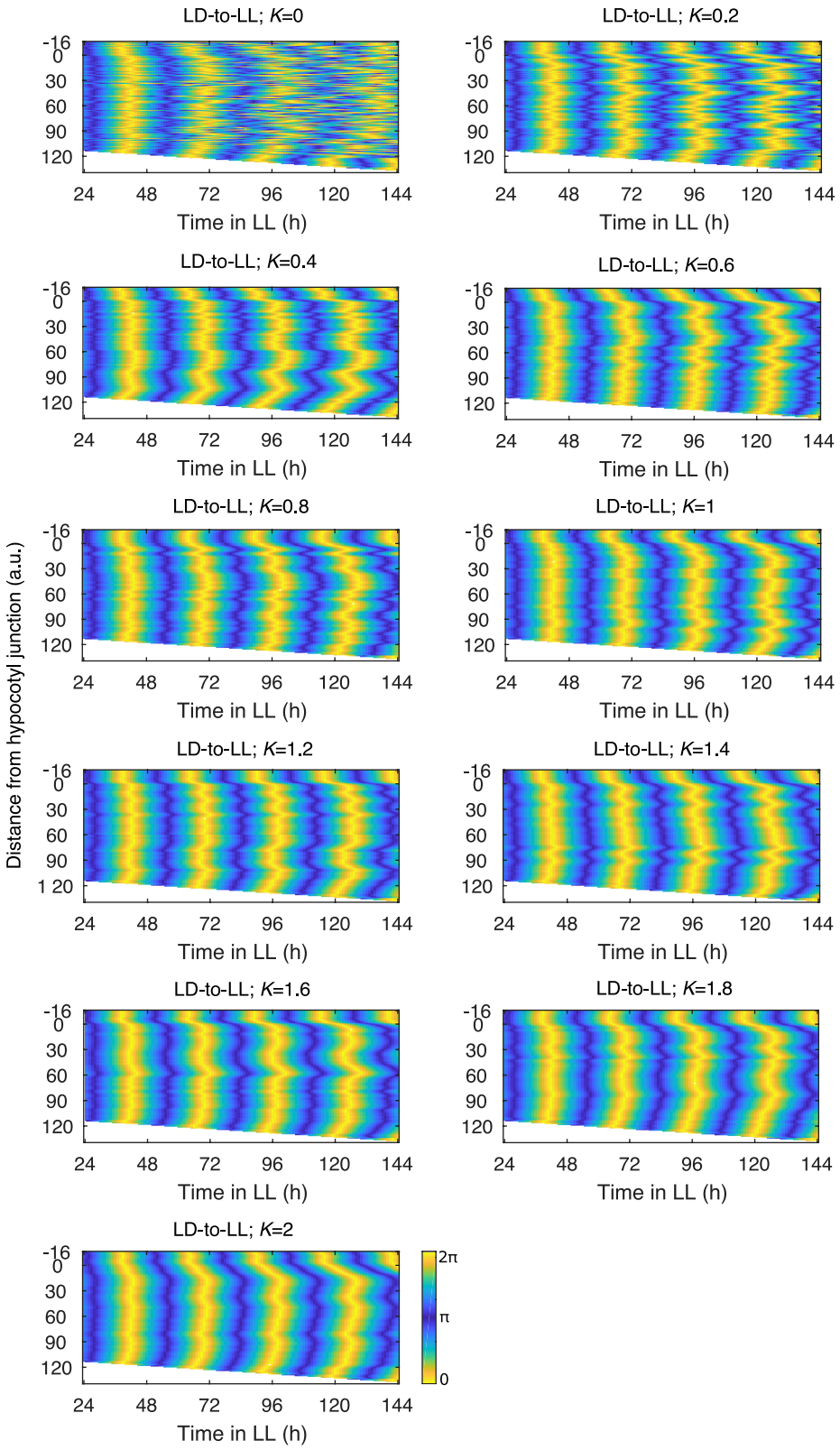

Fig. 3.13 Phase plots for LD-to-LL simulations with increasing strengths of coupling. Phase plots of simulated *GI* expression across longitudinal sections of the hypocotyl and root. Each phase plot is a simulation of a single seedling, each with a different strength of coupling (K).

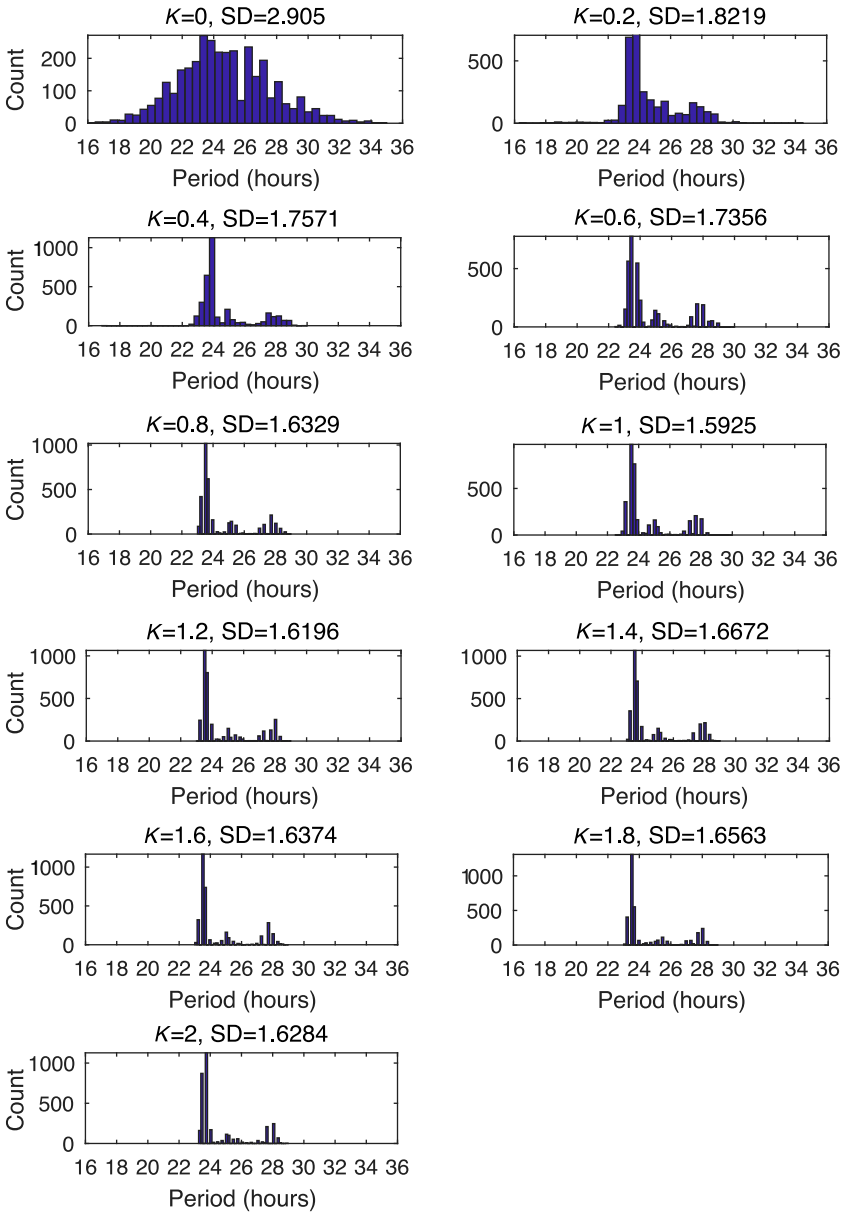

Fig. 3.14 The distribution of periods within a single seedling for simulations of the LD-to-LL condition with increasing strengths of coupling. The distribution of periods of simulated *GI* from individual pixels on the model template of a seedling is shown. Each plot shows the distribution for the simulation of a single seedling under the LD-to-LL condition with different strengths of coupling (K).

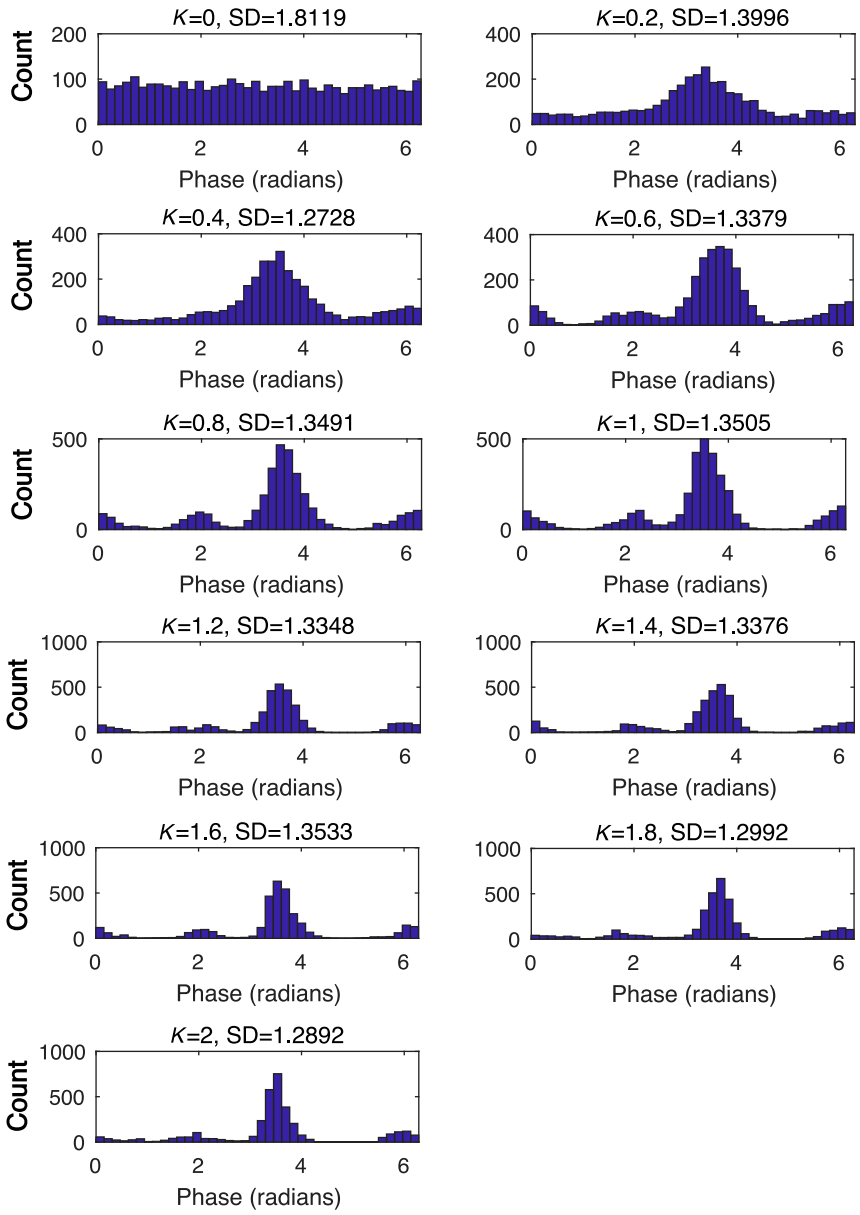

Fig. 3.15 The distribution of phases within a single seedling for simulations of the LD-to-LL condition with increasing strengths of coupling. The distribution of phases of simulated *GI* from individual pixels on the model template of a seedling is shown. Each plot shows the distribution for the simulation of a single seedling under the LD-to-LL condition with different strengths of coupling (K).

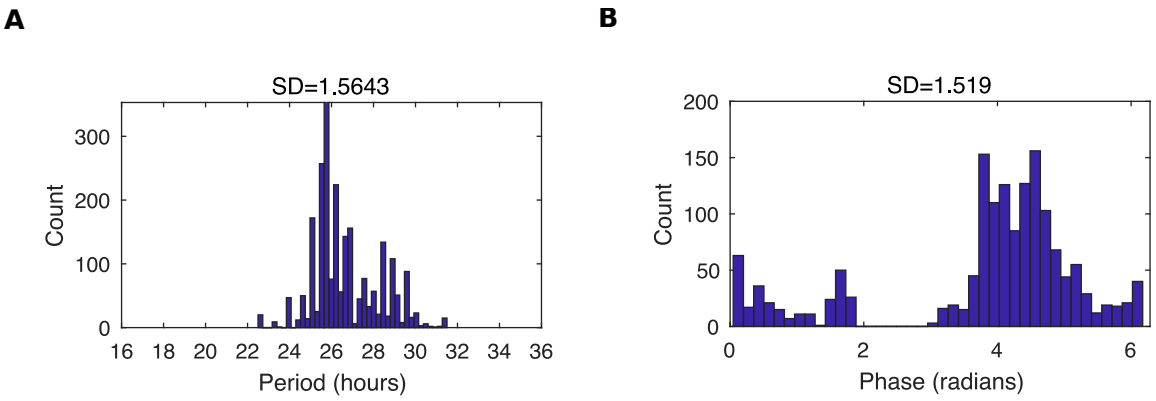

Fig. 3.16 The distribution of periods within a single seedling for *GI*::*LUC* expression under LD-to-LL condition. (A, B) The distribution of periods (A) and phases (B) within a single representative seedling expressing *GI*::*LUC*.

to entrainment to the external rhythm (Figure 3.12B). However, because of the mismatch between the intrinsic period and the entraining rhythm, organs entrained with different phases, matching those observed experimentally (Figure 3.12D).

3.5.6 Spatial waves of clock gene expression propagate within and between organs in simulations under LD

We next tested whether the presence of cell-to-cell coupling is sufficient to drive spatial waves, even when clocks are under LD cycles. Although small, phase shifts could be observed at the sub-tissue level; two short waves could be observed in the root (Figure 3.12F), as in experiments (Figure 3.12H). Unlike under LL, waves did not appear to increase with time, because the observed periods in organs were all close to 24 h due to entrainment to the LD cycle (Figure 3.12B). Nonetheless, our results show that even under LD cycles the underlying period differences, and coupling, are together sufficient to drive spatial waves of clock gene expression.

3.6 Local coupling limits de-synchrony

3.6.1 Simulations in the absence of entrainment

In a set of coupled oscillators, variation in period causes a decrease in synchrony, whereas coupling and external entrainment maintain or increase synchrony [20, 191, 192, 183]. In order to make predictions about the presence of local coupling in seedlings, we simulated our model in the absence of LD entrainment. We simulated the duration of the experiment

without entraining the oscillators, and thus assume that the phases are initially random (LL-to-LL; Figure 3.17A and subsection 2.5.1).

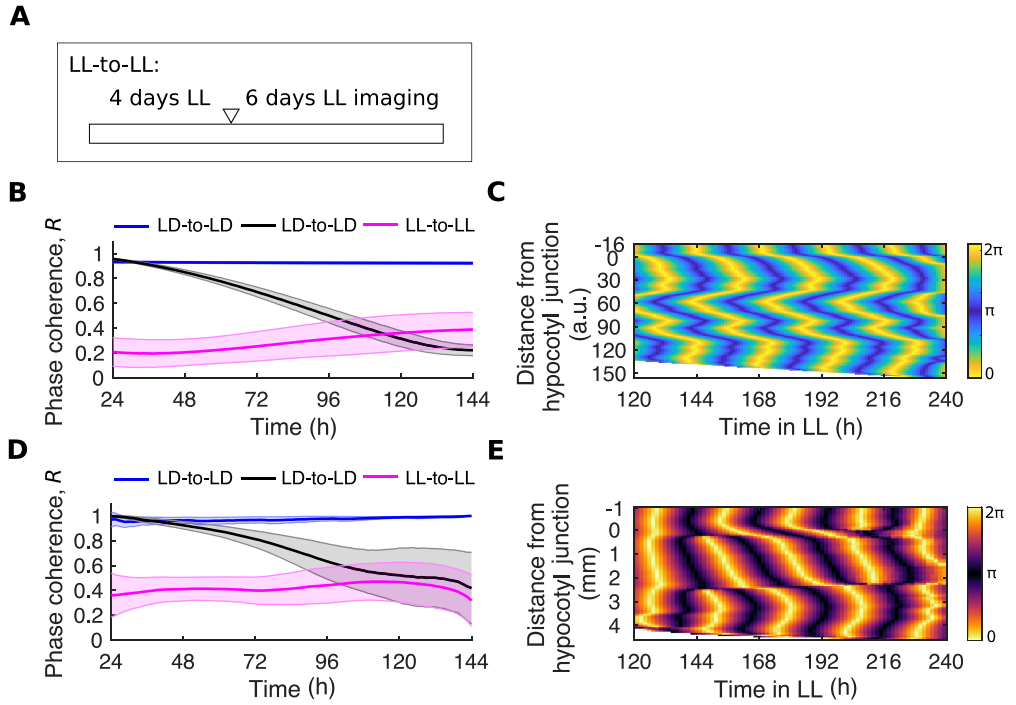

Fig. 3.17 Local coupling limits desynchrony in the absence of LD cycles. (A) Schematic depicting the experimental conditions used. Seedlings were grown for 4 d under LL and then imaged, also under LL (LL-to-LL), so that seedlings have never seen an LD cycle. The white triangle represents the beginning of imaging. (B) Quantification of phase coherence by time evolution of the Kuramoto order parameter, R, for simulated *GI* expression. Solid lines indicate the mean and the shaded region one standard deviation of the mean. (C) Representative phase plot of simulated *GI* expression across longitudinal sections of the hypocotyl and root of a single seedling under the LL-to-LL condition. (D) Quantification of phase coherence by time evolution of the Kuramoto order parameter, R, for *GI*::*LUC* expression. Solid lines indicate the mean and the shaded region one standard deviation of the mean. (E) Representative phase plot of *GI*::*LUC* expression across longitudinal sections of the hypocotyl and root of a single seedling under the LL-to-LL condition. For LL-to-LL *GI*::*LUC* data, $N = 3$ and $n = 30$; for *GI* model simulations, $n = 24$. N represents the number of independent experiments and n the total number of organs tracked.

3.6.2 A degree of synchrony is maintained in the absence of entrainment

We compared the phases of the pixels within seedlings to estimate the overall synchrony of the oscillators over time. We compared the order parameter between entrainment conditions

(LD-to-LD, LD-to-LL, and LL-to-LL) for simulation and experiment. An order parameter [183], *R*, value of 1 indicates a set of completely synchronised oscillators and a value of 0 a set of completely desynchronised oscillators.

Under LD-to-LD condition, we observed a high degree of synchrony over the entire experiment, in simulation (Figure 3.17B) and experiment (Figure 3.17D), due to entrainment to the LD cycle. In contrast, under the LD-to-LL condition oscillators desynchronised upon transition to LL. However, they did not completely desynchronise during the time-course. A similar rate of desynchronisation was observed between simulation (Figure 3.17B) and experiment (Figure 3.17D).

In LL-to-LL simulations, phases were set to be initially random (subsection 2.5.1). In theory, we would expect order parameter values close to 0 in the absence of any synchronising force. In LL-to-LL simulations, oscillators began less synchronous than under the other entrainment conditions, however, *R* values were substantially above 0 (Figure 3.17B). Further, oscillators maintained their order, not further desynchronising during the time course. These simulations suggest that local cell-to-cell coupling is sufficient to maintain a degree of synchrony across the seedling in the absence of entrainment.

3.6.3 Simulations in the absence of entrainment predict complex spatial phase patterns

We next analysed the LL-to-LL simulations at the sub-tissue to observe the spatial coordination. Interestingly, in the root, the model predicted a complex spatial pattern, with multiple phase clusters and spatial waves in a single seedling (Figure 3.17C and S4 Video, available from https://gitlab.com/slcu/teamJL/greenwood_etal_2019). These patterns of gene expression were similar to the zigzag patterns previously reported by others, when roots are grown on sucrose supplemented media [141, 147, 193]. We found that these zigzag patterns emerged with, but not without, local coupling (Figure 3.19). We note that in the LL-to-LL model, setting the phases to be in phase or close to in phase (e.g., approximately 11 h after the first measurement ±2 h [standard deviation]), we could not obtain the results seen. Thus, both coupling, and a high degree of phase disorder are required for the emergence of zig-zag patterns.

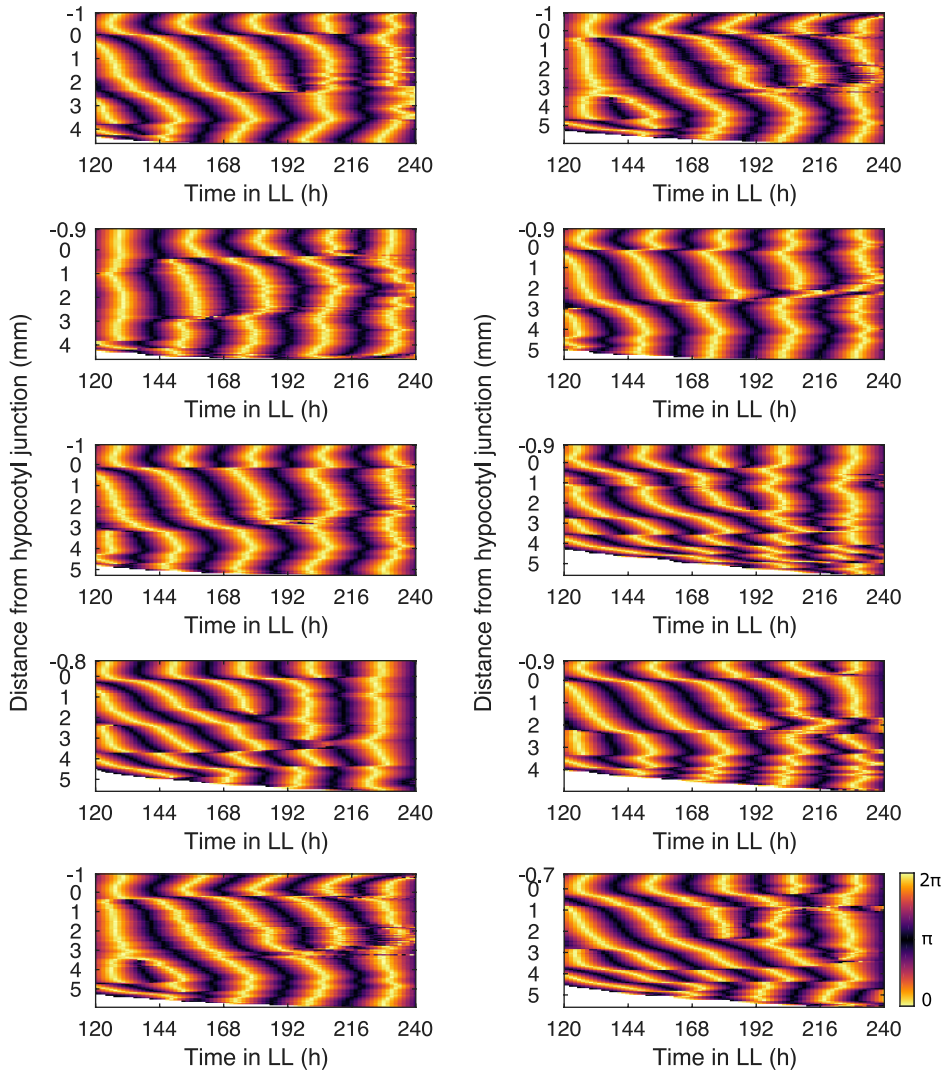

Fig. 3.18 Representative phase plots for the LL-to-LL condition. Phase plots of *GI*::*LUC* expression across longitudinal sections of the hypocotyl and root. Each phase plot is of a single seedling that is representative for the LL-to-LL condition. *N* and *n* are as presented in Figure 3.17. *N* represents the number of independent experiments and *n* the total number of organs tracked.

3.6.4 An alternative model without coupling fails to capture spatial patterns observed under the LL-to-LL condition

An alternative mechanism to explain the spatial patterns of rhythms that we observed can also be envisaged. If, within the tissue, there exists a gradient in the periods of oscillators, spatial waves may be seen in the absence of cellular coupling. Simulations of this plausible alternative model, without coupling but with a gradient of the intrinsic periods within the root, were indeed sufficient to generate simple waves similar to those we observed under the LD-to-LL condition (Figure 3.19C and D), but not the complex zigzag waves predicted in the LL-to-LL condition (Figure 3.19E and Figure 3.19F).

3.6.5 Testing the LL-to-LL prediction in experiments without entrainment

In order to test our model and validate the assumption of local coupling, we experimentally tested the LL-to-LL model prediction. We both grew and imaged seedlings under LL conditions (LL-to-LL; Figure 3.17A). Under this condition, seedlings do not see an entrainment cue beyond the synchronisation that occurs at germination [194, 195]. Given the small number of cells that exist at germination we do not expect it to have a significant effect on overall synchrony by the beginning of imaging. Seedlings maintained their coherence over the full time course (Figure 3.17D), as predicted from simulations with cell-to-cell coupling (Figure 3.17B). Within the root we observed a zigzag expression pattern (Figure 3.17E) and Figure 3.18), also as predicted by the model. This close match between experiment and model supports the hypothesis of weak, local coupling between clocks in seedlings.

3.7 Conclusions and discussion

In this chapter, we report how local period differences and coupling can generate spatial waves of circadian clock gene expression across the plant. Using time-lapse imaging we show that phase differences between organs, and spatial waves, exist both in constant and entrained conditions and do not require long-distance signals. Modelling and experiments show that local coupling with period differences can explain our results, including complex synchronisation patterns in plants that have never seen an entraining signal.

In the wild, plants are exposed to environmental cycles, and the interaction between the oscillator and the environment is of importance. It is therefore significant that we observed phase differences between clocks within a plant, both under LL and LD cycles (Figure 3.1).

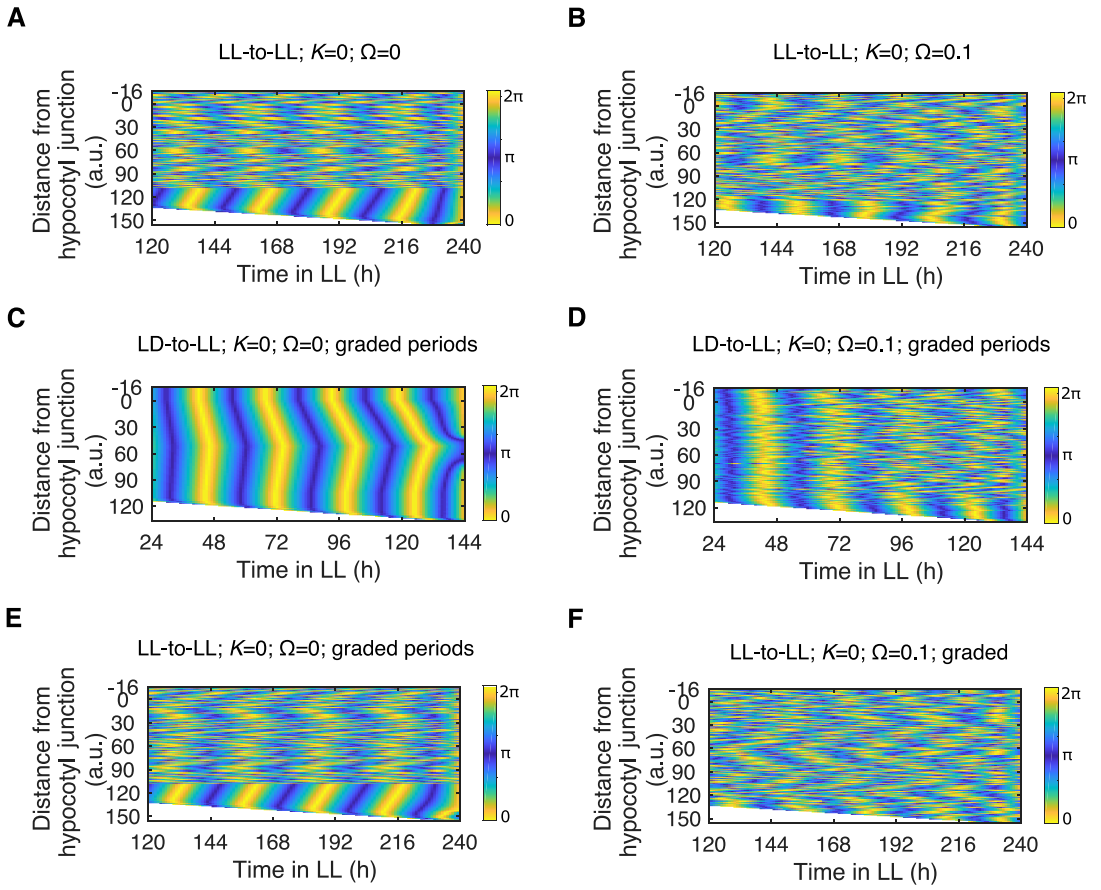

Fig. 3.19 Phase plots for alternative model simulations with different spatial structure of periods. (A, B) Phase plot of simulated *GI* expression across longitudinal sections of the hypocotyl and root of a single seedling for the LL-to-LL condition in the absence of coupling ($K = 0$), but with period differences. In A, periods of the pixels in each tissue are set to the mean periods measured in the LD-to-LL experimental data, without noise ($\omega = 0$). In B, a representative set of periods for each region are shown, as drawn from the period distributions described in subsection 2.5.4 ($\omega = 0.1$). (C, D) Phase plot of simulated *GI* expression across longitudinal sections of the hypocotyl and root of a single seedling for the LD-to-LL condition in the absence of coupling ($K = 0$). In C, periods in the root region are graded with a maximum period in the middle of the root, without noise ($\omega = 0$). In D, periods are also graded in the root, but periods are drawn from a distribution ($\omega = 0.1$). See subsection 2.5.4 for details. (E, F) Phase plot of simulated *GI* expression across longitudinal sections of the hypocotyl and root of a single seedling for the LL-to-LL condition in the absence of coupling ($K = 0$). In E, periods in the root region are graded with a maximum period in the middle of the root, without noise ($\omega = 0$). In F, periods are also graded in the root, but periods are drawn from a distribution ($\omega = 0.1$). See subsection 2.5.4 for details.

A previous high-resolution study in *Arabidopsis* observed phase differences within leaves after the transfer from LL to LD conditions, although rhythms were near synchronous after 3 d in LD cycles [139]. Phase differences have also been observed in *Lemna gibba* fronds, where cells in leaves entrain with different phases, causing a centrifugal pattern [121]. Phase differences under LD cycles may therefore be a common property of plant circadian systems, and will require further investigation.

A second key finding of this chapter was the observation of spatial waves of clock gene expression travelling within and between all major organs of the seedling (Figure 3.5). Interesting parallels can be made with the mammalian SCN, where spatial-temporal wave patterns are driven by intercellular coupling [188, 196–198]. In the SCN, recent studies have revealed that the mammalian spatial structure is changeable, and lacks a fixed hierarchy. For example, as the day length changes, coupling between cells is altered, and the spatial structure adapts [199, 200]. In future, it will be interesting to investigate whether the plant circadian system shares similar features.

The presence of local cell-to-cell coupling has been previously suggested to help maintain clock synchrony within *Arabidopsis* [4, 139–141, 121, 142]. In addition, long-distance signals [142, 129] and light piped from the shoot [143] have been proposed as mechanisms for coordination. Through a combination of experiments and modelling, we show that in seedlings, local signals alone are sufficient to maintain robust rhythms after 6 d in all organs, as well as generate the observed complex spatial patterns in clock gene expression. We note that our results do not exclude the possibility that phloem mobile signals, or light piped from the stem, additionally act to synchronise the root with the shoot. However, the waves that we observed in cut roots suggest that these signals do not drive the spatial wave patterns that we observe. In future work, it will be important to investigate whether coordination through local coupling also occurs in later stages of plant development and, if so, whether the coordination structure changes as the plant develops to compensate for its increasing size. Intuitively, it could be predicted that an increase in the points of coordination would allow the mechanism to scale.

Finally, we began to probe the mechanisms of local cell-to-cell coupling, revealing that the mobile signal may move through plasmodesmata. Partially restricting plasmodesmata transport using the *cals3m* system incompletely disrupted organ-level rhythms and spatial waves (Figure 3.10 and Figure 3.11). However, the effect on rhythms was organ conditional, likely due to the variation in the induction of callose between cells and regions that we observed (Figure 3.9). We hypothesise that this variation in callose induction is caused by the spatial expression pattern of the *G1090* promoter used in our inducible construct. Although we intended the promoter to be expressed ubiquitously, thereby inducing callose deposition

ubiquitously, spatial variation in the strength of the promoters expression was observed. In particular, our collaborators observed expression of the *G1090* promoter to be weakest in the middle region of the root (Matthieu Bourdon, personal communication), where we observed minimal effect on rhythms (Figure 3.10). The redesign of the construct represents a future direction for our work, as experiments such as these will be important for understanding the transport mechanisms behind the local cell-to-cell coupling.

Beyond the future directions for the investigation of cell-to-cell coupling that we discuss here, our results raise an important question not addressed in this chapter: what causes the period differences across the seedling? It is this question that we address in Chapter 4.

Acknowledgements / disclosures

The model was formulated by Mirela Domijan (University of Liverpool) and simulations performed by MG. Callose staining and associated confocal imaging (Figure 3.9) was completed by MG and Matthieu Bourdon (University of Cambridge). The results of this chapter are published as part of Greenwood et al., 2019 [1] and Gould et al., 2018 [4].

Chapter 4

Local inputs to the *Arabidopsis* circadian clock

In Chapter 3 we found a simple model with period differences and local coupling can generate spatial waves, matching our experimental data. Here, we attempted to test the model by manipulating the periods in specific organs and modulate the spatial waves of gene expression. In the most severe case, removing all period differences across the plant should result in perfectly coherent rhythms. We tested this with chemical and genetic perturbations, and in doing so demonstrated that the periods across the plant are set locally by the environmental inputs.

4.1 Core clock network mutations effect the robustness of oscillations but not the specificity of periods

The specificity of periods across the plant could be due to the clock network being wired differently in different parts, or that the sensitivity of the clock to environmental inputs varies across the plant. We tested the former hypothesis by imaging rhythms of *GI*::*LUC* from different organs in seedlings carrying mutations to the core clock network. We found in organs scored as rhythmic, mutations to the clock network either lengthened or shortened periods depending on the gene (Figure 4.1A). These period effects matched reports from previous whole plant experimental assays [92, 201, 88, 202, 41]. However, we observed that the change in period length in each region of the seedling was approximately equal (Figure 4.1A), and thus the specificity of periods was not altered. We note that we cannot rule out that mutations to other clock components could have a larger effect on the organ specificity of periods.

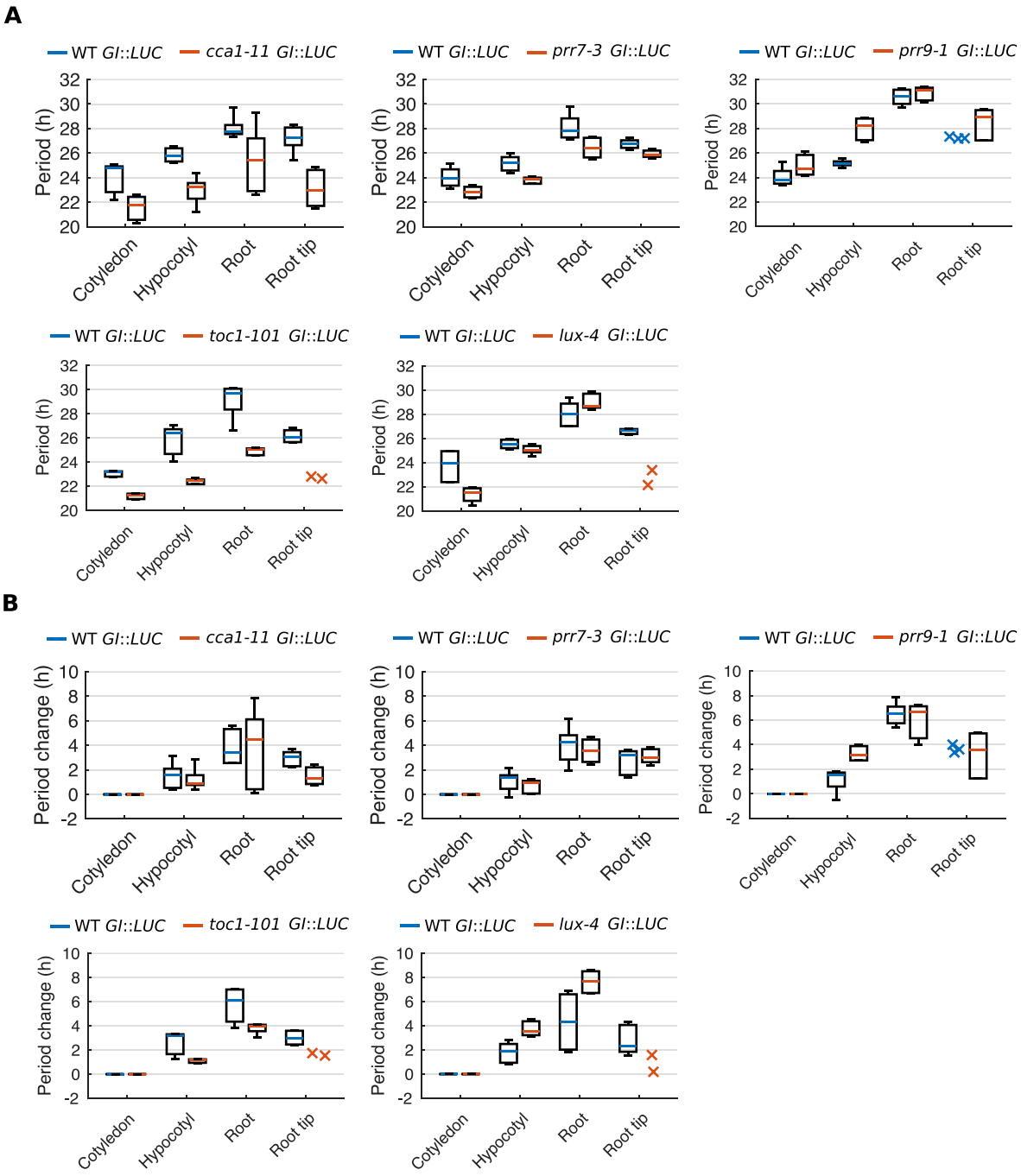

Fig. 4.1 Core clock network mutations effect the period of different regions proportionately. (A) Period estimates for *GI*::*LUC* expression from different organs imaged under the LD-to-LL condition in circadian mutant lines. (B) Period change relative to the cotyledon for *GI*::*LUC* expression from different organs imaged under the LD-to-LL condition in circadian mutant lines. For *cca1-11*, $N = 4$; *prr7-3*, $N = 4$; *prr9-1*, $N = 2$; *toc1-101*, $N = 2$; *lux-4*, $N = 2$. For all, $n = 5$–18. N represents the number of independent experiments and n the total number of organs tracked. Box plots indicate the median and upper and lower quartiles, and whiskers the 9th and 91st percentiles of organs scored as rhythmic. Individual data points are shown when the number of rhythmic plants is less than five. Horizontal position of scatter points is for clarity and has no meaning.

We did, however, observe some organ-specific effects on rhythmicity (Table 4.1). We observed that some mutations caused a decrease in the proportion of organs scored as rhythmic. This effect was larger in some organs than others. For example less than half of rhythms from the root tip were scored as rhythmic in *toc1-101* and *lux-4* lines. Our results suggest that mutations to the clock network effect the robustness rather than the periods organ specifically.

Table 4.1 Core clock network mutations effects rhythmicity region-conditionally

Organ	*CCA1*		*PRR7*		*PRR9*		*TOC1*		*LUX*	
	WT	*cca1-11*	WT	*prr7-3*	WT	*prr9-1*	WT	*toc1-101*	WT	*lux-4*
Cotyledon	91	100	100	89	100	100	80	88	100	62
Hypocotyl	100	94	100	67	100	100	90	100	100	85
Root	100	56	100	100	100	100	90	75	100	69
Root tip	100	94	100	100	60	86	100	25	100	15

Note: Values indicate the percentage of tracked organs classed as rhythmic.

4.2 Local light inputs set organ-specific periods

4.2.1 Organ-specific periods are altered under constant darkness

Next, we tested whether we could alter periods in an organ-specific manner by modulating inputs to the clock. We first tested the effect of light input by growing seedlings under LD cycles before imaging seedlings under constant darkness (DD). Under DD, we observed a drastic slowing of periods in the cotyledon and hypocotyl, whereas the middle region of the root maintained its speed compared with LL (Figure 4.2A). This is in contrast to previous lower-resolution work that found the period of the root as a whole increased under DD [111, 143]. The lengthening of periods in the aerial organs reduced the phase differences between the aerial organs and the root (Figure 4.2B and Figure 4.3). As predicted by the modelling (chapter 3), a change in periods resulted in modulation of the spatial waves. The spatial waves travelling from the hypocotyl down the root were lost (Figure 4.2C and S5 Video, available from https://gitlab.com/slcu/teamJL/greenwood_etal_2019). Inversely, in the root tip we observed a decrease in period compared with LL (Figure 4.2A), causing larger phase shifts between the root tip and the root (Figure 4.2B and Figure 4.3) and resulting in longer spatial waves travelling from the root tip upwards into the root (Figure 4.2C and S5 Video, available from https://gitlab.com/slcu/teamJL/greenwood_etal_2019).

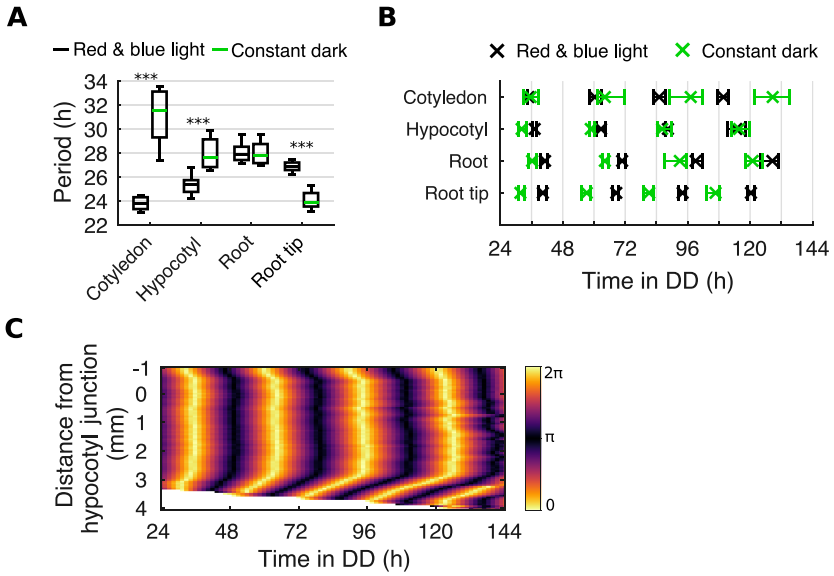

Fig. 4.2 Local light inputs modulate the spatial coordination of the clock. (A) Period estimates for different organs under constant red and blue light or DD. ***$p < 0.001$, by two-tailed t test, Welch correction. (B) Times of peaks of *GI*::*LUC* expression in different organs under constant red and blue light or DD. Plots represent the 25th percentile, median, and the 75th percentile for the peak times of organs scored as rhythmic. (C) Representative phase plot of *GI*::*LUC* expression across longitudinal sections of the hypocotyl and root of a single seedling under DD. For red and blue light data, N and n are as presented in Figure 3.1. For DD, $N = 3$, $n = 26$–31. N represents the number of independent experiments and n the total number of seedlings. Box plots indicate the median and upper and lower quartiles, and whiskers the 9th and 91st percentiles of organs scored as rhythmic.

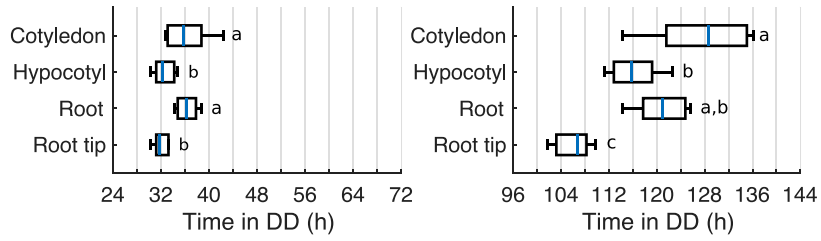

Fig. 4.3 Phase shifts between aerial organs and the root are reduced under DD. Times of peaks of *GI*::*LUC* expression in different organs during the first (left) and final (right) observed oscillations under DD. Means are statistically different ($p < 0.05$, one-way ANOVA, Tukey post hoc tests) if they do not have a letter in common. N and n are as presented in Figure 4.2. N represents the number of independent experiments and n the total number of organs tracked. Box plots indicate the median and upper and lower quartiles, and whiskers the 9th and 91st percentiles of organs scored as rhythmic.

4.2.2 Direct entrainment of the root to light does not set periods under DD

The altered periods under DD suggests that light sets the periods differently in individual organs. Of particular interest is the root tip, which runs faster under DD (Figure 4.2). This is in contrast to the other organs, and previous reports at the whole-plant level, where periods lengthened [60, 203, 111, 143]. However, in our experiments the roots are grown under light before imaging under DD, and the observed fast periods in the root tip could potentially be an after-effect or artefact of this exposure to light. To test this possibility, we grew seedlings in an optimised growth system so that the roots were not exposed to light during entrainment, and then imaged under DD as before (Figure 4.4A and subsection 2.1.2) [170]. We observed similar periods in all organs under DD whether roots were exposed to light or not during growth (Figure 4.4B). The spatial structure under DD is therefore unlikely to be a consequence of prior exposure to light.

4.2.3 The wavelength of light input sets organ-specific periods

It could be hypothesised that the periods are fixed, but have two different states, LL and DD. Alternatively, it could be that the periods are plastic, and influenced by multiple environmental factors. To distinguish between the two we varied the light wavelength under LL, to see if periods are fixed. We imaged rhythms under monochromatic red or blue light and compared rhythms to those imaged under a mixture of red and blue light (Figure 4.5). Under blue light, rhythms in the aerial organs slowed (Figure 4.5A). However, the root tip decreased in speed (Figure 4.5A). These changes in period are qualitatively the same as observed under DD (Figure 4.2), albeit lesser in size. Under red light, the aerial organs also slowed, however a change in the speed of the root tip was less clear (Figure 4.5B). These results show that the periods are plastic to the light properties, rather than being of fixed value under LL. Further, the light input can either increase or decrease the speed, depending on the region.

4.2.4 Red light sets periods locally in a *PHYB* dependent manner

We next tested whether the effect of light on organ specificity is direct, through known light signalling pathways. *PHYB* is the primary red light photoreceptor in *Arabidopsis* (subsection 1.3.2) [204, 205], and has a tissue-specific expression pattern in the plant [69, 70, 66, 19]. Expression is highest in the aerial organs, low in the roots, but increases in the root tip. We therefore reasoned that its period-shortening effect under red light [17] may be organ specific.

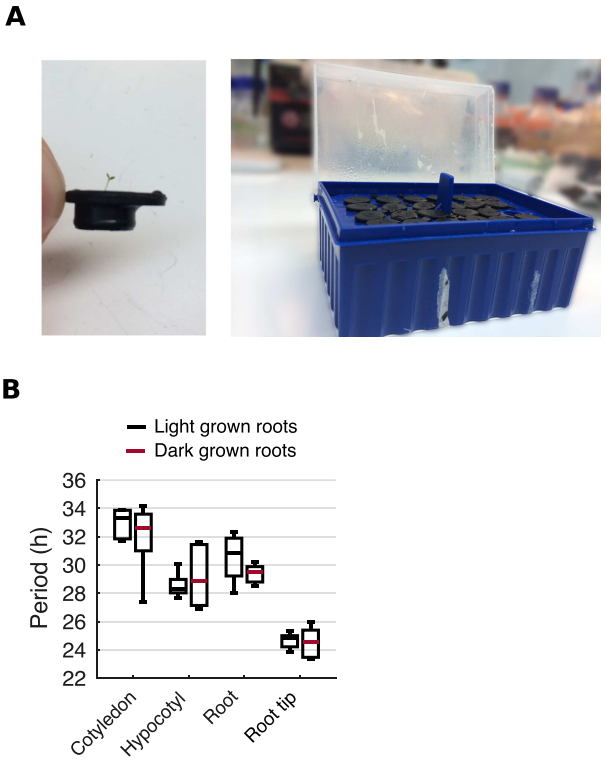

Fig. 4.4 Exposing roots to light during entrainment has minimal effects on circadian dynamics observed during imaging. (A) Seeds are sown on agar-filled black micro-centrifuge tube lids with a piercing in the lid (left), and suspended in MS liquid in a floating micro-centrifuge tube rack (right), as described previously [170]. Seedlings are entrained for 4 d, with the roots either exposed to light or kept in the dark using this system. Seedlings are then imaged under DD. Note that images include a blur selectively on the background in order to highlight these components. (B) Period estimates of *GI*::*LUC* expression for the different organs when roots are exposed to light during entrainment or when kept in the dark. All comparisons between period estimates are not significant, $p < 0.05$, by two-tailed t test, Welch correction. Box plots indicate the median and upper and lower quartiles, and whiskers the 9th and 91st percentiles of organs scored as rhythmic. $N = 3$; $n = 14–15$. N represents the number of independent experiments and n the total number of organs tracked.

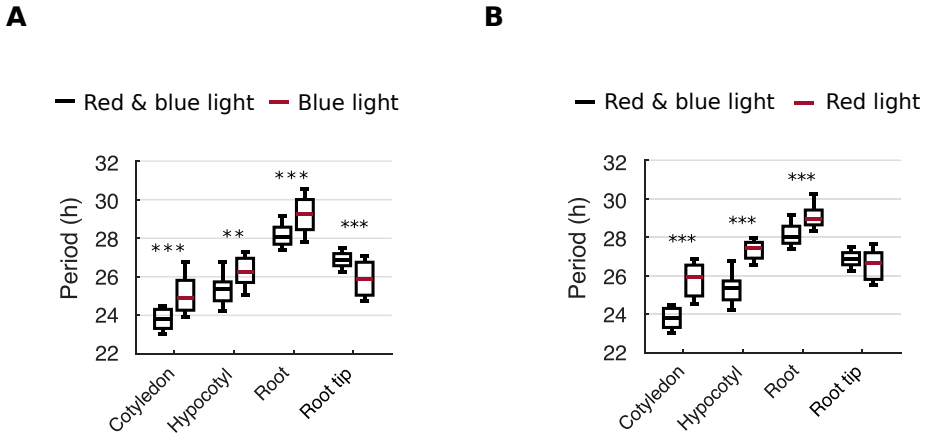

Fig. 4.5 The wavelength of light influences the clock in an organ-specific manner. (A, B) Period estimates of *GI*::*LUC* expression for different organs under constant red and blue light, plotted against blue-light-only (A) or red-light-only data (B). ***$p < 0.001$, two-tailed *t* test, Welch correction. Box plots indicate the median and upper and lower quartiles, and whiskers the 9th and 91st percentiles of organs scored as rhythmic. For constant blue light, $N = 2$; constant red light, $N = 2$. For both, $n = 22$–25. N represents the number of independent experiments and n the total number of organs tracked.

We imaged *GI*::*LUC* expression in the *phyb-9* background, a null mutant for *PHYB* [204, 205]. Under red light, in the *phyb-9* mutant we observed the loss of period differences between the cotyledon, hypocotyl, and root (Figure 4.6A). This caused the loss of phase shifts between the aerial organs and the root (Figure 4.6B and Figure 4.7) and the loss of distinct spatial waves travelling down the root (Figure 4.6C and and S6 Video, available from https://gitlab.com/slcu/teamJL/greenwood_etal_2019). We also observed a decrease in rhythmicity across the seedling (Table 4.2). The effect was particularly large in the root tip, with only 24% of root tips classed as rhythmic compared with 96% in the WT. In the root tips classed as rhythmic, the period ran approximately 3 h slower, at approximately the same speed as the middle of the root (Figure 4.6A). Therefore, after 6 d under constant red light, the phase shifts between the root tip and root (Figure 4.6B) and (Figure 4.7), and the spatial waves travelling from the root tip upwards, were attenuated (Figure 4.6C and S5 Video, available from https://gitlab.com/slcu/teamJL/greenwood_etal_2019).

4.2.5 *PHYB* does not cause the fast periods in the root tip under DD

The *phyb-9* mutation caused a slowing of periods in all organs under red light (Figure 4.6). However, under DD we observed a shortening of periods in the root tip (Figure 4.2). Since *PHYB* can also influence the amplitude of rhythms in the absence of light [61] we hypoth-

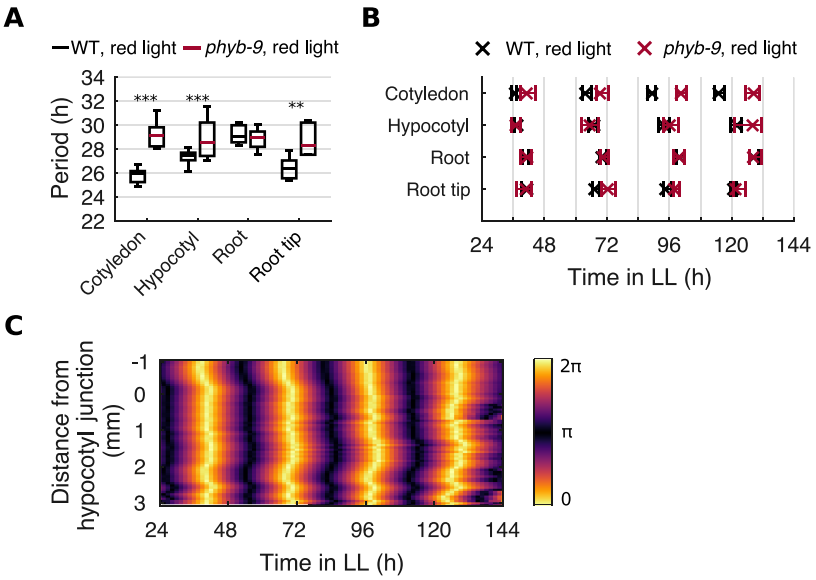

Fig. 4.6 Light input through *PHYB* modulates the spatial coordination of the clock. (A) Period estimates of *GI*::*LUC* for different organs under constant red light in the *phyb-9* mutant. $^{**}p < 0.01$, $^{***}p < 0.001$, by two-tailed t test, Welch correction. (B) Times of peaks of *GI*::*LUC* expression in different organs under constant red light in the *phyb-9* mutant. Plots represent the 25th percentile, median, and the 75th percentile for the peak times of organs scored as rhythmic. (C) Representative phase plot of *GI*::*LUC* expression across longitudinal sections of the hypocotyl and root of a single seedling under constant red light in the *phyb-9* mutant. For *phyb-9* red light, $N = 4$, $n = 23$–35. N represents the number of independent experiments and n the total number of seedlings. Box plots indicate the median and upper and lower quartiles, and whiskers the 9th and 91st percentiles of organs scored as rhythmic.

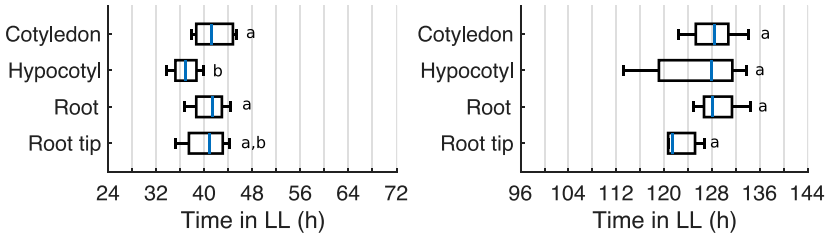

Fig. 4.7 Phase shifts between regions are reduced in the *phyb-9* mutant under red light. Times of peaks of *GI*::*LUC* expression in different organs during the first (left) and final (right) observed oscillations in the *phyb-9* mutant imaged under constant red light. Means are statistically different ($p < 0.05$, one-way ANOVA, Tukey post hoc tests) if they do not have a letter in common. N and n are as presented in Figure 4.6. N represents the number of independent experiments and n the total number of organs tracked. Plots represent the 25th percentile, median, and the 75th percentile for the peak times of organs scored as rhythmic.

Table 4.2 *PHYB* mutations effects the period of rhythms region-conditionally

Organ	WT	*phyb-9*
Cotyledon	100	70
Hypocotyl	96	79
Root	100	77
Root tip	96	24

Note: Values indicate the percentage of tracked organs classed as rhythmic.

esised that *PHYB* caused the fast periods in the root tip under DD. The *phyb-9* mutation, however, did not abolish the faster periods observed in the root tip under DD (Figure 4.8A), and phase difference between the root tip and the middle region of the root persisted (Figure 4.8B). The mechanism driving the fast periods in the root tip under DD therefore appears to be separate from the *PHYB* mediated effect we observed under red light.

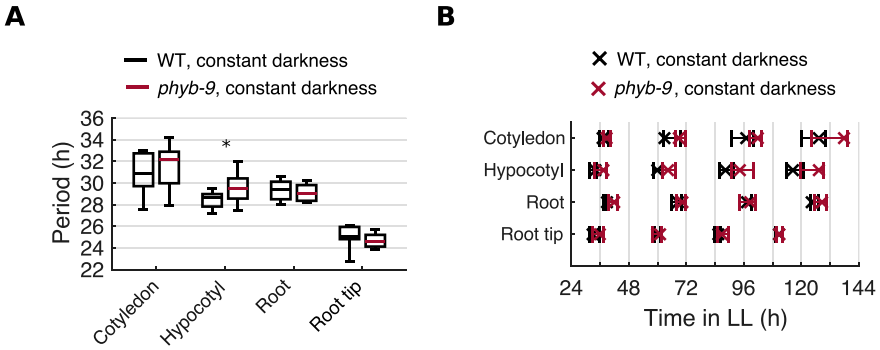

Fig. 4.8 *PHYB* has minimal effect on rhythms under DD. (A) Period estimates of *GI*::*LUC* expression for different organs in the *phyb-9* mutant imaged under DD. $*p < 0.05$, two-tailed *t* test, Welch correction. Box plots indicate the median and upper and lower quartiles, and whiskers the 9th and 91st percentiles of organs scored as rhythmic. (B) Times of peaks of *GI*::*LUC* expression in different organs in the *phyb-9* mutant imaged under DD. For *phyb-9* DD, $N = 2$, $n = 17–18$. *N* represents the number of independent experiments and *n* the total number of organs tracked. Plots represent the 25th percentile, median, and the 75th percentile for the peak times of organs scored as rhythmic.

4.3 Local metabolic inputs set organ-specific periods

4.3.1 Photosynthesis drives fast rhythms in the cotyledon and hypocotyl

In addition to the external environment, the circadian clock is exposed to biochemical signals from within the cell (Table 1.1). Many of these signals are concentrated in particular cells or tissues. For example, the outputs from photosynthesis might be higher in leaves, where they are produced. Using photosynthesis as an example, we investigated whether these endogenous signals could alter periods in an organ-specific manner, modulating the spatial waves of clock gene expression. First, we monitored seedlings under LL in the presence of 3-(3,4-dichlorophenyl)-1,1-dimethylurea (DCMU), a specific inhibitor of photosynthesis. We imaged seedlings on media containing DCMU and maintained low light levels, under which the effects of photosynthesis are clear [92]. During inhibition, we observed a slowing of periods specifically in the cotyledon and hypocotyl (Figure 4.9A), causing a loss of phase shifts between the hypocotyl and root (Figure 4.9B and Figure 4.10) and the loss of spatial waves down the root (Figure 4.9C).

4.3.2 Exogenous sugar drives spatial waves of clock gene expression

Photosynthesis can modulate the clock through the production of sugars, which feed into the oscillator [203, 92, 93]. We next tested whether the application of sucrose to part of the plant could locally reduce clock periods and generate spatial waves. This is a direct test of the hypothesis that local period differences drive spatial waves of gene expression. We designed a protocol that allowed us to rest only the top portion of the root on sugar-supplemented media and observe the effect throughout the root. We did this with roots cut at the hypocotyl junction to minimize developmental effects, and under DD, where we ordinarily observe no spatial waves down the root (Figure 4.2C). In comparison with mannitol (a poorly metabolized sugar that acts as an osmotic control), contact with sucrose-supplemented media caused a larger decrease in period length (Figure 4.11B). This caused larger phase shifts from the top to the middle of the root (Figure 4.11C and Figure 4.12). Within the root, clear spatial waves of clock gene expression propagated down from the top of the root when in contact with the sucrose (Figure 4.13A and S7 Video, available from https://gitlab.com/slcu/teamJL/greenwood_etal_2019) but not mannitol (Figure 4.13B and S8 Video, available from https://gitlab.com/slcu/teamJL/greenwood_etal_2019) supplemented media. Together these results show that altering the speed of clocks locally, either via modulating light perception or the addition of sugars derived from photosynthesis, can drive spatial waves of clock gene expression.

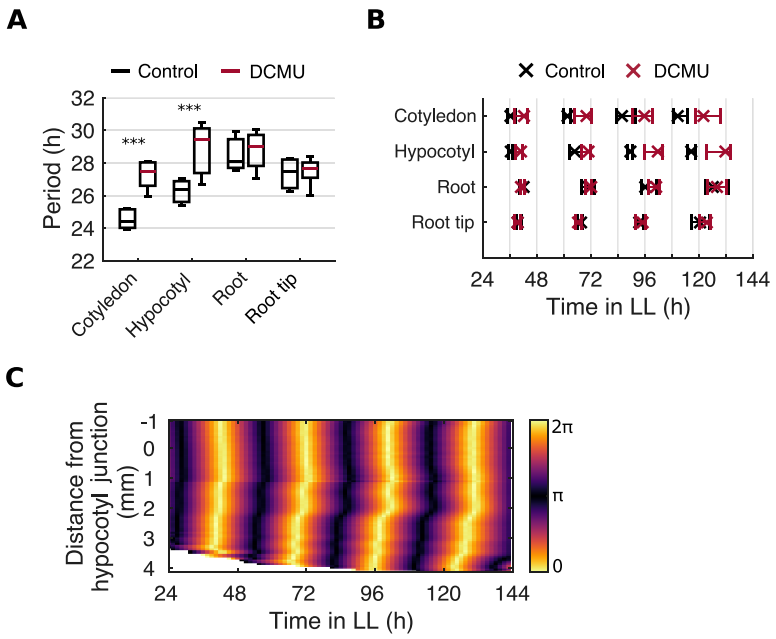

Fig. 4.9 Photosynthesis related signals can drive spatial waves of clock gene expression by altering periods locally. (A) Period estimates of *GI*::*LUC* for different organs during the inhibition of photosynthesis by DCMU. ***$p < 0.001$, by two-tailed t test, Welch correction. (B) Times of peaks of *GI*::*LUC* expression in different organs during the inhibition of photosynthesis by DCMU. Color legend is as in A. Plots represent the 25th percentile, median, and the 75th percentile for the peak times of organs scored as rhythmic. (C) Representative phase plot of *GI*::*LUC* expression across longitudinal sections of the hypocotyl and root of a single seedling during the inhibition of photosynthesis by DCMU. For DCMU, $N = 3$, $n = 14–15$. N represents the number of independent experiments and n the total number of organs tracked. Box plots indicate the median and upper and lower quartiles, and whiskers the 9th and 91st percentiles of organs scored as rhythmic.

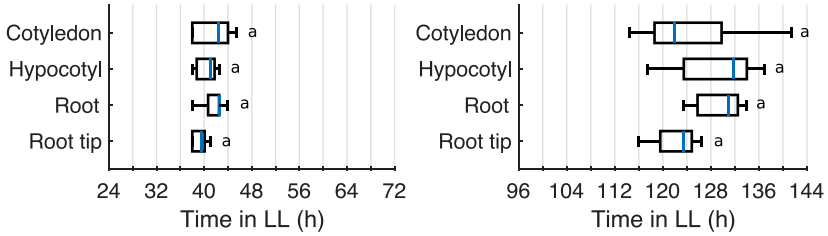

Fig. 4.10 Phase shifts between aerial organs and the root are reduced following the inhibition of photosynthesis by DCMU. Times of peaks of *GI*::*LUC* expression in different organs during the first (left) and final (right) observed oscillations during the inhibition of photosynthesis by DCMU. Means are statistically different ($p < 0.05$, one-way ANOVA, Tukey post hoc tests) if they do not have a letter in common. N and n are as presented in Figure 4.9. N represents the number of independent experiments and n the total number of organs tracked. Box plots indicate the median and upper and lower quartiles, and whiskers the 9th and 91st percentiles of organs scored as rhythmic.

4.4 Conclusions and discussion

In this chapter, we report how exogenous and endogenous environmental inputs set periods across the plant, and drive spatial waves of circadian clock gene expression. We demonstrate this using light and metabolic signals, as well as with genetic perturbations.

It is interesting to note that we observed the *lux-4* mutant to be rhythmic, an apparent contradiction with previous work. Early molecular studies reported null mutants to have arrhythmic whole-plant luciferase and Northern blot rhythms, but a considerable proportion of plants to have rhythmic leaf movements, albeit with lower robustness and more variable periods [41, 206]. Our data shows a higher proportion of plants to be rhythmic than these studies, but still a considerably lower proportion than the WT (Table 4.1). We speculate that the discrepancies between whole-plant, leaf movement, and our higher resolution luciferase assay are due to the differences in resolution. This could suggest a role for *LUX* in the molecular mechanism of cellular coupling, and warrants further investigation.

It is significant that we found the inputs to the clock to have a large effect on the organ-specificity of periods. This supports the recently proposed idea that the plant circadian clock is dynamically plastic, able to adjust its period and phase to the environment, both externally and internally to the status of the cell [207]. Our results suggest this plasticity extends to within a plant, due to differences in inputs. It could be hypothesised that this enables the clock to have a more flexible role in development, which we outline in Chapter 6. However, an obvious consequence of this plasticity is that it causes some internal de-synchrony within the seedling. It has been suggested that this internal jet-lag would be detrimental for an organism, and perhaps why we feel so groggy after travelling across time zones [208–210].

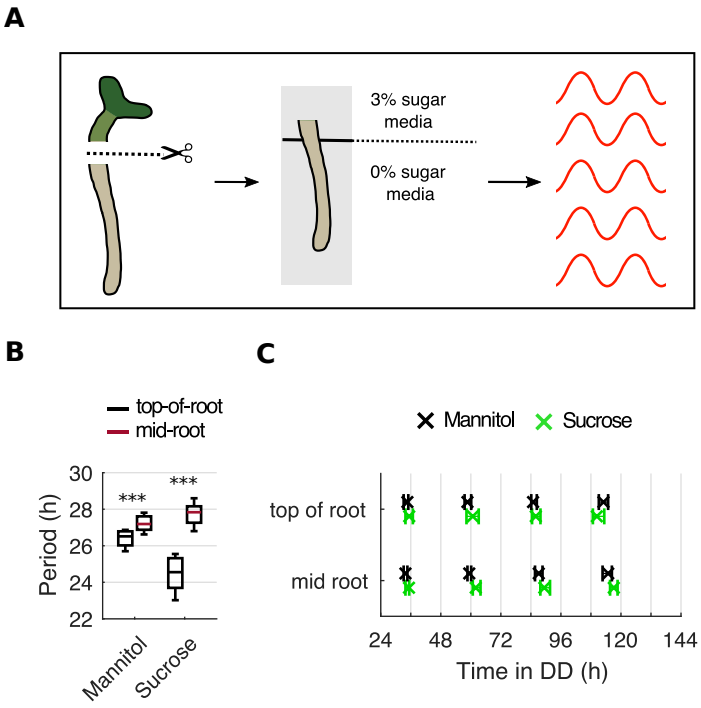

Fig. 4.11 Exogenous sugar alters periods locally. (A) Schematic representing the experimental design. Seedlings are cut at the hypocotyl junction and the excised root laid across two adjacent agar pads, one containing sugar-supplemented media and the other not, so that only the top part of the root is in contact with sugar. Roots are then imaged under DD. (B) Period estimates of *GI*::*LUC* for the top and middle regions of the root during the partial contact of the root with sucrose or mannitol, under DD. ***p < 0.001, by two-tailed *t* test, Welch correction. (C) Times of peaks of *GI*::*LUC* expression for the top and middle regions of the root during the partial contact of the root with exogenous sucrose or mannitol, under DD. Plots represent the 25th percentile, median, and the 75th percentile for the peak times of organs scored as rhythmic. For exogenous sucrose, N= 3; exogenous mannitol, N = 2. For both, n = 20–30. N represents the number of independent experiments and n the total number of organs tracked. Box plots indicate the median and upper and lower quartiles, and whiskers the 9th and 91st percentiles of organs scored as rhythmic.

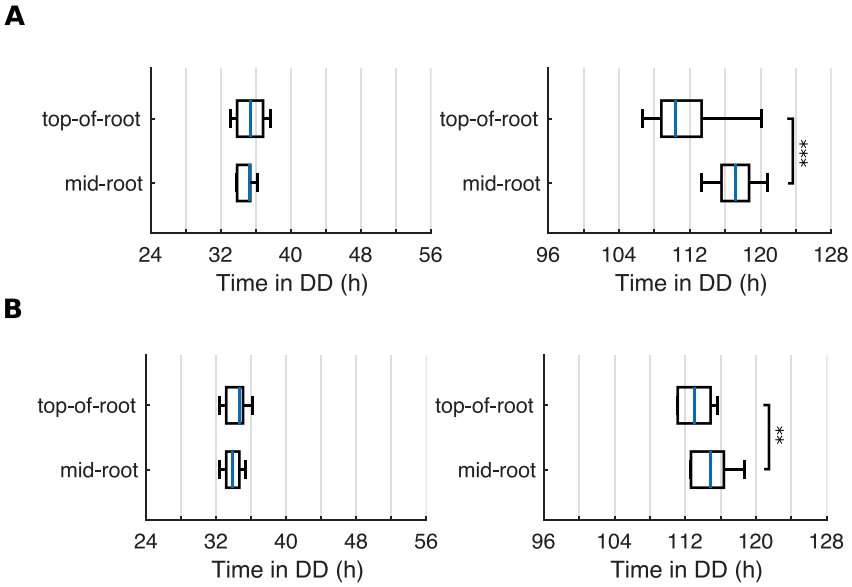

Fig. 4.12 The application of sugar to the top of the root creates a phase shift from the top to the middle of the root under DD. (A) Times of peaks of *GI*::*LUC* expression in different regions during the first (left) and final (right) observed oscillations during the partial contact of the root with sucrose. $***p < 0.001$, Wilcoxon rank-sum test. (B) Times of peaks of expression in different regions during the first (left) and final (right) observed oscillations during the partial contact of the root with mannitol. $**p < 0.01$, Wilcoxon rank-sum test. N and n are as presented in Figure 4.11. N represents the number of independent experiments and n the total number of organs tracked. Box plots indicate the median and upper and lower quartiles, and whiskers the 9th and 91st percentiles of organs scored as rhythmic.

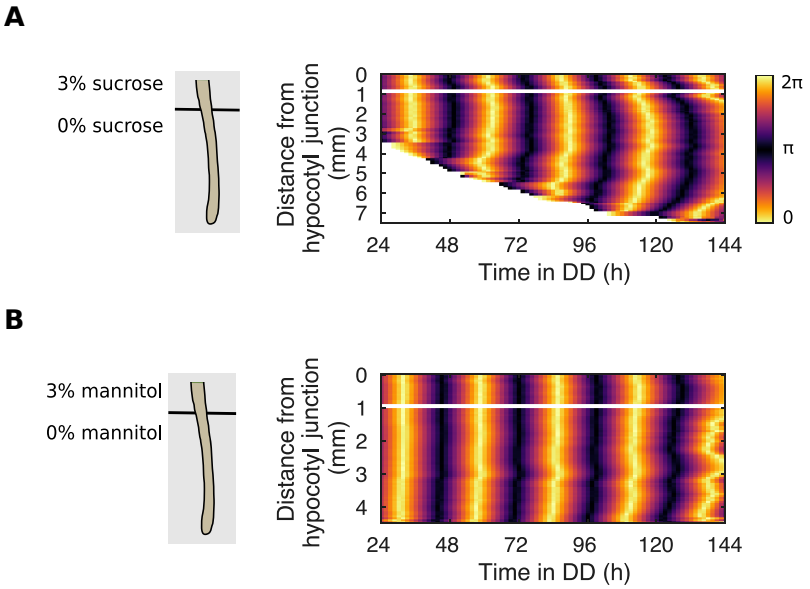

Fig. 4.13 Exogenous sugar can drive spatial waves of clock gene expression. (A, B) Representative phase plot of *GI*::*LUC* expression across longitudinal sections of the hypocotyl and root of a single seedling during the partial contact of the root with exogenous sucrose (A) or mannitol (B), under DD. Schematic shows the approximate position of the root on the agar pads. Colour bar is as in A. *N* and *n* are as presented in Figure 4.11. *N* represents the number of independent experiments and *n* the total number of organs tracked. Box plots indicate the median and upper and lower quartiles, and whiskers the 9th and 91st percentiles of organs scored as rhythmic.

However, a recent study in mice observed only small effects on fitness when the SCN was desynchronised from peripheral oscillators [211]. It will be important to understand the potential trade-off between plasticity and synchrony and the overall fitness effects in both mammals and plants.

Our results revealed that regions of the seedling respond to environmental inputs differently, in both quantitative and qualitative ways. Quantitatively, the clocks in different regions of the seedling had distinct sensitivities to identical levels of light exposure. It can be hypothesised that this is caused by the distribution of light sensing proteins across the plant. The phytochromes and cryptochromes have a apical distribution in *Arabidopsis* seedlings, with the highest levels of their transcription approximately corresponding to the fastest oscillating rhythms [69, 70, 66, 19, 71]. There were however, regions that demonstrated qualitatively different responses to perturbations than would be expected from this hypothesis. For example, under DD when the aerial regions of the seedling slow, the root tip shows a dramatic increase in speed (Figure 4.2). This is an apparent violation of Aschoff's rule, a long standing observation that periods lengthen with decreasing light intensity [212]. We anticipate our molecular understanding of this will come from the emerging understanding that darkness can be perceived as an active signal, rather than simply the absence of light [213].

A molecular understanding of how photosynthesis modulates periods tissue specifically is also absent from this chapter. Perturbations to photosynthesis may have a number of indirect effects on the clock, perhaps via the cell cycle or growth pathways [214, 97]. To distinguish between these effects, further molecular studies utilising sugar sensing mutants will be required. Experiments with the sugar-responsive transcription factor *bZIP63* will be particularly informative for testing if the effect of sugars on organ specificity of periods is direct [93]. However, irrespective of the molecular mechanisms, our results succeed in demonstrating how multiple different inputs can set the periods within a seedling.

In this study, our experiments were limited to light and metabolic signals. There are, however, many other signals known to modulate the speed of the clock (section 1.3). In future work, it will be important to test how these interact and the consequence to spatial coordination when plants are under physiological conditions. Of particular interest will be temperature, which is known to differ between the air and the ground [112] and deviate from the photoperiod [215]. In fact, it has already been demonstrated that temperature is preferentially sensed by the clock in specific cell types [123, 126]. Comprehensive in vivo studies under a range of environmental conditions will be required to understand the full complexity.

Our results suggest that the clock is not only spatially complex, but also dynamic as it flexes to the environment. In Chapter 5, we begin to investigate whether this complexity persists under more realistic LD conditions.

Acknowledgements / disclosures

The results of this chapter are published as part of Greenwood et al., 2019 [1].

Chapter 5

Circadian coordination under more realistic LD cycles

In Chapter 3 we reported the surprising observation of phase differences and spatial waves of clock gene expression within seedlings under LD cycles (section 3.2). However, experiments were conducted under a simplified on-off type LD condition containing low intensity (40 $\mu mol\,m^{-2}\,s$) red and blue wavelength light (RB) only (subsection 2.2.5). The relevance under more realistic environmental conditions therefore remained unclear. Here we monitored the clock under two more realistic conditions, containing higher intensity, broad spectrum white light (WL) in either an on-off (60 $\mu mol\,m^{-2}\,s$), or graded (maximum 95 $\mu mol\,m^{-2}\,s$) 12-h light–12-h dark cycle. Henceforth, we refer to these three entrainment conditions as 'RB on-off', 'WL on-off' and 'WL graded' LD respectively (Figure 5.1 and subsection 2.2.5).

We firstly monitored expression of the *GI* promoter region fused to the *LUC* reporter gene with near cellular resolution. We observed altered phasing and spatial coordination of rhythms, both in comparison to the RB on-off LD condition of Chapter 3, and between the WL on-off and WL graded LD condition used here. We therefore went on to image luciferase reporters for the core clock genes *CCA1*, *PRR9*, *PRR7*, and *TOC1* to better evaluate the temporal and spatial organisation under more natural light conditions.

5.1 *GI* expression under RB and WL on-off LD cycles

5.1.1 *GI* expression is acutely induced by light under WL but not RB on-off LD cycles

GI is core clock gene stabilised by light, and expression is phased to the evening under constant light [18]. In Chapter 3 we reported phase differences between organs under RB

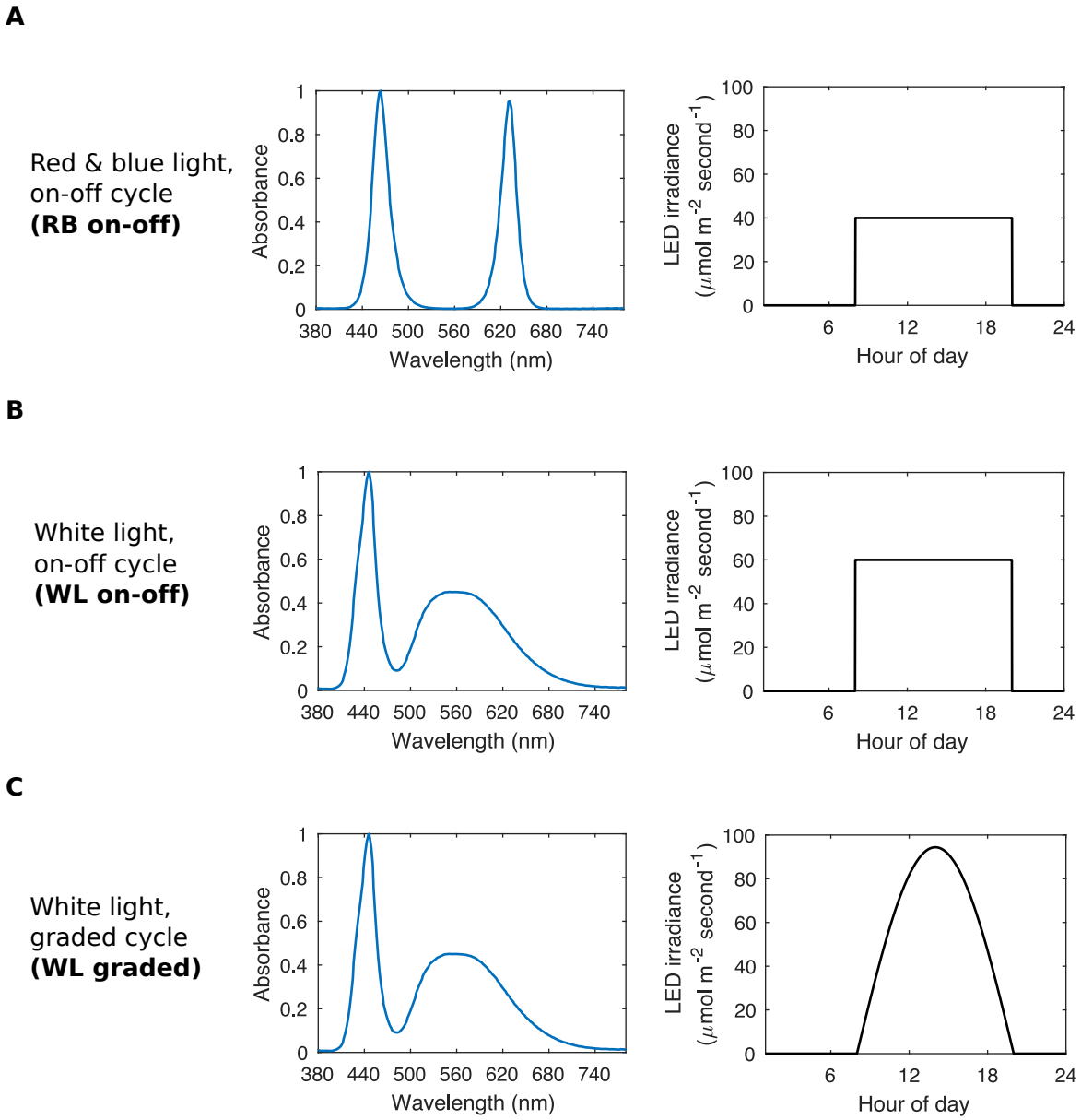

Fig. 5.1 Laboratory conditions make approximations of LD cycles. (A) In Chapter 3 we used red and blue wavelength (left) with on-off light cycles (right). We refer to this condition here as 'RB on-off'. (B) In 'WL on-off' condition we used broad spectrum white light (left) with on-off light cycles (right). (C) In 'WL graded' condition we used broad spectrum white light (left) with graded light cycles (right).

on-off LD conditions (subsection 3.1.2 and Figure 5.2). Here, we firstly monitored rhythms of *GI*::*LUC* expression under WL on-off light conditions, to see whether organ specificity of rhythms persists with increased light quality. Under the WL on-off light condition, rhythms of *GI*::*LUC* showed clear rhythmic patterns but in some organs atypical waveforms (Figure 5.2). *GI*::*LUC* was acutely induced at dawn in the cotyledon and hypocotyl, causing a spike of expression. The acute peak was not observed in the root regions (Figure 5.2), but has been previously reported in whole-plant molecular assays [216, 217]. These spikes of expression were also not visible in any organ under the RB on-off LD condition (Figure 5.2). This could be because the lower intensity, or the narrow wavelength, was insufficient to induce the acute transcriptional response at dawn.

5.1.2 *GI* peaks earlier under WL on-off than RB on-off LD cycles in the hypocotyl and mid-root

We next analysed the times of the peaks of *GI*:*LUC* expression occurring in the evening (see subsection 2.3.3), in individual organs. We chose to analyse this peak only, ignoring any acute peaks at dawn. We did this because it corresponds to the timing of the peak of GI expression under LL (chapter 3), so likely represents the natural peak. Previously, under RB on-off LD conditions, we observed that the cotyledon and hypocotyl peaked earlier than the middle region of the root, with the root tip peaking before the middle region of the root (subsection 3.1.2 and Figure 5.3). Under WL on-off LD cycles we observed a change in the relative times of the peaks of expression between organs (Figure 5.3A). This can be seen clearer by plotting the peaks for the final day of the time course (Figure 5.3B and Figure 5.4). The root regions peaked first, with the root tip at 130.23 ± 0.37 h (versus 130.75 ± 1.49 under RB on-off) peaking slightly before the middle region of the root at 130.71 ± 1.46 h (versus 132.25 ± 2.08). The aerial organs peaked afterwards, as under RB on-off. However, under WL on-off the hypocotyl peaked at 131.30 ± 1.00 h (versus 132.25 ± 0.85) and before the cotyledon at 132.05 ± 0.87 h (versus 131.43 ± 1.84. Thus, the relative timing of *GI* expression between organs was altered between RB on-off and WL on-off LD cycles.

5.1.3 The spatial coordination of rhythms of *GI* are altered between RB and WL on-off LD cycles

Finally, we analysed rhythms at the sub-tissue level to test whether the spatial coordination was modulated under WL conditions. We previously observed that spatial waves propagated within and between tissues under RB on-off LD cycles (subsection 3.1.2 and Figure 5.5A).

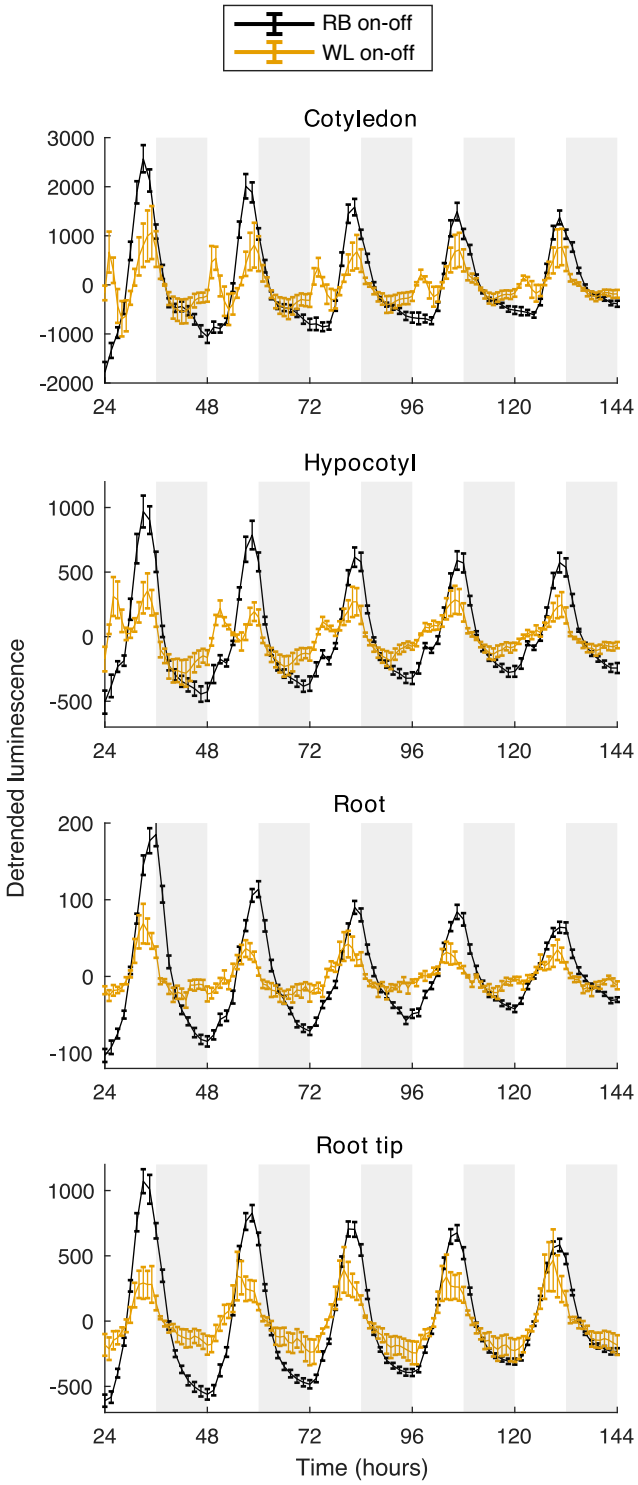

Fig. 5.2 *GI* expression under RB on-off and WL on-off LD cycles. Expression of *GI*::*LUC* from different organs under RB on-off or WL on-off LD cycles. Data represent the mean ± standard error of tracked organs. For WL on-off, $N = 2$, $n = 8$. For RB on-off, $N = 3$; WL on-off $N = 2$. For both, $n = 8$-35. N represents the number of independent experiments and n the total number of organs tracked.

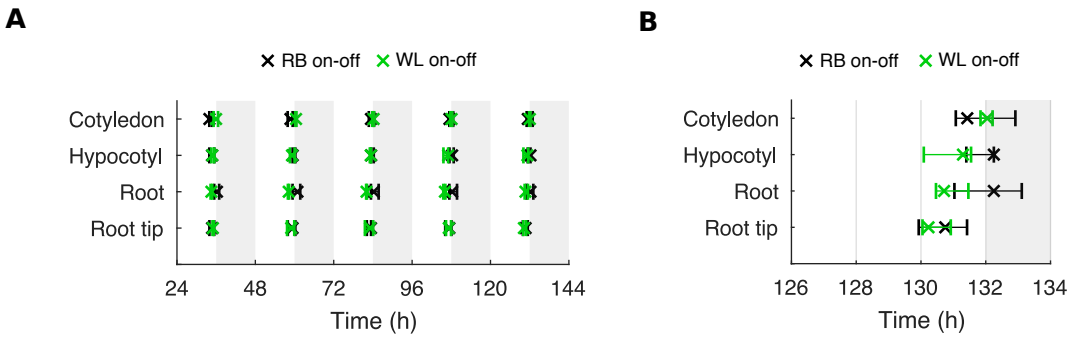

Fig. 5.3 Times of peaks of *GI* expression in different organs are phase shifted between RB on-off and WL on-off LD cycles. (A) Times of all observed peaks of *GI*::*LUC* expression in different organs under RB on-off or WL on-off LD cycles. Plots represent the 25th percentile, median, and the 75th percentile for the peak times of organs scored as rhythmic. (B) Times of the final observed peak of *GI*::*LUC* expression under RB on-off or WL on-off LD cycles. For on-off WL, *N* and *n* are as in Figure 5.2. *N* represents the number of independent experiments and *n* the total number of organs tracked. Box plots indicate the median and upper and lower quartiles, and whiskers the 9th and 91st percentiles of organs scored as rhythmic.

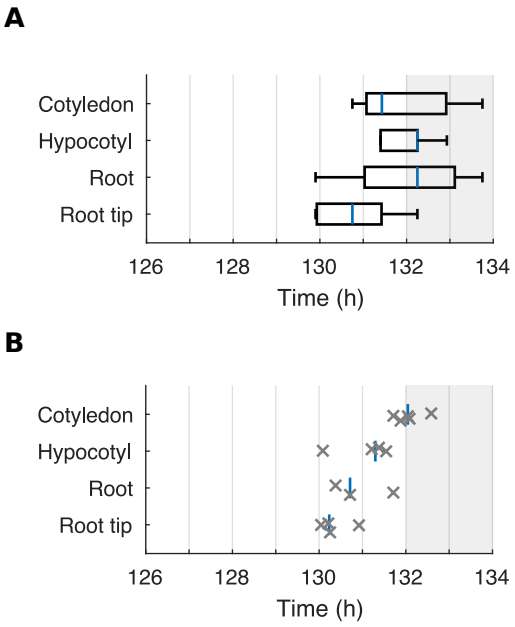

Fig. 5.4 Times of the final observed peaks of *GI* expression in different organs are shifted between RB on-off and WL on-off LD cycles. (A, B) Times of the final observed peak of *GI*::*LUC* expression in different organs for the final observed oscillation under RB on-off (A) or WL on-off (B) LD cycles. *N* and *n* are as in Figure 5.2. *N* represents the number of independent experiments and *n* the total number of organs tracked. Box plots indicate the median and upper and lower quartiles, and whiskers the 9th and 91st percentiles of organs scored as rhythmic. Individual data points are plotted when $n < 5$.

As before, we extracted the phase of the luminescence signal across longitudinal sections of seedlings (Figure 2.4 and section 2.4) and present phase plots of single seedlings representative for each light condition (Figure 5.5). In the cotyledon, a phase wave of *GI*::*LUC* expression propagated from the tip to the base under RB on-off LD cycles (Figure 5.5A, top and subsection 3.1.2). A spatial wave was also observed under the WL on-off LD cycles. However, the wave propagated in the opposite direction, from the base out to the tip (Figure 5.5B, top). Spatial wave patterns in clock gene expression have previously been reported to be variable within leaves of *Arabidopsis* [139]. Further analysis will therefore be required to ascertain whether this change is a result of the WL conditions.

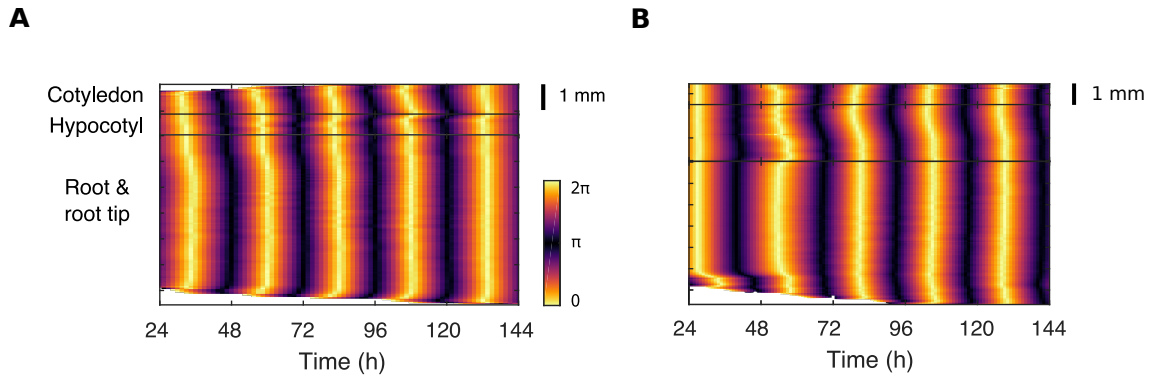

Fig. 5.5 Spatial waves of *GI*::*LUC* expression propagate within and between tissues under RB on-off and WL on-off LD cycles. (A, B) Representative phase plot of *GI*::*LUC* expression across longitudinal sections of the cotyledon (top), hypocotyl (middle), and root (bottom) of a single seedling under RB on-off (A) and WL on-off (B) LD cycles.

In the root we previously observed two waves under RB on-off LD cycles. One propagated from the hypocotyl junction down into the root and the second from the root tip upwards into the root (subsection 3.1.2 and Figure 5.5A, bottom). Under WL on-off LD cycles we also observed two waves however their direction was altered. One wave propagated from the lower region of the root into the hypocotyl and a second from the lower region of the root into the root tip (Figure 5.5B, bottom). Phase shifts were also visible in the hypocotyl under both RB and WL on-off condition, however, the direction of waves was difficult to discern (subsection 3.1.2 and Figure 5.5A and B, middle). Together our analysis suggests that the spatial coordination of rhythms across the plant may be altered between RB and WL on-off LD cycles.

5.2 *GI* expression under WL graded LD cycles

5.2.1 *GI* expression is more gradually induced under WL graded than WL on-off LD cycles

Thus-far we have imaged plants under on-off type LD cycles. However, in the field, the natural light cycle is more gradual (Figure 1.6). We therefore imaged expression of *GI*::*LUC* under graded LD cycles, and compared rhythms to WL on-off LD condition, to see how the clock responds to more natural light cycles. Under WL on-off LD cycles we observed acute induction of *GI* expression at dawn in the cotyledons and hypocotyls (subsection 5.1.1 and Figure 5.6). In contrast, under WL graded LD cycles *GI*::*LUC* was gradually induced in all organs, and the spike of expression was lost (Figure 5.6). It is interesting to note that the acute induction of *GI* occurred under WL on-off (Figure 5.6), but not RB on-off (Figure 5.2) or WL graded LD conditions (Figure 5.6). This indicates that the acute peak of *GI*::*LUC* expression at dawn was a result of the abrupt transition of WL specifically, but not a natural property of the network under more realistic graded cycles.

5.2.2 *GI* expression peaks earlier under WL graded than WL on-off LD cycles in all organs

We again analysed the times of what we now deemed to be the natural peaks of *GI*:*LUC* expression, occurring in the evening (see subsection 5.2.1). We again observed a change in the relative times of the peaks of expression between organs (Figure 5.7A). This can be seen clearer by plotting the peaks for the final day of the time course (Figure 5.7B and Figure 5.8). Under WL graded LD cycles *GI*::*LUC* peaked approximately 2 h earlier in all organs imaged. The cotyledon peaked at 153.50 ± 0.88 h (versus 155.75 ± 0.43 h under WL on-off LD), the hypocotyl 153.17 ± 0.30 h (versus 155.21 ± 0.38 h), and the middle region of the root at 152.67 ± 0.76 h (versus 154.21 ± 0.38 h). Finally, the root tip peaked at 152.50 ± 0.30 h (versus 154.73 ± 1.71 h) causing it to peak before rather than after the middle region of the root, as observed under WL on-off LD (Figure 5.7 and Figure 5.8). Thus, the evening phased *GI* responded to WL graded LD cycles with a more gradual induction by light and an earlier phase of expression in all organs.

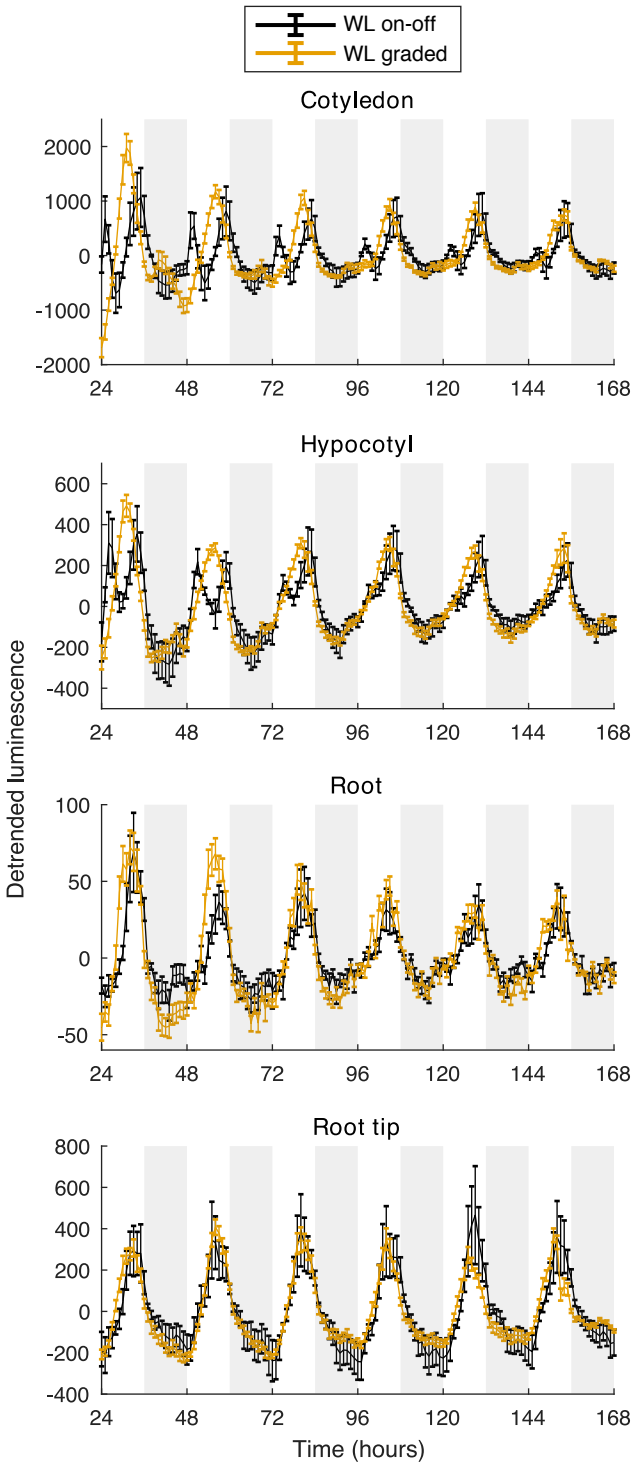

Fig. 5.6 *GI* expression under WL on-off and WL graded LD cycles. Expression of *GI*::*LUC* from different organs under WL on-off or WL graded LD cycles. Data represent the mean ± standard error of tracked organs. $N = 2$, $n = 8$. N represents the number of independent experiments and n the total number of organs tracked.

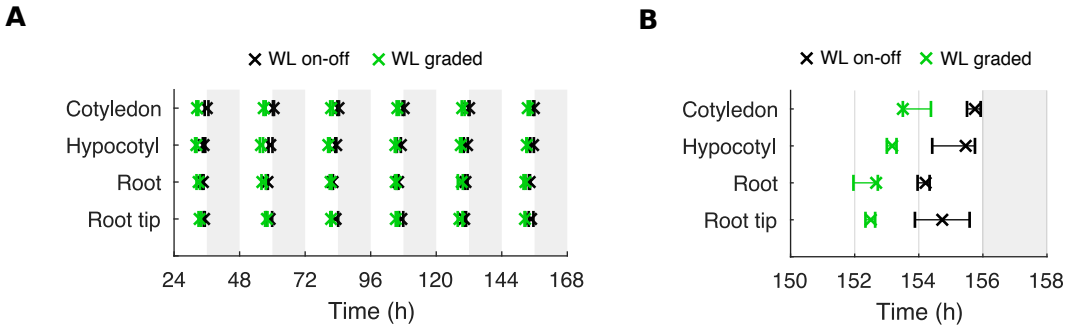

Fig. 5.7 Times of peaks of *GI* expression in different organs are phase shifted between WL on-off and WL graded LD cycles. (A) Times of all observed peaks of *GI*::*LUC* expression in different organs under WL on-off or WL graded LD cycles. Plots represent the 25th percentile, median, and the 75th percentile for the peak times of organs scored as rhythmic. (B) Times of the final observed peak of *GI*::*LUC* expression under WL on-off or WL graded LD cycles. *N* and *n* are as in Figure 5.6. *N* represents the number of independent experiments and *n* the total number of organs tracked. Box plots indicate the median and upper and lower quartiles, and whiskers the 9th and 91st percentiles of organs scored as rhythmic.

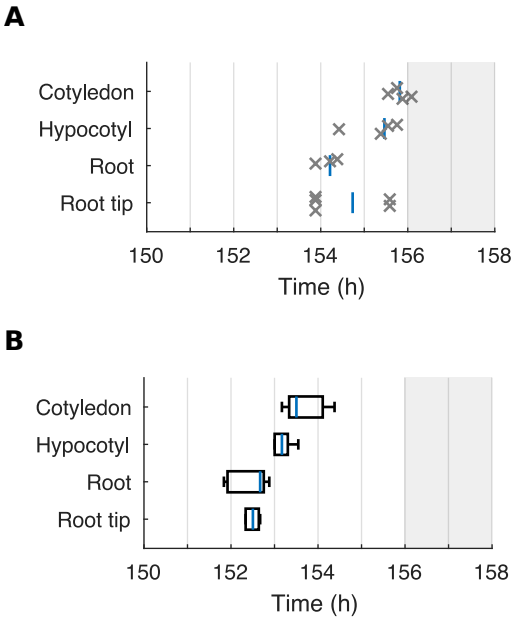

Fig. 5.8 Times of the final observed peaks of *GI* expression in different organs are shifted between WL on-off and WL graded LD cycles. (A, B) Times of the final observed peak of *GI*::*LUC* expression in different organs for the final observed oscillation under WL on-off (A) or WL graded (B) LD cycles. *N* and *n* are as in Figure 5.6. *N* represents the number of independent experiments and *n* the total number of organs tracked. Box plots indicate the median and upper and lower quartiles, and whiskers the 9th and 91st percentiles of organs scored as rhythmic. Individual data points are plotted when $n < 5$.

5.2.3 Spatial waves of *GI*::*LUC* are modulated between WL on-off and WL graded LD cycles

Spatial waves of *GI*::*LUC* could also be seen within and between tissues under WL graded LD cycles. As under WL on-off cycles, a phase wave propagated from the base of the cotyledon out to the tip (Figure 5.9A and B, top). Wave patterns in the hypocotyl and root were also similar. A wave travelled from the base of the cotyledon down the hypocotyl under both on-off and graded WL (Figure 5.9A and B, middle). In the root, one wave propagated up the root into the hypocotyl and a second down the root into the tip (Figure 5.9A and B, bottom). However, this second wave into the root tip was less clear under graded WL (Figure 5.9B, bottom). Overall, the spatial coordination between WL on-off and graded cycles appeared similar, despite the differences in phases observed at the organ level (subsection 5.2.2). .

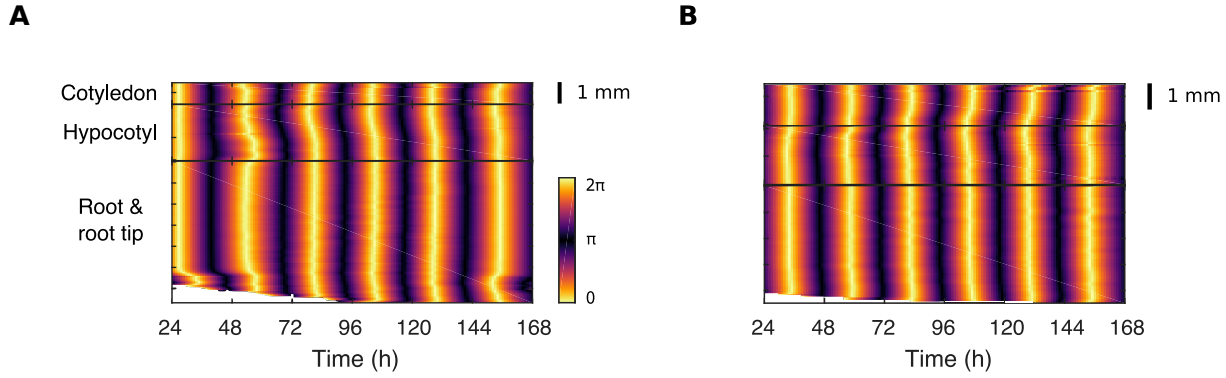

Fig. 5.9 Spatial waves of *GI*::*LUC* expression propagate within and between tissues under WL on-off and WL graded LD cycles. (A, B) Representative phase plot of *GI*::*LUC* expression across longitudinal sections of the cotyledon (top), hypocotyl (middle), and root (bottom) of a single seedling under WL on-off (A) and WL graded (B) LD cycles.

5.3 *CCA1* expression under WL graded LD cycles

5.3.1 *CCA1* oscillates with phase differences between organs under WL on-off LD cycles

We next imaged additional clock genes to see if sensitivity to the light gradient is a general property of the clock. *CCA1* is a light-induced core clock gene and dawn phased under constant light [21, 22]. We monitored expression of the *CCA1* promoter region fused to the *LUC* reporter gene. We observed sustained rhythms of *CCA1*::*LUC* in all the major organs of the seedling under both WL on-off and WL graded LD cycles (Figure 5.10). Close

inspection of the times of the peaks of expression revealed phase differences between organs. Under WL on-off LD cycles the root tip peaked first at 147.96 ± 1.25 h (median $\pm$ IQR), followed shortly by the middle section of the root (148.21 ± 0.33 h). The aerial organs peaked approximately 30-60 minutes later, with the cotyledon (148.55 ± 0.83 h) peaking before the hypocotyl (149.05 ± 0.67 h; Figure 5.11 and Figure 5.12).

5.3.2 *CCA1* peaks later under WL graded than WL on-off LD cycles in the cotyledon and hypocotyl

We also observed phase differences between organs under WL graded LD cycles, although the times of the peaks were shifted in some organs. The root regions peaked first, at approximately the same time as under WL on-off LD cycles (Figure 5.11 and Figure 5.12). However, in the cotyledon and hypocotyl the induction of *CCA1*::*LUC* at dawn was slower than under WL on-off LD cycles (Figure 5.10). This caused a delay in the peak of expression by 1-2 h (Figure 5.11 and Figure 5.12). The cotyledon peaked at 150.13 ± 1.50 h (versus 148.55 ± 0.83 h under WL on-off cycles) and the hypocotyl at 150.05 ± 0.50 h (versus 149.05 ± 0.67 h). Thus *CCA1* expression in the aerial organs peaked later, but the root regions at a similar time under WL graded cycles versus WL on-off LD cycles.

5.3.3 Spatial waves of *CCA1*::*LUC* are modulated between WL on-off and WL graded LD cycles

We next analysed rhythms of *CCA1*::*LUC* at the sub-tissue level, to see if the coordination is also altered under graded cycles. We observed spatial waves of *CCA1*::*LUC* propagating within and between tissues under both WL on-off and WL graded LD cycles, however the waves were modulated. A phase wave propagated from the tip to the base of the cotyledon (Figure 5.13A and B, top), and downwards into the hypocotyl (Figure 5.13A and B, middle) under both LD conditions.

In the root, we observed a wave travel up the root (Figure 5.13A and B, bottom) and into the hypocotyl under both conditions (Figure 5.13A and B, middle). Under WL on-off condition careful observation revealed a short wave propagated from the bottom region of the root down into the root tip (Figure 5.13A, bottom). However, by the sixth day, this wave was lost under graded on-off condition (Figure 5.13A, bottom). The modulation of the wave into the root tip was also observed in *GI* expression (Figure 5.5). Indeed, the overall coordination structure looked similar across the entire seedling for *CCA1* and *GI* expression in both conditions.

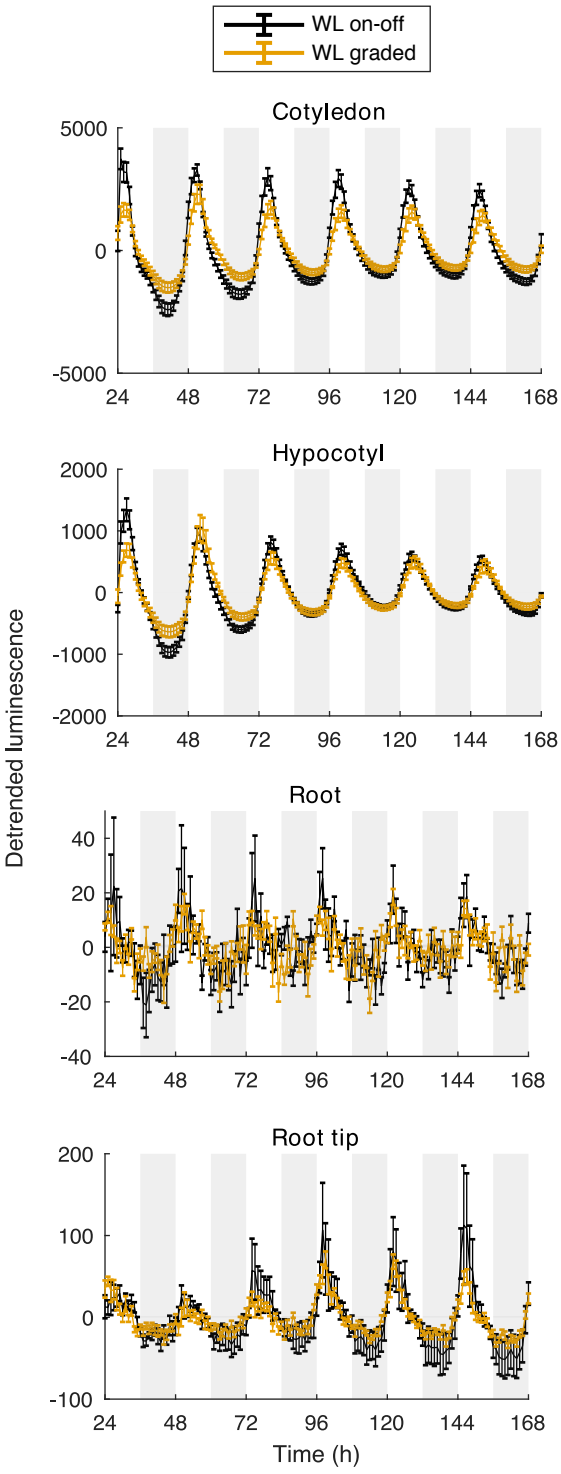

Fig. 5.10 *CCA1* expression under WL on-off and WL graded LD cycles. Expression of *CCA1*::*LUC* from different organs under WL on-off or WL graded LD cycles. Data represent the mean ± standard error of tracked organs. $N = 2$, $n = 8$. N represents the number of independent experiments and n the total number of organs tracked.

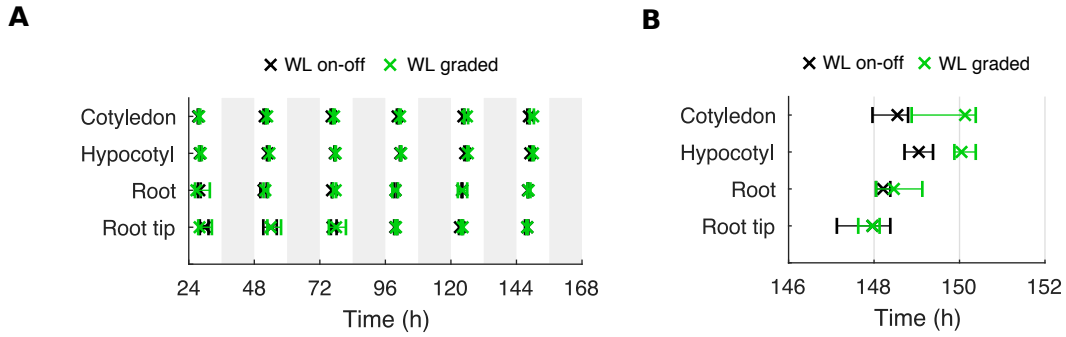

Fig. 5.11 Times of peaks of *CCA1* expression in different organs are phase shifted between WL on-off and WL graded LD cycles. (A) Times of all observed peaks of *CCA1*::*LUC* expression in different organs under WL on-off or WL graded LD cycles. Plots represent the 25th percentile, median, and the 75th percentile for the peak times of organs scored as rhythmic. (B) Times of the final observed peak of *CCA1*::*LUC* expression under WL on-off or WL graded LD cycles. *N* and *n* are as in Figure 5.10. *N* represents the number of independent experiments and *n* the total number of organs tracked. Box plots indicate the median and upper and lower quartiles, and whiskers the 9th and 91st percentiles of organs scored as rhythmic.

5.4 *PRR9* expression under WL graded LD cycles

5.4.1 *PRR9* oscillates with phase differences between organs under WL on-off LD cycles

PRR9 is a light induced transcription factor that forms a feedback loop in the morning with *CCA1/LHY* [218, 88]. We next monitored expression of the *PRR9* promoter region fused to the *LUC* reporter gene. Rhythms of *PRR9*::*LUC* were robust and sustained for the full 7 days of imaging in all organs (Figure 5.14). As for *CCA1* and *GI* expression, we observed phase differences in rhythms between organs. Under WL on-off LD cycles the middle region of the root peaked first (148.96 ± 0.67 h), with the root tip (149.38 ± 0.50 h) and the cotyledons (149.38 ± 2.33 h) peaking quickly afterwards. Finally, the hypocotyl lagged behind by approximately 2 h (151.63 ± 1.83 h; Figure 5.15 and Figure 5.16).

5.4.2 *PRR9* peaks later under WL graded than WL on-off LD cycles in all organs

We observed changes in the times of the peaks of *PRR9* expression when seedlings were imaged under WL graded rather than WL on-off cycles (Figure 5.15 and Figure 5.16). Under WL graded LD the middle region of the root peaked first at 150.71 ± 0.83 h (versus $148.96 \pm$

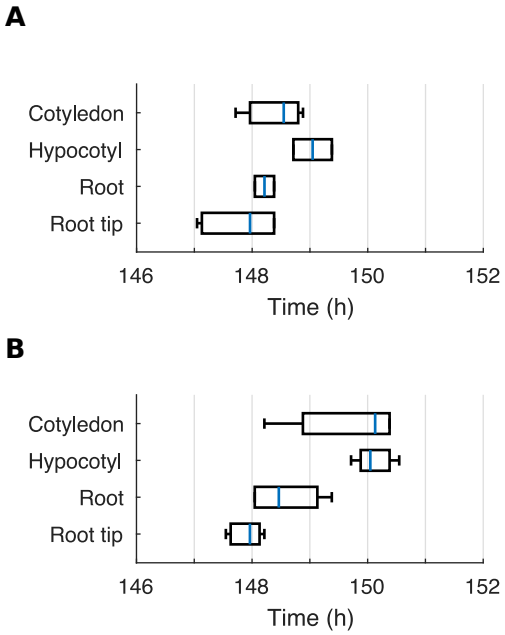

Fig. 5.12 Times of the final observed peaks of *CCA1* expression in different organs are shifted between WL on-off and WL graded LD cycles. (A, B) Times of the final observed peak of *CCA1*::*LUC* expression in different organs for the final observed oscillation under WL on-off (A) or WL graded (B) LD cycles. *N* and *n* are as in Figure 5.10. *N* represents the number of independent experiments and *n* the total number of organs tracked. Box plots indicate the median and upper and lower quartiles, and whiskers the 9th and 91st percentiles of organs scored as rhythmic.

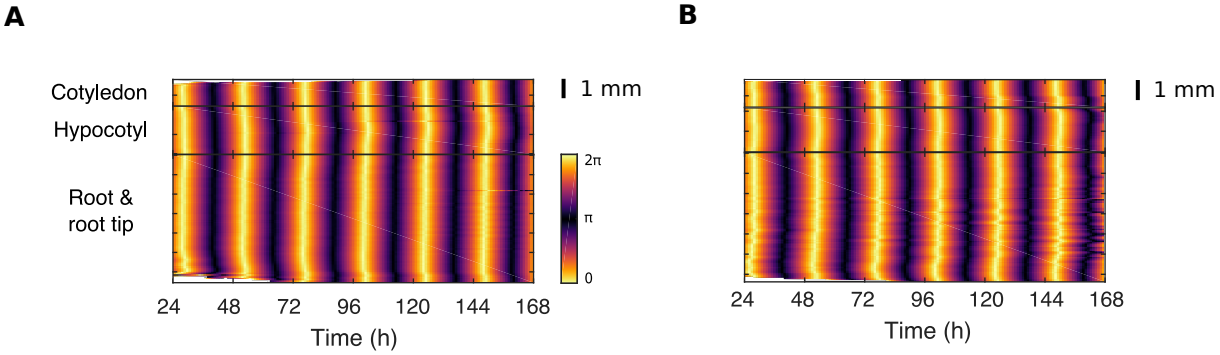

Fig. 5.13 Spatial waves of *CCA1*::*LUC* expression propagate within and between tissues under WL on-off and WL graded LD cycles. (A, B) Representative phase plot of *CCA1*::*LUC* expression across longitudinal sections of the cotyledon (top), hypocotyl (middle), and root (bottom) of a single seedling under WL on-off (A) and WL graded LD (B) LD cycles.

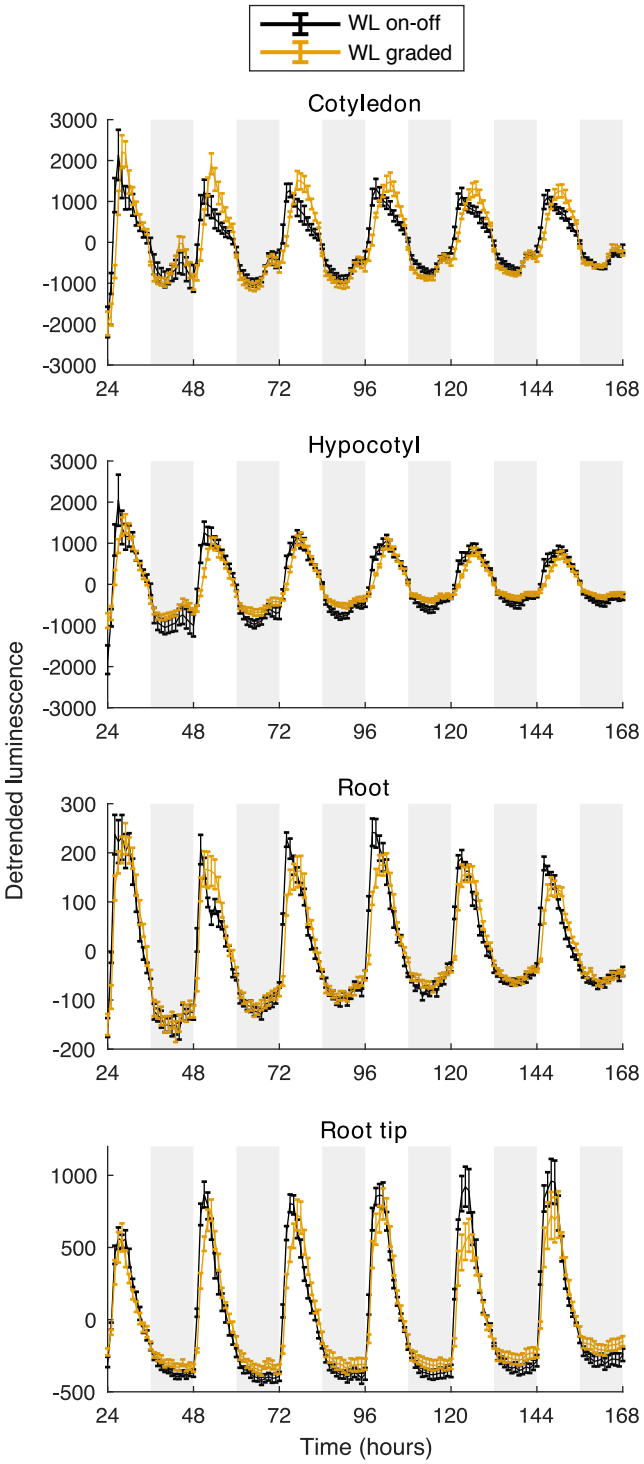

Fig. 5.14 *PRR9*::*LUC* expression under WL on-off and WL graded LD cycles. Expression of *PRR9*::*LUC* from different organs under WL on-off or WL graded LD cycles. Data represent the mean ± standard error of tracked organs. $N = 2$, $n = 8$. N represents the number of independent experiments and n the total number of organs tracked.

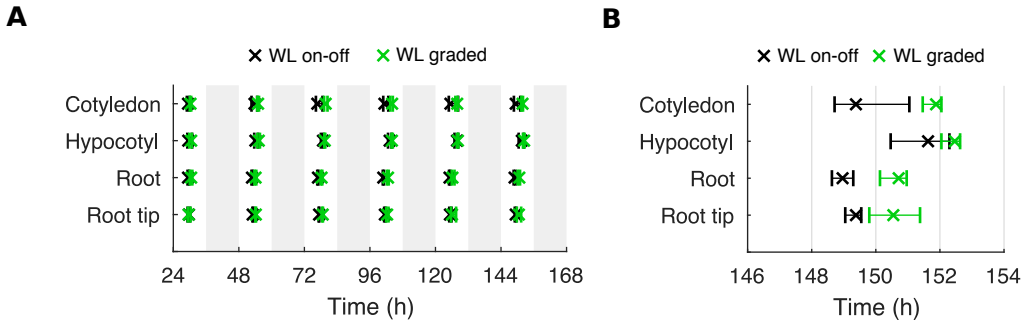

Fig. 5.15 Times of peaks of *PRR9* expression in different organs are shifted between WL on-off and WL graded LD cycles. (A) Times of all observed peaks of *PRR9*::*LUC* expression in different organs under WL on-off or WL graded LD cycles. Plots represent the 25th percentile, median, and the 75th percentile for the peak times of organs scored as rhythmic. (B) Times of the final observed peak of *PRR9*::*LUC* expression under WL on-off or WL graded LD cycles. *N* and *n* are as in Figure 5.14. *N* represents the number of independent experiments and *n* the total number of organs tracked. Box plots indicate the median and upper and lower quartiles, and whiskers the 9th and 91st percentiles of organs scored as rhythmic.

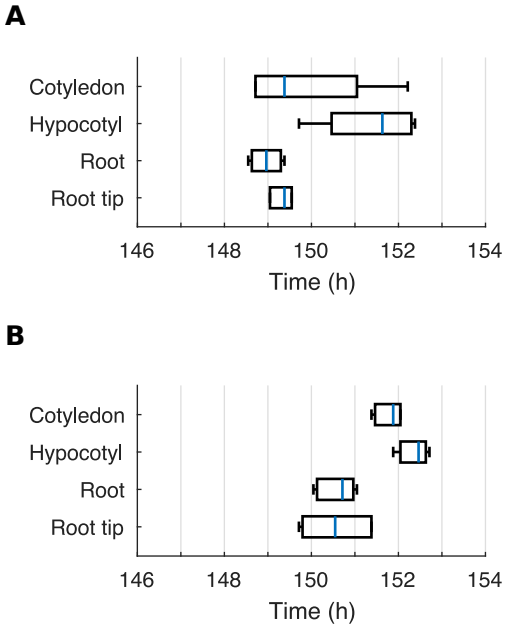

Fig. 5.16 The times of the final observed peaks of *PRR9* expression in different organs are shifted between WL on-off and WL graded LD cycles. (A, B) Times of the final observed peak of *PRR9*::*LUC* expression in different organs for the final observed oscillation under WL on-off (A) or WL graded (B) LD cycles. *N* and *n* are as in Figure 5.14. *N* represents the number of independent experiments and *n* the total number of organs tracked. Box plots indicate the median and upper and lower quartiles, and whiskers the 9th and 91st percentiles of organs scored as rhythmic.

0.67 h under WL on-off LD), followed shortly afterwards by the root tip 150.55 ± 1.58 h (versus 149.38 ± 0.50 h), and the cotyledon 151.88 ± 0.58 h (versus 149.38 ± 2.33 h). The hypocotyl again peaked last at 152.46 ± 0.58 h (versus 151.63 ± 1.83 h). Thus *PRR9* expression in all organs peaked later under WL graded cycles versus WL on-off LD cycles.

5.4.3 Spatial waves of *PRR9*::*LUC* are modulated between WL on-off and WL graded LD cycles

At the sub-tissue level, this time in rhythms of *PRR9*::*LUC*, we again observed the modulation of spatial waves under WL graded LD cycles. A similar coordination structure of *PRR9* expression was observed as for rhythms of *GI* and *CCA1* (Figure 5.17A and B). In the cotyledon a wave propagated from the base to the tip under both WL on-off and WL graded LD cycles (Figure 5.17A and B, top). This was alike *GI* expression in the cotyledons (Figure 5.9A and B, top), but in the opposite direction to the wave of *CCA1* expression (Figure 5.13A and B, top). Two waves were also observed in the hypocotyl and root under WL on-off condition (Figure 5.17A and B, middle and bottom). As with *GI* and *CCA1* expression, the wave from the root into the root tip did not persist under WL graded condition. The wave of *PRR9*::*LUC* from the root into the root tip was attenuated by the final day of imaging under WL graded cycles (Figure 5.17B, bottom).

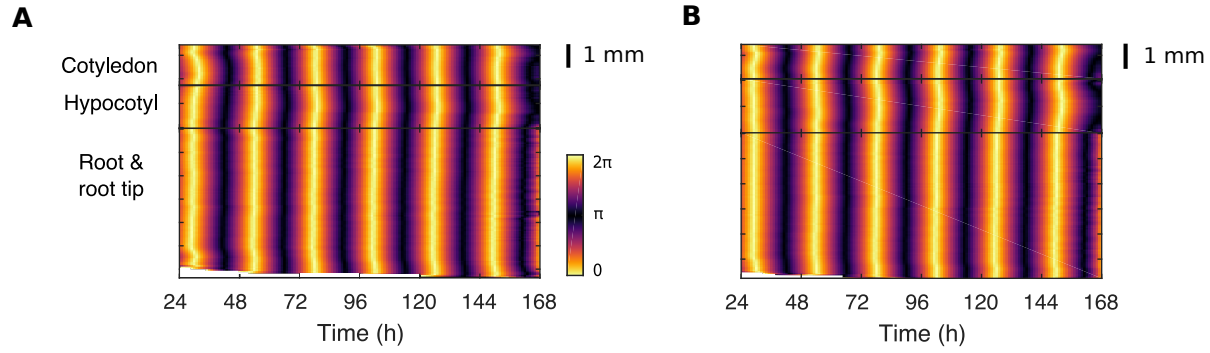

Fig. 5.17 Spatial waves of *PRR9*::*LUC* expression propagate within and between tissues under WL on-off and WL graded LD cycles. (A, B) Representative phase plot of *PRR9*::*LUC* expression across longitudinal sections of the cotyledon (top), hypocotyl (middle), and root (bottom) of a single seedling under WL on-off (A) and WL graded (B) LD cycles.

5.5 *PRR7* expression under natural LD cycles

5.5.1 *PRR7* oscillates with phase differences between organs under WL on-off LD cycles

PRR7 is a close relative of *PRR9*, with overlapping function and a similar phase of expression [218, 88]. Rhythms were sustained for the full 7 days of imaging (Figure 5.18). Intriguingly, in the root tip we observed an increase in amplitude of rhythms over time. This could be due to the difference in light conditions between the growth and imaging cabinet (subsection 2.2.5).

Phase differences were also observed between organs (Figure 5.19). Under WL on-off LD cycles, *PRR7*::*LUC* was rapidly induced by light in the cotyledons at dawn (Figure 5.18), creating the earliest peak of expression in the seedling (149.13 ± 1.08 h). The middle region of the root (150.05 ± 1.92 h) peaked less than 30 minutes after the cotyledon, whilst the root tip (151.30 ± 0.50 h) and hypocotyl (151.46 ± 1.42 h) lagged behind by approximately 1-2 h (Figure 5.19 and Figure 5.20).

5.5.2 *PRR7* peaks later under WL graded than WL on-off LD cycles in all organs

Under WL graded LD cycles, we observed altered waveforms and phases in comparison to WL on-off. The effect was most dramatic in the cotyledons, where *PRR7*::*LUC* was gradually induced, avoiding the acute spike of expression that occurs under WL on-off LD cycles (Figure 5.18).

The times of the peaks of expression also differed between conditions. The peak of *PRR7*::*LUC* expression was approximately 3 h later in the cotyledon under WL graded LD cycles (152.05 ± 1.92 h versus 149.13 ± 1.08 h under WL on-off LD). The hypocotyl and root regions were induced more gradually, and peaked 0.5-2 h later in the day (Figure 5.19 and Figure 5.20). The hypocotyl peaked at 153.30 ± 0.50 h (versus 151.46 ± 1.42 h under WL on-off LD), the middle region of the root at 152.21 ± 1.33 h (versus 150.05 ± 1.92 h), and the root tip peaked at 152.30 ± 0.92 h (versus 151.30 ± 0.50 h). Thus, *PRR7* peaked later in all organs imaged.

5.5.3 Spatial waves of *PRR7*::*LUC* are modulated between WL on-off and WL graded LD cycles

At the sub-tissue level, we observed qualitatively the same spatial structure of *PRR7*::*LUC* expression under WL on-off LD cycles to that described earlier for *PRR9*::*LUC* (Figure 5.21).

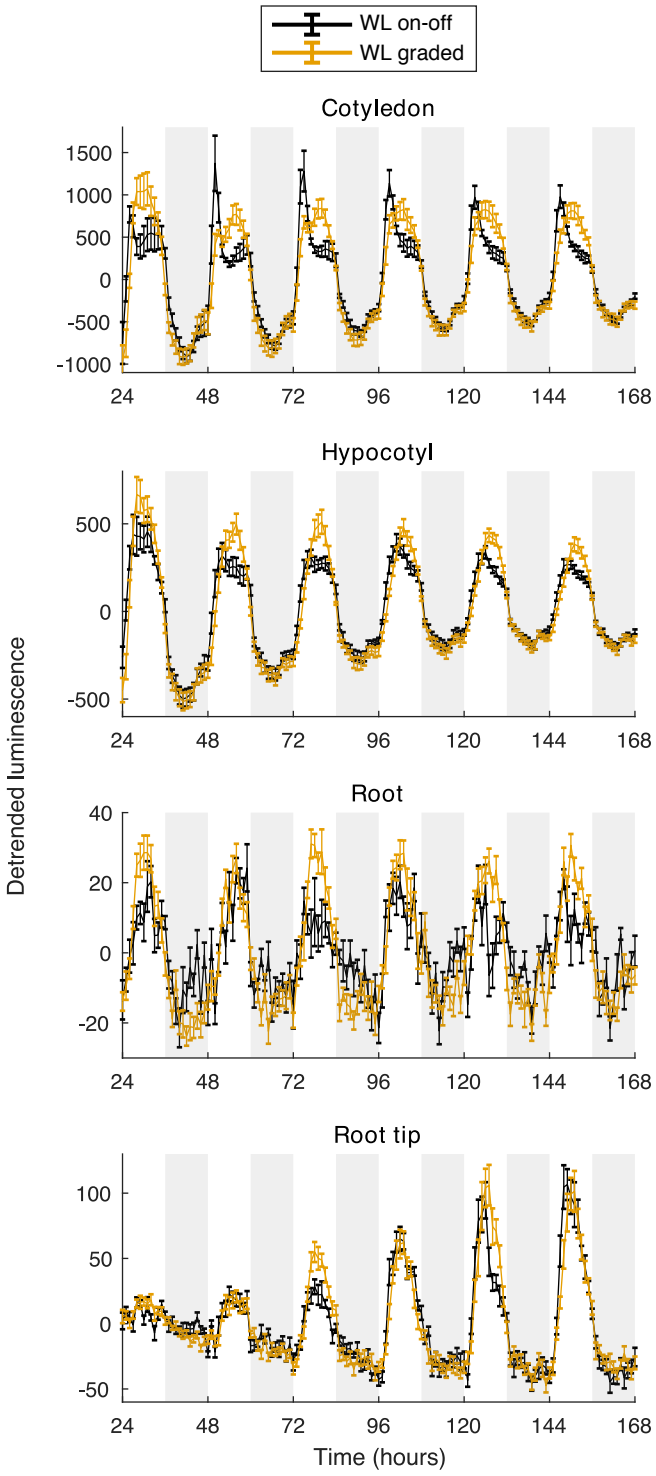

Fig. 5.18 *PRR7* expression under WL on-off and WL graded LD cycles. Expression of *PRR7*::*LUC* from different organs under WL on-off or WL graded LD cycles. Data represent the mean ± standard error of tracked organs. $N = 2$, $n = 8$. N represents the number of independent experiments and n the total number of organs tracked.

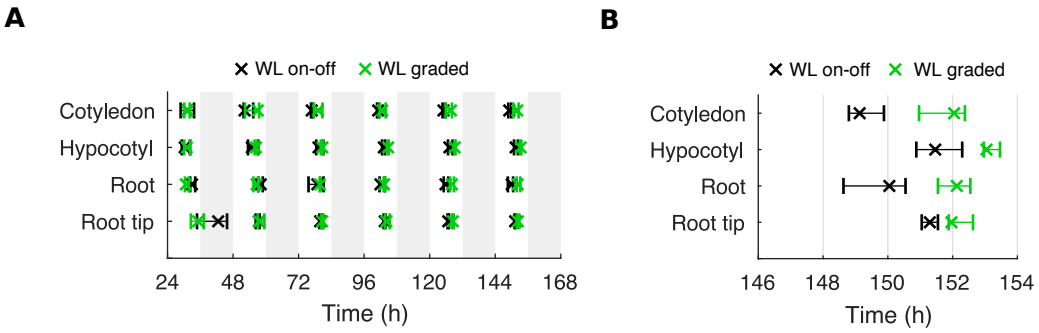

Fig. 5.19 Times of peaks of *PRR7* expression in different organs are shifted between WL on-off and WL graded LD cycles. (A) Times of all observed peaks of *PRR7*::*LUC* expression in different organs under WL on-off or WL graded LD cycles. Plots represent the 25th percentile, median, and the 75th percentile for the peak times of organs scored as rhythmic. (B) Times of the final observed peak of *PRR7*::*LUC* expression under WL on-off or WL graded LD cycles. *N* and *n* are as in Figure 5.18. *N* represents the number of independent experiments and *n* the total number of organs tracked. Box plots indicate the median and upper and lower quartiles, and whiskers the 9th and 91st percentiles of organs scored as rhythmic.

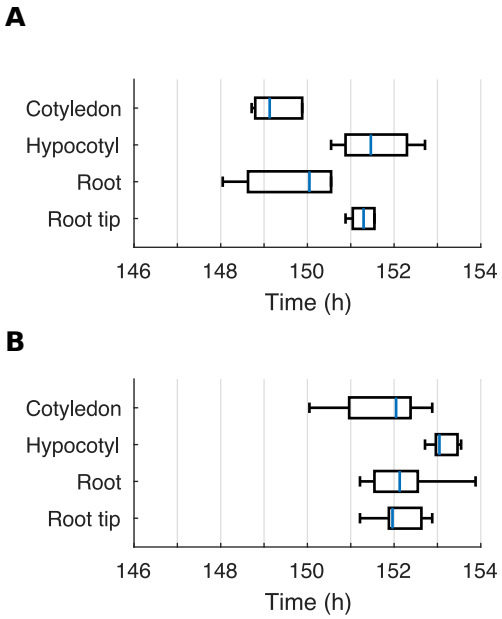

Fig. 5.20 The times of the final observed peaks of *PRR7* expression in different organs are shifted between WL on-off and WL graded LD cycles. (A, B) Times of the final observed peak of *PRR7*::*LUC* expression in different organs for the final observed oscillation under WL on-off (A) or WL graded (B) LD cycles. *N* and *n* are as in Figure 5.18. *N* represents the number of independent experiments and *n* the total number of organs tracked. Box plots indicate the median and upper and lower quartiles, and whiskers the 9th and 91st percentiles of organs scored as rhythmic.

Spatial waves of *PRR7*::*LUC* were also modulated between WL on-off and WL graded LD conditions. The wave of clock gene expression down the root into the root tip was again attenuated (Figure 5.21B, bottom), as for *GI*, *CCA1*, and *PRR9*.

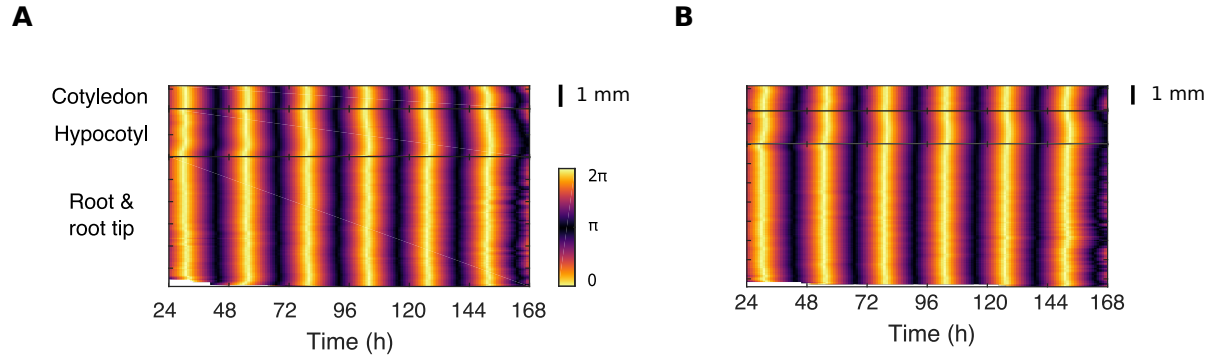

Fig. 5.21 Spatial waves of *PRR7*::*LUC* expression propagate within and between tissues under on-off and WL graded LD cycles. (A, B) Representative phase plot of *PRR7*::*LUC* expression across longitudinal sections of the cotyledon (top), hypocotyl (middle), and root (bottom) of a single seedling under WL on-off (A) and WL graded (B) LD cycles.

5.6 *TOC1* expression under WL graded LD cycles

5.6.1 *TOC1* is bimodal under WL on-off and WL graded LD cycles

We next monitored expression of a reporter for the core clock gene *TOC1*. Unlike the genes imaged thus-far, *TOC1* is not activated by light, and is instead repressed by the light active clock genes [219, 26]. Plots of *TOC1*::*LUC* showed clear rhythmic patterns but atypical waveforms (Figure 5.22). Rhythms peaked at the beginning of the night-time in all organs imaged, as observed previously in whole-plants [12, 216, 190]. However, we also observed a second increase in expression towards the end of the night under both WL on-off and WL graded LD cycles. This can be most clearly seen in the root regions (Figure 5.22 and Figure 5.23), as additional induction of *TOC1*::*LUC* may be present in the aerial organs at dawn (Figure 5.22 and Figure 5.23). Thus, *TOC1* showed complex waveforms in all regions, indicating additional levels of regulation which will require further investigation.

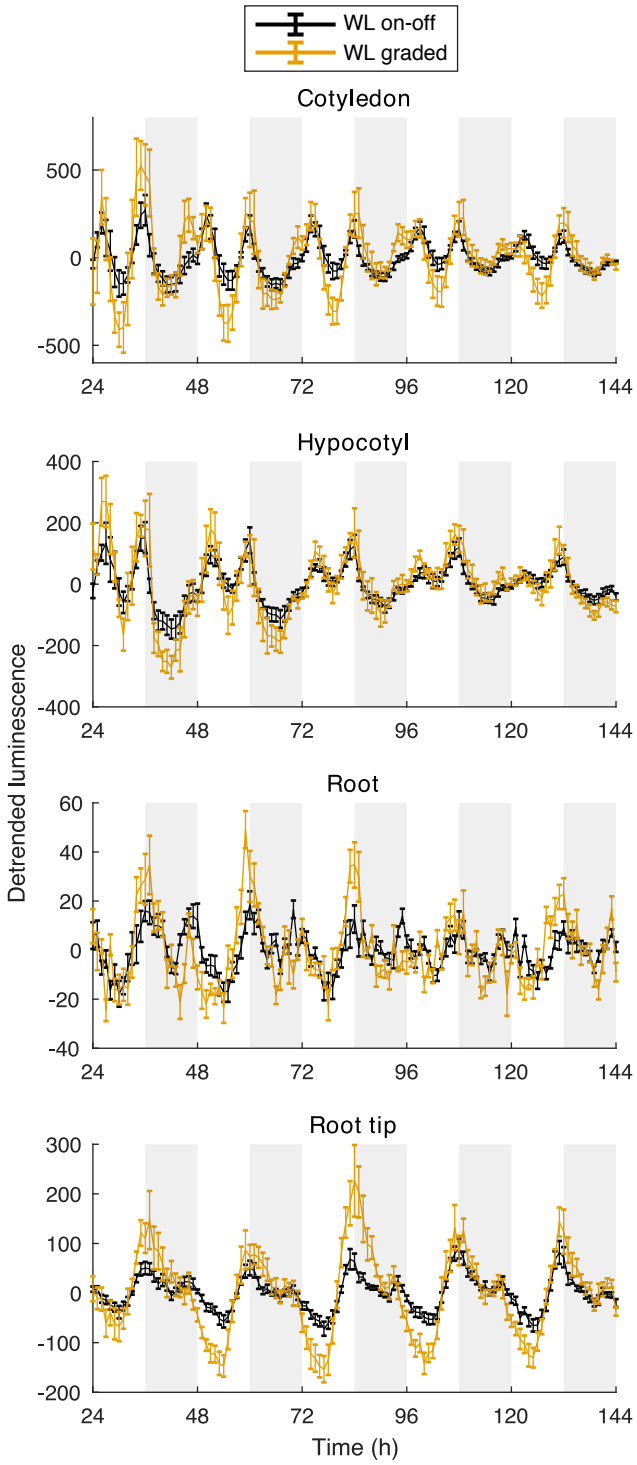

Fig. 5.22 *TOC1* expression under WL on-off and WL graded LD cycles. Expression of *TOC1*::*LUC* from different organs under WL on-off or WL graded LD cycles. Data represent the mean ± standard error of tracked organs. N = 2-3, n = 6-12. N represents the number of independent experiments and n the total number of organs tracked.

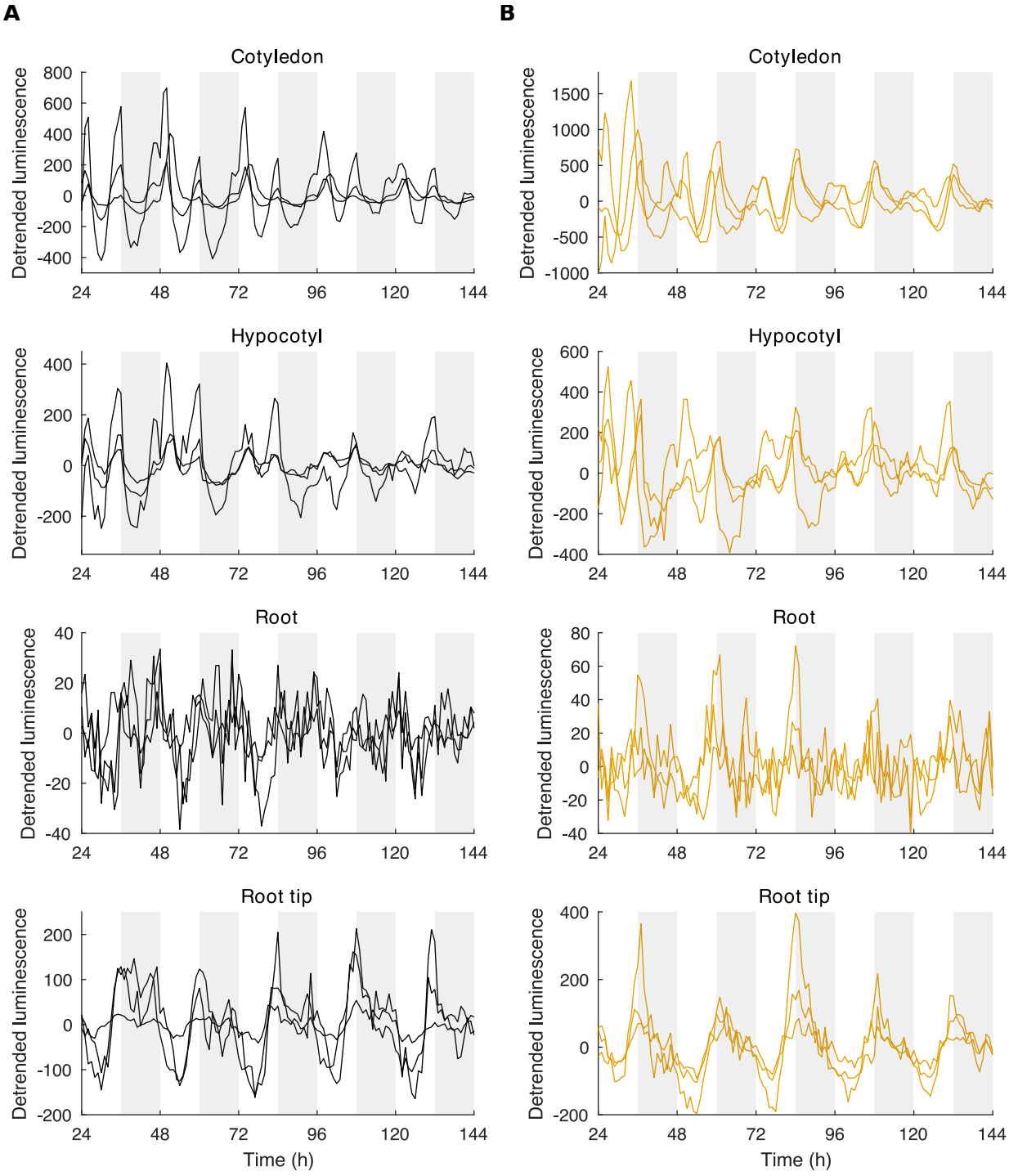

Fig. 5.23 Individual organ oscillations of *TOC1* expression under WL on-off and WL graded LD cycles. Expression of *TOC1*::*LUC* from individual organs under WL on-off (A) or WL graded LD cycles (B). For each condition 3 individual organs were randomly selected and plotted. *N* and *n* are as in Figure 5.22. *N* represents the number of independent experiments and *n* the total number of organs tracked.

5.6.2 *TOC1* peaks after dusk under WL on-off and WL graded LD cycles

We analysed the times of peaks of *TOC1*::*LUC* expression to see if the phasing is altered as for the light activated clock genes. We analysed the peaks occurring at the beginning of the night because its large size made detection feasible. In contrast to *CCA1*, *PRR9*, *PRR7*, and *GI*, differences in the times of peaks of *TOC1*::*LUC* expression were minimal. Under WL on-off LD cycles, although small phase differences may be present, all organs peaked at the beginning of the dark period, and within approximately 1 h of each other (Figure 5.24 and Figure 5.25). Under WL graded LD cycles we observed minimal changes in phase (Figure 5.24 and Figure 5.25).

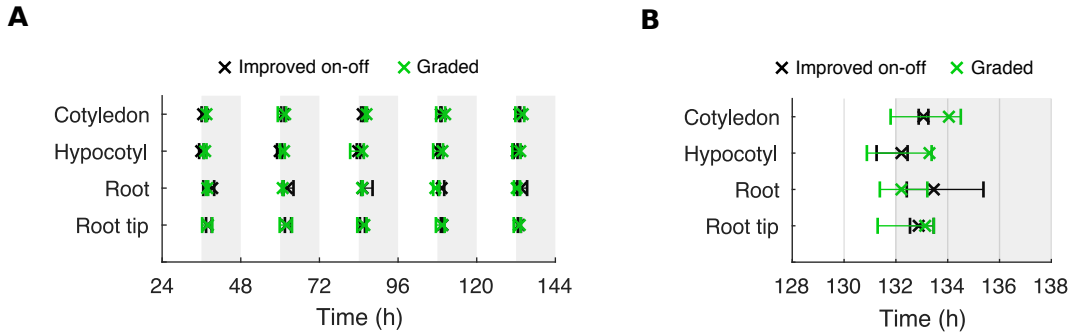

Fig. 5.24 Times of peaks of *TOC1* expression in different organs is comparable between WL on-off and WL graded LD cycles. (A) Times of all observed peaks of *TOC1*::*LUC* expression in different organs under WL on-off or WL graded LD cycles. Plots represent the 25th percentile, median, and the 75th percentile for the peak times of organs scored as rhythmic. (B) Times of the final observed peak of *TOC1*::*LUC* expression under WL on-off or WL graded LD cycles. *N* and *n* are as in Figure 5.22. *N* represents the number of independent experiments and *n* the total number of organs tracked. Box plots indicate the median and upper and lower quartiles, and whiskers the 9th and 91st percentiles of organs scored as rhythmic.

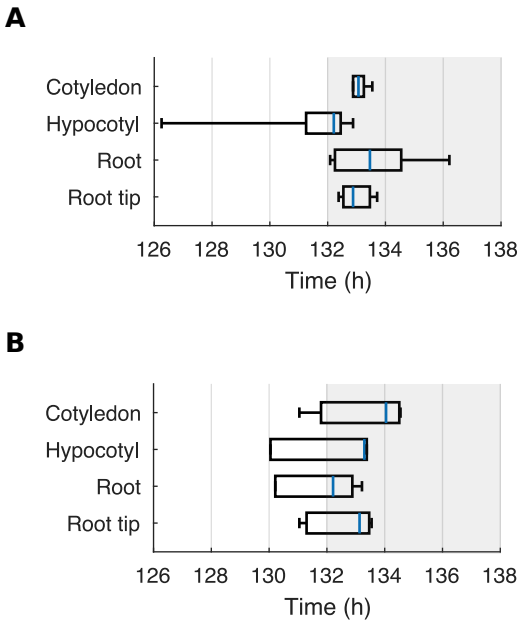

Fig. 5.25 Times of the final observed peaks of *TOC1* expression in different organs is comparable between WL on-off and WL graded LD cycles (A, B) Times of the final observed peak of *TOC1*::*LUC* expression in different organs for the final observed oscillation under WL on-off (A) or WL graded (B) LD cycles. *N* and *n* are as in Figure 5.22. *N* represents the number of independent experiments and *n* the total number of organs tracked. Box plots indicate the median and upper and lower quartiles, and whiskers the 9th and 91st percentiles of organs scored as rhythmic.

5.7 The overall network organisation of the clock under LD cycles

5.7.1 The temporal organisation of the clock is organ-specific under WL on-off LD cycles

By plotting the phase of the core clock genes together we can observe their temporal order. Under WL on-off LD cycles, *CCA1* peaked earliest in the cotyledons, followed very quickly afterwards by *PRR9* and *PRR7*. *GI* peaked later in the day, just prior to the transition to night, followed by *TOC1* at the beginning of the dark period (Figure 5.26A). The phases of these core clock genes expressed in the cotyledon are approximately the same as those observed previously at the whole-plant level [216, 217, 220].

In the hypocotyl, root, and root tip, this order of expression was approximately maintained. However, of note is how expression of *PRR9* and *PRR7* are shifted further in time from *CCA1*. Additionally, expression of *PRR9* and *PRR7* were more shifted from one another in the root regions (Figure 5.26A). Thus, the temporal organisation of the clock was slightly shifted between organs under WL on-off LD cycles.

5.7.2 The temporal organisation of the clock is altered between WL on-off and WL graded LD cycles

As described in subsection 5.2.2, subsection 5.3.2, subsection 5.4.2, and subsection 5.5.2, we observed changes in the phase of many of the imaged clock genes under WL graded LD cycles. Plotting the phases of the genes together we can observe the effect on the temporal order of the network. Under WL graded LD cycles, in the cotyledons *CCA1* again peaked earliest. *PRR9* and *PRR7* peaked next, however, they were more shifted from *CCA1* in comparison to expression in the cotyledon under WL on-off LD cycles (Figure 5.26B). Similarly, the phase advance of *GI* under WL graded LD cycles resulted in it peaking much earlier than *TOC1*. It is interesting to see how together these changes resulted in the clock genes being more evenly staggered across the day under WL graded LD cycles in the cotyledon (Figure 5.26B).

We also observed altered timing of genes in other regions of the seedling. In the hypocotyl, root, and root tip the relative timing of the clock genes was the approximately the same. They did however, differ from the timings in the cotyledon. In the hypocotyl, root, and root tip, expression of *PRR9* and *PRR7* were more shifted from one another, as observed in the root regions under WL on-off LD cycles. Expression of *PRR7* instead peaked at a similar time

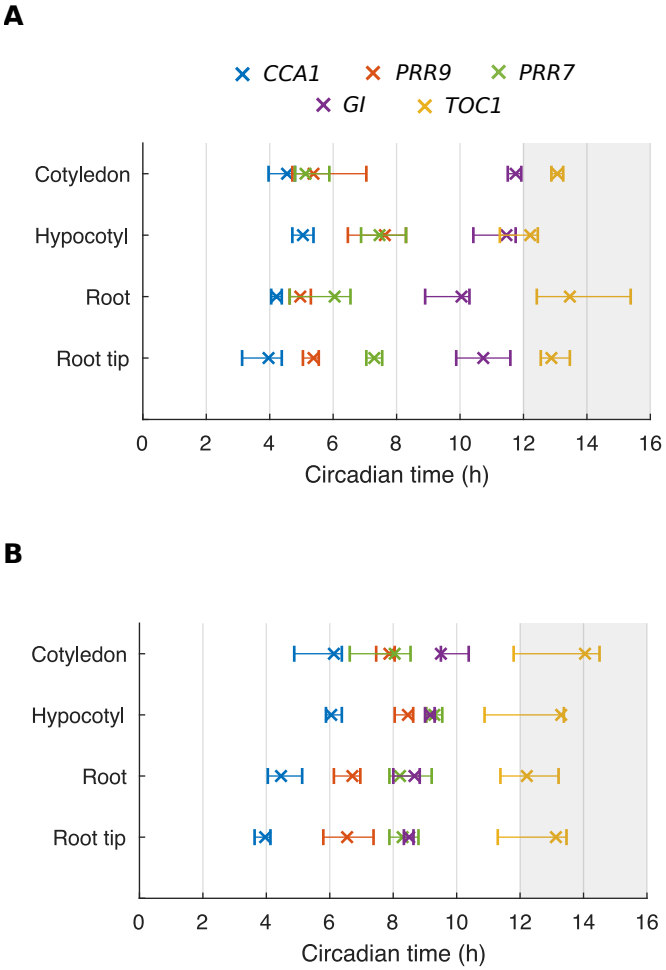

Fig. 5.26 Phase differences in core clock genes occur between organs under WL on-off and WL graded LD cycles. Circadian phase of *CCA1*::*LUC*, *PRR9*::*LUC*, *PRR7*::*LUC*, *GI*::*LUC*, and *TOC1*::*LUC* in different organs under WL on-off (A) or WL graded (B) LD cycles. Circadian phase was determined from the final observed peak of expression. Plots represent the 25th percentile, median, and the 75th percentile for the peak times of organs scored as rhythmic. *N* and *n* are as in Figure 5.10, Figure 5.14, Figure 5.18, Figure 5.6, and Figure 5.22. *N* represents the number of independent experiments and *n* the total number of organs tracked.

as *GI*, which was phase advanced by a number of hours (Figure 5.26B). Thus, under WL graded LD cycles the temporal organisation is altered, but organ-specificity is retained.

5.7.3 The spatial organisation of the clock is similar between clock genes under WL on-off LD cycles

To gain a picture of the overall spatial structure of the clock, it is useful to summarise the results of our sub-tissue analyses with multiple clock genes. We observed a similar spatial structure for the day expressed genes *GI*, *CCA1*, *PRR9*, and *PRR7* under WL on-off LD cycles (Figure 5.9A, Figure 5.13A, Figure 5.17A, and Figure 5.21A). We note here the potential differences.

In the cotyledon, we observed spatial waves of clock gene expression travel from the base to the tip for *GI* and *PRR9* expression (Figure 5.9A and Figure 5.17A, top), but in the opposite direction for *CCA1* and *PRR7* expression under WL on-off LD cycles (Figure 5.13A and Figure 5.21A, top). Spatial waves patterns have previously been reported under LL in leaves of *Arabidopsis*, and were variable in direction. The variation that we observed between genes could in fact be this variation between seedlings. Further spatial-level analyses of our data set will be required to test this hypothesis.

In the hypocotyl, we observed two waves in all genes analysed at the sub-tissue level. One travelled from the cotyledon down the hypocotyl, and the second from the root junction upwards (Figure 5.9A, Figure 5.13A, Figure 5.17A, and Figure 5.21A, middle). In the root also, we observed a wave travel up the root into the hypocotyl in all genes analysed (Figure 5.9A, Figure 5.13A, Figure 5.17A, and Figure 5.21A, bottom). This suggests that these spatial wave patterns are a general property of the clock network under WL on-off LD cycles.

In all clock genes anaylsed at the sub-tissue level we observed a spatial wave travel from the lower root into the root tip under WL on-off LD cycles (Figure 5.9A, Figure 5.13A, Figure 5.17A, and Figure 5.21A, bottom). Intriguingly, we did not observe this wave under RB on-off LD cycles (Figure 5.9A) or under RB constant light in Chapter 3 (Figure 3.5B). This suggests the wave travelling down into the root tip is a product of the higher intensity, WL on-off LD cycles.

5.7.4 The spatial organisation of the clock is modulated between LD conditions in all analysed clock genes

Although generally the spatial structure remained similar between WL on-off and WL graded LD cycles, some modulation of wave direction was observed for all clock genes. Under WL on-off LD cycles we observed a spatial wave travel from the lower root down into the root tip in all clock genes analysed (Figure 5.9A, Figure 5.13A, Figure 5.17A, and Figure 5.21A, bottom). Intriguingly, we did not observe this wave under RB on-off LD cycles (Figure 5.9A) or under RB constant light in Chapter 3 (Figure 3.5B). Additionally, we consistently observed the attenuation of this wave under WL graded LD cycles. By the final day of imaging the wave was no longer visible (Figure 5.9A, Figure 5.13A, Figure 5.17A, and Figure 5.21A, bottom). This demonstrates that both the light type (RB or WL) and the cycle type (on-off or graded) modulates the spatial coordination of the clock system.

5.8 Conclusion and discussion

In this chapter, we report how the temporal and spatial coordination of the clock changed under different LD conditions. The phasing of many core clock genes was altered by the both light wavelength and intensity (RB on-off versus WL on-off) and the light cycle type (WL on-off versus WL graded). Spatial waves of circadian clock gene expression propagated within and between the organs, and were modulated between the conditions. Thus, the temporal and spatial coordination of the clock is flexible to the environment, even under LD cycles.

In Chapter 3, we reported phase differences and spatial waves of clock gene expression within and between organs under RB on-off LD cycles. However, it remained unclear whether these phenomenon were relevant under more realistic conditions, or a consequence of weak entrainment. Our observation of these dynamics under more realistic LD conditions confirms them to be a natural property of the circadian system in plants. It is intriguing that the spatial structure varied slightly depending on the clock gene imaged. Such variation in the structure has also been observed in the mammalian SCN. Rhythms of the core clock gene *PERIOD 1* (*PER1*) and *PER2* in SCN slices showed spatially organised coherent waves travelling from the dorsal to the ventral region [196, 221]. However, rhythms of cytosolic free calcium ions, which are a direct output of the clock, did not show a wave pattern across the SCN. Instead, shorter, local phase waves could be observed [222].

It is notable that the core clock genes responded qualitatively differently to changes in light cycles. Differences in the regulation of the clock genes could account for these distinct

responses. For example, although *CCA1*, *PRR9*, *PRR7*, and *GI* are all transcriptionally activated by light, under constant light *CCA1*, *PRR9*, and *PRR7* are phased to the morning whereas *GI* is phased to the evening [184, 218, 88, 21, 22]. The difference in phase could account for how *GI* responds to graded LD cycles by peaking earlier, whereas the morning phased genes are delayed. This suggests the phase is a product of the genetic and light regulation. In future experiments it will be important to test more differentially phased clock genes, such as the night expressed *ELF3*, *ELF4*, and *LUX*, to better understand how genetic and light regulation interact during entrainment.

Our luciferase imaging approach enabled a high spatial and temporal resolution, revealing previously unseen dynamics under LD cycles. However, features of the luciferase timeseries should be interpreted with care. Firstly, comparisons of luciferase data and endogenous RNA timeseries in a previous study revealed that the luciferase signal peaks significantly later [12]. This is likely due to the translation time and the stability of the *LUC* protein. Secondly, there may be a metabolic effect of the luciferase reporter enzyme. Controls using a constitutively expressed *35S*::*LUC* reporter line showed approximately a 15 % increase in signal at dawn [12]. Alternative molecular methods will therefore be required to further validate our results.

An appealing alternative method would be the use of fluorescent reporter proteins. Fluorescent reporters together with time-lapse microscopy enable tracking of clock gene expression at the single cell level with high temporal resolution. Although technically challenging this has been done previously in *Arabidopsis* [4, 120, 142] and would allow us to resolve the finer-grain spatial structure that our organ-level analysis missed. For example, the substructure within the root, with multiple waves (e.g. Figure 5.9), was not captured by our arbitrarily defined root and root tip regions of interest (e.g. Figure 5.7). Further, the bi-modal expression of *TOC1* at the organ-level (Figure 5.22) could represent two sub-populations of cells with unimodal expression. To resolve such ambiguities and understand the full complexity within the circadian system it will be important to employ single cell imaging methods.

Our more natural LD cycles represent a first step towards understanding how clocks behave under realistic environmental conditions. However, in the field plants will be under much more complex environments. For example, the root will be exposed to different light levels in comparison to the shoot due to the soil (Figure 1.7). Understanding how clocks entrain and coordinate under these more complex environments will be important for plant research. Recently a couple of technical advancements have been made in this direction, helping to bridge the gap between imaging power and physiological relevance. The GLO-Roots systems allows imaging of luminescence at sub-tissue resolution in soil, however, images are limited to the root system [223]. A second system, developed by Bordage et al., utilised robotics to allow for simultaneous imaging of roots and shoots, whilst not exposing

roots to light [111]. However, here only organ-level resolution is achieved. The development of methods with coverage of all organs under physiologically relevant conditions, with sub-tissue, or cellular resolution, will be important for the future study of clock coordination.

To conclude, our results show that the coordination of rhythms through local cell-to-cell communication remains active under more natural LD cycles. However, the temporal and spatial structure of the clock is altered under different LD conditions.

Chapter 6

Conclusions and outlook

6.1 Conclusions

In this thesis we have demonstrated a decentralised mechanism for the coordination of circadian rhythms, consisting of locally set periods and cell-to-cell communication. We began by examining rhythms in all the major individual organs of a seedling to inspect the spatial structure of periods and phases. The cotyledon and hypocotyl ran faster than the root regions, but the tip of the root ran faster than the middle region of the root under LL. To understand how plants coordinate these individual clocks, despite the differences, we then analysed rhythms at the sub-tissue level. We found spatial phase waves propagated within and between organs. Modelling and experiments show that local cell-to-cell coupling can explain our results, including complex synchronisation patterns in plants that have never seen an entraining signal. Then, by manipulation of environmental inputs, we are able to modulate the waves in a predictable manner by locally altering periods. Thus we propose a decentralised model of circadian coordination with local inputs integrated by cell-to-cell signalling. Finally, we demonstrated the relevance of this model under more realistic environmental conditions. Preliminary results in Chapter 5 demonstrated the modulation of the spatial structure and the reorganisation of the clock network under more realistic LD cycles. Here, we summarise the key findings, and the caveats, before discussing them in the wider context of plant biology.

In Chapter 3, we used a mixture of high resolution luciferase imaging and mathematical modelling to show that local cell-to-cell coupling coordinates individual circadian clocks. Our imaging approach allowed us to observe previously unseen circadian dynamics but also had limitations. To achieve sub-tissue level resolution, we adapted luciferase imaging methods to younger seedlings (subsection 2.2.1). Work in more mature plants has hypothesised long-distance mechanisms of circadian coordination [142, 129], which we did not observe here. In future work it will be important to develop methods for imaging the clock at high

resolution in larger plants. This will allow us to ascertain whether different mechanisms of circadian coordination operate together, and how they interact.

Our simple mathematical model was based on the Kuramoto framework [183]. The Kuramoto model describes the phase of each individual clock of the system by a single differential equation (subsection 2.5.1). The molecular details of the network, as well as amplitudes and expression levels of the oscillations are ignored for the sake of simplicity. Our simple model was able to capture the synchronisation dynamics that we observed under a variety of entrainment conditions. However, further experiments with reporters for other core clock genes in Chapter 5 revealed gene specific effects which can not be captured by such a modelling approach. To better understand the overall spatial structure of the clock network the development of models including the full gene regulatory network will be crucial.

In Chapter 4 we altered periods locally by manipulating the environmental inputs and demonstrated that this drives spatial waves of clock gene expression. Genetic and chemical perturbations to input pathways demonstrated that these period differences were set under LL by exogenous and endogenous environmental inputs. However, in the field clocks exist under LD cycles, not LL (subsection 1.3.7). Further, the number, and type of environmental inputs to clocks will be different under natural conditions (subsection 1.3.7 and Figure 1.7). It therefore remained to be seen how relevant period effects under constant light are to the coordination of clocks in the field. In future work, and indeed more generally for the study of clocks, our understanding will benefit greatly from probing clock regulation under environmental cycles.

In Chapter 5 we began to address this limitation by monitoring clock gene expression under more realistic environmental cycles. We imaged luciferase reporters for multiple core clock genes under two increasingly realistic LD conditions and in both cases found altered spatial and temporal coordination. Our results were sufficient to demonstrate the flexibility of coordination in the circadian system, even under LD cycles. However, the observation of gene specific effects means that our understanding remains limited by the number of genes we imaged. Further experiments with reporters for other clock genes, and manipulations to the network, will help to build an understanding of spatial and temporal coordination under physiological conditions. Mathematical modelling will also play an important part in developing this understanding.

Beyond the availability of genetic data, our understanding of the clock system in the field remains limited by our laboratory conditions, which still represents a simplification (subsection 1.3.7). However, a decentralised mechanism with organ specific inputs is likely to only be more relevant under a variable and complex natural environment. We look forward to our ideas being put to the test by ourselves and others, in the laboratory or field.

6.2 Outlook

As discussed, our work advances the field of circadian research in a few key areas. It is interesting to place these advances in the wider context of developmental biology and hypothesise on where the direction our work, together with the recent work of others, may lead the field. We hypothesise that the clock acts as a multi-scale developmental timekeeper (Figure 6.1) [2]. To enable this the clock is plastic to the environment (Figure 6.2, left), coordinates internally via cell-to-cell signalling (Figure 6.2, centre), and controls distinct outputs in different tissues (Figure 6.2, right).

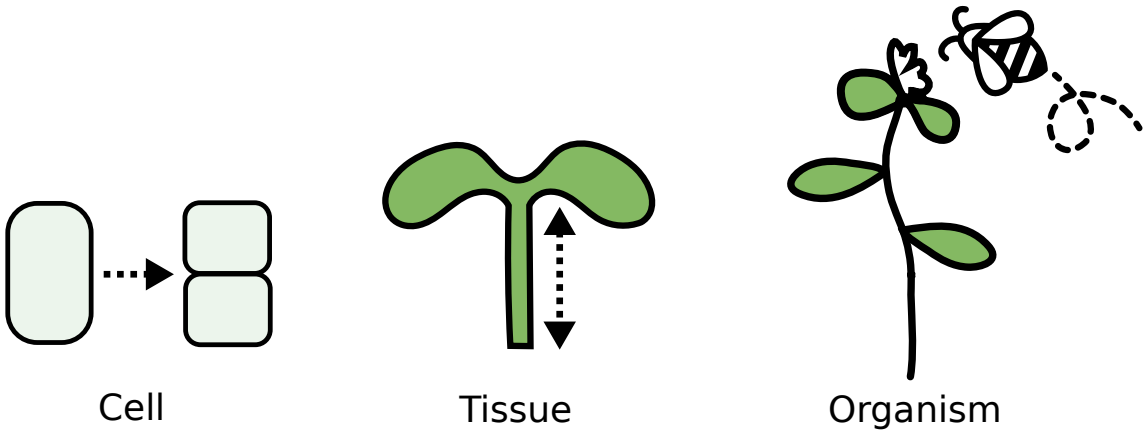

Fig. 6.1 The circadian clock coordinates plant development at multiple scales. The clock regulates development at the cellular level, e.g. by timing cell division (left), at the tissue level, e.g. by timing hypocotyl growth (middle), and coordinates the whole plant's interactions with its ecosystem, e.g. by modulating interactions with pollinators (right).

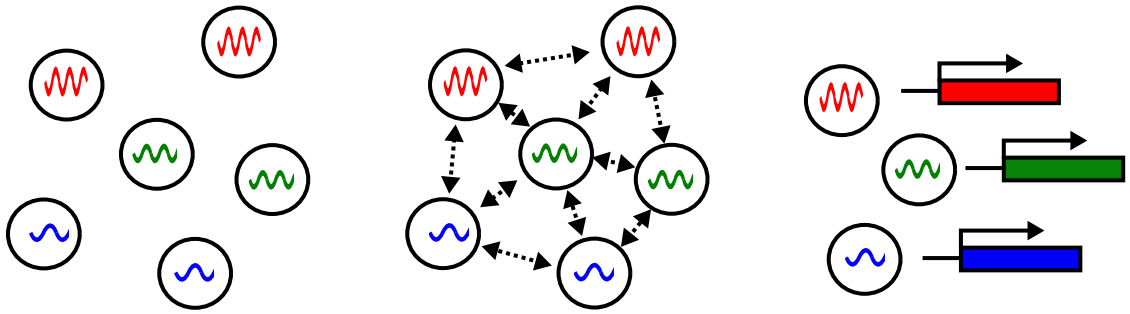

Fig. 6.2 The *Arabidopsis* circadian clock is a decentralised coordinator of development. We hypothesise that to enable such a range of control, the clock runs at different speeds in individual cells (left), coordinates internally via cell-to-cell signalling (middle), and controls distinct outputs in different tissues (right).

Plasticity of period and phase appears to be a common property in circadian clocks across organisms [224]. In Chapter 4, we demonstrated that this extends to within *Arabidopsis* seedlings, causing internal differences in period and phase (Figure 6.2, left). A fundamental challenge in biology is to understand the link between form and function; why has the *Arabidopsis* clock evolved to be plastic? It has previously been shown that plasticity in the fungal circadian clock increases the robustness of oscillations in LD cycles [225]. It is also interesting to hypothesise whether the measured differences in rhythms have other physiological effects. For example, if variations in clock amplitude or phase effects division timing due to the coupling of the clock to the cell cycle. Further investigation will reveal whether these differences in timing allow for different phasing of developmental outputs.

Plasticity creates differences in period and phase within a plant. However, for many developmental processes, cells and tissues must act in a coordinated way. Oscillations must therefore coordinate in order to time development (Figure 6.2, middle). A decentralised structure with organ-specific inputs to clocks that are coupled together could allow some plasticity whilst ensuring synchronised developmental control. In the future, it will be important to better understand the importance of this design principle in terms of development.

In addition to entraining to different environments, clocks specialise in terms of their outputs. It has been previously shown that the clock in different tissues regulates distinct sets of target genes (Figure 6.2, right). This causes the appropriate change in physiology in that tissue (subsection 1.4.2). We hypothesise that it is these three functions together, plasticity in period and phase, cell-to-cell coordination, and specialisation of target regulation that enables the clock to act as a multi-scale developmental timekeeper (Figure 6.1).

The circadian clock has for some time been a promising target for genetic engineering in crops. The potential is exemplified by the fact that the domestication of tomatoes and barley have in large part been driven by selection on the circadian clock, altering their development [226, 227]. However, despite our impressive molecular understanding of the clock, derived mainly from experiments at the whole-organism level, direct targets for manipulation are not obvious. As development, and circadian timing, happens at the level of cells and tissues, in order to improve crop productivity efforts should be directed here. Our work in this thesis contributes to understanding how circadian clocks function at this scale. We hope that in some small way this will help in allowing us to engineer development with the clock at greater precision.

References

[1] Greenwood M, Domijan M, Gould PD, Hall AJ, and Locke JC. Coordinated circadian timing through the integration of local inputs in Arabidopsis thaliana. *PLoS Biology*, 17(8):e3000407, 2019.

[2] Greenwood M and Locke JC. The circadian clock coordinates plant development through specificity at the tissue and cellular level. *Current Opinion in Plant Biology*, 53:65–72, 2020.

[3] Rees H, Duncan S, Gould P, Wells R, Greenwood M, Brabbs T, and Hall A. A high-throughput delayed fluorescence method reveals underlying differences in the control of circadian rhythms in Triticum aestivum and Brassica napus. *Plant Methods*, 15(1):51, 2019.

[4] Gould PD, Domijan M, Greenwood M, Tokuda IT, Rees H, Kozma-Bognar L, Hall AJ, and Locke JC. Coordination of robust single cell rhythms in the Arabidopsis circadian clock via spatial waves of gene expression. *eLife*, 7:e31700, 2018.

[5] Bell-Pedersen D, Cassone VM, Earnest DJ, Golden SS, Hardin PE, Thomas TL, and Zoran MJ. Circadian rhythms from multiple oscillators: lessons from diverse organisms. *Nature Reviews Genetics*, 6(7):544–556, 2005.

[6] Green RM, Tingay S, Wang ZY, and Tobin EM. Circadian rhythms confer a higher level of fitness to Arabidopsis plants. *Plant Physiology*, 129(2):576–84, 2002.

[7] Dodd AN, Salathia N, Hall A, Kevei E, Toth R, Nagy F, Hibberd JM, Millar AJ, Webb AAR, Kévei E, *et al.* Plant Circadian Clocks Increase Photosynthesis, Growth, Survival, and Competitive Advantage. *Science*, 309(5734):630–633, 2005.

[8] Young MW and Kay SA. Time zones: a comparative genetics of circadian clocks. *Nature Reviews Genetics*, 2(9):702–715, 2001.

[9] McClung CR. The Plant Circadian Oscillator. *Biology*, 8(1):14, 2019.

[10] Cheng P, Yang Y, and Liu Y. Interlocked feedback loops contribute to the robustness of the Neurospora circadian clock. *Proceedings of the National Academy of Sciences*, 98(13):7409–7413, 2002.

[11] Shalit-Kaneh A, Kumimoto RW, Filkov V, and Harmer SL. Multiple feedback loops of the Arabidopsis circadian clock provide rhythmic robustness across environmental conditions. *Proceedings of the National Academy of Sciences of the United States of America*, 115(27):7147–7152, 2018.

[12] Edwards KD, Akman OE, Knox K, Lumsden PJ, Thomson AW, Brown PE, Pokhilko A, Kozma-Bognar L, Nagy F, Rand DA, *et al.* Quantitative analysis of regulatory flexibility under changing environmental conditions. *Molecular Systems Biology*, 6(1):424, 2010.

[13] Troein C, Locke JCW, Turner MS, and Millar AJ. Weather and Seasons Together Demand Complex Biological Clocks. *Current Biology*, 19(22):1961–4, 2009.

[14] Pittendrigh CS. Circadian Systems: Entrainment. In *Biological Rhythms*, pages 95–124. Springer US, Boston, MA, 1981.

[15] Chaix A, Zarrinpar A, and Panda S. The circadian coordination of cell biology. *Journal of Cell Biology*, 215(1):15–25, 2016.

[16] Covington MF, Maloof JN, Straume M, Kay SA, and Harmer SL. Global transcriptome analysis reveals circadian regulation of key pathways in plant growth and development. *Genome Biology*, 9(8):R130, 2008.

[17] Somers DE, Devlin PF, and Kay SA. Phytochromes and cryptochromes in the entrainment of the Arabidopsis circadian clock. *Science*, 282(5393):1488–90, 1998.

[18] Kim WY, Fujiwara S, Suh SS, Kim J, Kim Y, Han L, David K, Putterill J, Nam HG, and Somers DE. ZEITLUPE is a circadian photoreceptor stabilized by GIGANTEA in blue light. *Nature*, 449(7160):356–360, 2007.

[19] Tóth R, Kevei E, Hall A, Millar AJ, Nagy F, and Kozma-Bognár L. Circadian clock-regulated expression of phytochrome and cryptochrome genes in Arabidopsis. *Plant Physiology*, 127(4):1607–16, 2001.

[20] Winfree AT. *The geometry of biological time*. Springer-Verlag, New York, 2 edition, 1960. ISBN 9783662224922.

[21] Schaffter R, Ramsay N, Corden S, Putterill J, Carré IA, Samach A, Schaffer R, Coupland G, Ramsay N, Samach A, *et al.* The late elongated hypocotyl Mutation of Arabidopsis Disrupts Circadian Rhythms and the Photoperiodic Control of Flowering. *Cell*, 93(7):1219–1229, 1998.

[22] Wang ZYY and Tobin EM. Constitutive expression of the CIRCADIAN CLOCK ASSOCIATED 1 (CCA1) gene disrupts circadian rhythms and suppresses its own expression. *Cell*, 93(7):1207–17, 1998.

[23] Mizoguchi T, Wheatley K, Hanzawa Y, Wright L, Mizoguchi M, Song HRR, Carré IA, and Coupland G. LHY and CCA1 Are Partially Redundant Genes Required to Maintain Circadian Rhythms in Arabidopsis. *Developmental Cell*, 2(5):629–641, 2002.

[24] Matsushika A, Makino S, Kojima M, and Mizuno T. Circadian waves of expression of the APRR1/TOC1 family of pseudo-response regulators in Arabidopsis thaliana: Insight into the plant circadian clock. *Plant and Cell Physiology*, 41(9):1002–1012, 2000.

[25] Khanna R, Shen Y, Toledo-Ortiz G, Kikis EA, Johannesson H, Hwang YS, and Quail PH. Functional profiling reveals that only a small number of phytochrome-regulated early-response genes in Arabidopsis are necessary for optimal deetiolation. *The Plant Cell*, 18(9):2157–71, 2006.

[26] Nakamichi N, Kiba T, Henriques R, Mizuno T, Chua NH, and Sakakibara H. PSEUDO-RESPONSE REGULATORS 9, 7, and 5 are transcriptional repressors in the Arabidopsis circadian clock. *The Plant Cell*, 22(3):594–605, 2010.

[27] Gendron JM, Pruneda-Paz JL, Doherty CJ, Gross AM, Kang SE, and Kay SA. Arabidopsis circadian clock protein, TOC1, is a DNA-binding transcription factor. *Proceedings of the National Academy of Sciences of the United States of America*, 109(8):3167–72, 2012.

[28] Huang W, Pérez-García P, Pokhilko A, Millar AJ, Antoshechkin I, Riechmann JL, and Mas P. Mapping the core of the Arabidopsis circadian clock defines the network structure of the oscillator. *Science*, 336(6077):75–9, 2012.

[29] Adams S, Manfield I, Stockley P, Carre IA, Dowidar N, and Dunaway D. Revised Morning Loops of the Arabidopsis Circadian Clock Based on Analyses of Direct Regulatory Interactions. *PLoS ONE*, 10(12):e0143943, 2015.

[30] Gould PD, Locke JCW, Larue C, Southern MM, Davis SJ, Hanano S, Moyle R, Milich R, Putterill J, Millar AJ, *et al.* The Molecular Basis of Temperature Compensation in the Arabidopsis Circadian Clock. *The Plant Cell*, 18:1177–1187, 2006.

[31] Martin-Tryon EL, Kreps JA, and Harmer SL. GIGANTEA acts in blue light signaling and has biochemically separable roles in circadian clock and flowering time regulation. *Plant Physiology*, 143(1):473–86, 2007.

[32] Más P, Kim WY, Somers DE, and Kay SA. Targeted degradation of TOC1 by ZTL modulates circadian function in Arabidopsis thaliana. *Nature*, 426(6966):567–570, 2003.

[33] Nusinow DA, Helfer A, Hamilton EE, King JJ, Imaizumi T, Schultz TF, Farré EM, and Kay SA. The ELF4-ELF3-LUX complex links the circadian clock to diurnal control of hypocotyl growth. *Nature*, 475:398–402, 2011.

[34] Li Y, Huang Y, Bergelson J, Nordborg M, and Borevitz JO. Association mapping of local climate-sensitive quantitative trait loci in Arabidopsis thaliana. *Proceedings of the National Academy of Sciences of the United States of America*, 107(49):21199–204, 2010.

[35] Box M, Huang B, Domijan M, Jaeger K, Khattak A, Yoo S, Sedivy E, Jones D, Hearn T, Webb A, *et al.* ELF3 Controls Thermoresponsive Growth in Arabidopsis. *Current Biology*, 25(2):194–199, 2015.

[36] Ezer D, Jung JH, Lan H, Biswas S, Gregoire L, Box MS, Charoensawan V, Cortijo S, Lai X, Stöckle D, *et al.* The Evening Complex coordinates environmental and endogenous signals in Arabidopsis. *Nature Plants*, 3:17087, 2017.

[37] Mizuno T, Nomoto Y, Oka H, Kitayama M, Takeuchi A, Tsubouchi M, and Yamashino T. Ambient temperature signal feeds into the circadian clock transcriptional circuitry through the EC night-time repressor in Arabidopsis thaliana. *Plant & Cell Physiology*, 55(5):958–76, 2014.

[38] Yu JW, Rubio V, Lee NY, Bai S, Lee SY, Kim SS, Liu L, Zhang Y, Irigoyen ML, Sullivan JA, *et al.* COP1 and ELF3 Control Circadian Function and Photoperiodic Flowering by Regulating GI Stability. *Molecular Cell*, 32(5):617–630, 2008.

[39] Kim Y, Lim J, Yeom M, Kim H, Kim J, Wang L, Kim WY, Somers DE, and Nam HG. ELF4 Regulates GIGANTEA Chromatin Access through Subnuclear Sequestration. *Cell Reports*, 3(3):671–677, 2013.

[40] Doyle MR, Davis SJ, Bastow RM, McWatters HG, Kozma-Bognár L, Nagy F, Millar AJ, and Amasino RM. The ELF4 gene controls circadian rhythms and flowering time in Arabidopsis thaliana. *Nature*, 419(6902):74–77, 2002.

[41] Hazen SP, Schultz TF, Pruneda-Paz JL, Borevitz JO, Ecker JR, and Kay SA. LUX ARRHYTHMO encodes a Myb domain protein essential for circadian rhythms. *Proceedings of the National Academy of Sciences of the United States of America*, 102(29):10387–92, 2005.

[42] Hicks KA, Albertson TM, and Wagner DR. EARLY FLOWERING3 encodes a novel protein that regulates circadian clock function and flowering in Arabidopsis. *The Plant Cell*, 13(6):1281–92, 2001.

[43] Hsu PY, Devisetty UK, and Harmer SL. Accurate timekeeping is controlled by a cycling activator in Arabidopsis. *eLife*, 2:e00473, 2013.

[44] Farinas B and Mas P. Functional implication of the MYB transcription factor RVE8/LCL5 in the circadian control of histone acetylation. *The Plant Journal*, 66(2):318–329, 2011.

[45] Rawat R, Takahashi N, Hsu PY, Jones MA, Schwartz J, Salemi MR, Phinney BS, and Harmer SL. REVEILLE8 and PSEUDO-REPONSE REGULATOR5 form a negative feedback loop within the arabidopsis circadian clock. *PLoS Genetics*, 7(3):e1001350, 2011.

[46] Nakamichi N, Kiba T, Kamioka M, Suzukie T, Yamashino T, Higashiyama T, Sakakibara H, and Mizuno T. Transcriptional repressor PRR5 directly regulates clock-output pathways. *Proceedings of the National Academy of Sciences of the United States of America*, 109(42):17123–17128, 2012.

[47] Liu TL, Newton L, Liu MJ, Shiu SH, and Farré EM. A G-box-like motif is necessary for transcriptional regulation by circadian pseudo-response regulators in arabidopsis 1. *Plant Physiology*, 170(1):528–539, 2016.

[48] Yakir E, Hilman D, Hassidim M, and Green RM. CIRCADIAN CLOCK ASSOCIATED1 Transcript Stability and the Entrainment of the Circadian Clock in Arabidopsis. *Plant Physiology*, 145(3):925–932, 2007.

[49] Hernando CE, Romanowski A, and Yanovsky MJ. Transcriptional and post-transcriptional control of the plant circadian gene regulatory network. *Biochimica et Biophysica Acta (BBA) - Gene Regulatory Mechanisms*, 1860(1):84–94, 2017.

[50] Du S, Chen L, Ge L, and Huang W. A Novel Loop: Mutual Regulation Between Epigenetic Modification and the Circadian Clock. *Frontiers in Plant Science*, 10:22, 2019.

[51] Seo PJ and Mas P. Multiple Layers of Posttranslational Regulation Refine Circadian Clock Activity in Arabidopsis. *The Plant Cell*, 26(1):79–87, 2014.

[52] Foo M, Somers DE, and Kim PJ. Kernel Architecture of the Genetic Circuitry of the Arabidopsis Circadian System. *PLoS Computational Biology*, 12(2):e1004748, 2016.

[53] De Caluwé J, Xiao Q, Hermans C, Verbruggen N, Leloup JC, and Gonze D. A Compact Model for the Complex Plant Circadian Clock. *Frontiers in Plant Science*, 7:74, 2016.

[54] Tokuda IT, Akman OE, and Locke JC. Reducing the complexity of mathematical models for the plant circadian clock by distributed delays. *Journal of Theoretical Biology*, 463:155–166, 2019.

[55] Jones MA, Morohashi K, Grotewold E, and Harmer SL. Arabidopsis JMJD5/JMJ30 Acts Independently of LUX ARRHYTHMO Within the Plant Circadian Clock to Enable Temperature Compensation. *Frontiers in Plant Science*, 10:57, 2019.

[56] Devlin PF and Kay SA. Circadian Photoperception. *Annual Review of Physiology*, 63(1):677–694, 2001.

[57] Covington MF, Panda S, Xing Liang Liu, Strayer CA, Wagner DR, and Kay SA. ELF3 modulates resetting of the circadian clock in Arabidopsis. *The Plant Cell*, 13(6):1305–1315, 2001.

[58] Millar AJ. Input signals to the plant circadian clock. *Journal of Experimental Botany*, 55(395):277–283, 2004.

[59] Sanchez SE, Rugnone ML, and Kay SA. Light Perception: A Matter of Time, 2020.

[60] Millar AJ, Straume M, Chory J, Chua NH, Kay SA, Más P, Panda S, Kreps JA, and Kay SA. The regulation of circadian period by phototransduction pathways in Arabidopsis. *Science*, 267(5201):1163–1166, 1995.

[61] Jones MA, Hu W, Litthauer S, Lagarias JC, and Harmer SL. A Constitutively Active Allele of Phytochrome B Maintains Circadian Robustness in the Absence of Light. *Plant Physiology*, 169(1):814–825, 2015.

[62] Somers DE, Kim WY, and Geng R. The F-box protein ZEITLUPE confers dosage-dependent control on the circadian clock, photomorphogenesis, and flowering time. *The Plant Cell*, 16(3):769–82, 2004.

[63] Fehér B, Kozma-Bognár L, Kevei É, Hajdu A, Binkert M, Davis SJ, Schäfer E, Ulm R, Nagy F, Zs Fehé B, *et al.* Functional interaction of the circadian clock and UV RESISTANCE LOCUS 8-controlled UV-B signaling pathways in Arabidopsis thaliana. *The Plant Journal*, 67(1):37–48, 2011.

[64] Litthauer S, Battle MW, Lawson T, and Jones MA. Phototropins maintain robust circadian oscillation of PSII operating efficiency under blue light. *The Plant Journal*, 83(6):1034–1045, 2015.

[65] Litthauer S, Battle MW, and Jones MA. Phototropins do not alter accumulation of evening-phased circadian transcripts under blue light. *Plant Signaling & Behavior*, 11(2):e1126029, 2016.

[66] Bognár LK, Hall A, Adám E, Thain SC, Nagy F, and Millar AJ. The circadian clock controls the expression pattern of the circadian input photoreceptor, phytochrome B. *Proceedings of the National Academy of Sciences of the United States of America*, 96(25):14652–7, 1999.

[67] Harmer SL, Hogenesch JB, Straume M, Chang HS, Han B, Zhu T, Wang X, Kreps JA, and Kay SA. Orchestrated transcription of key pathways in Arabidopsis by the circadian clock. *Science*, 290(5499):2110–3, 2000.

[68] Sharrock RA and Clack T. Patterns of Expression and Normalized Levels of the Five Arabidopsis Phytochromes. *Plant Physiology*, 130(1):442–56, 2002.

[69] Somers DE and Quail PH. Temporal and spatial expression patterns of PHYA and PHYB genes in Arabidopsis. *The Plant Journal*, 7(3):413–427, 1995.

[70] Somers DE, Quail PH, Elich T, Fagan M, and Chory J. Phytochrome-Mediated Light Regulation of PHYA- and PHYB-GUS Transgenes in Arabidopsis thaliana Seedlings. *Plant Physiology*, 107(2):523–534, 1995.

[71] Hall A, Kozma-Bognár L, Tóth R, Nagy F, and Millar AJ. Conditional circadian regulation of PHYTOCHROME A gene expression. *Plant Physiology*, 127(4):1808–18, 2001.

[72] Yamaguchi R, Nakamura M, Mochizuki N, Kay SA, and Nagatani A. Light-dependent translocation of a phytochrome B-GFP fusion protein to the nucleus in transgenic Arabidopsis. *Journal of Cell Biology*, 145(3):437–445, 1999.

[73] Kircher S, Gil P, Kozma-Bognár L, Fejes E, Speth V, Husselstein-Muller T, Bauer D, Ádám É, Schäfer E, and Nagy F. Nucleocytoplasmic partitioning of the plant photoreceptors phytochrome A, B, C, D, and E is regulated differentially by light and exhibits a diurnal rhythm. *Plant Cell*, 14(7):1541–1555, 2002.

[74] Huang H, McLoughlin KE, Sorkin ML, Burgie ES, Bindbeutel RK, Vierstra RD, and Nusinow DA. PCH1 regulates light, temperature, and circadian signaling as a structural component of phytochrome B-photobodies in Arabidopsis. *Proceedings of the National Academy of Sciences of the United States of America*, 116(17):8603–8608, 2019.

[75] Liu X, Covington MF, Fankhauser C, Chory J, and Wagner DR. ELF3 encodes a circadian clock-regulated nuclear protein that functions in an Arabidopsis PHYB signal transduction pathway. *Plant Cell*, 13(6):1293–1304, 2001.

[76] Yeom M, Kim H, Lim J, Shin AY, Hong S, Kim JI, and Gil Nam H. How Do Phytochromes Transmit the Light Quality Information to the Circadian Clock in Arabidopsis? *Molecular Plant*, 7(11):1701–04, 2014.

[77] Huang H, Alvarez S, Bindbeutel R, Shen Z, Naldrett MJ, Evans BS, Briggs SP, Hicks LM, Kay SA, and Nusinow DA. Identification of Evening Complex Associated Proteins in Arabidopsis by Affinity Purification and Mass Spectrometry. *Molecular & cellular proteomics : MCP*, 15(1):201–17, 2016.

[78] Jung JH, Domijan M, Klose C, Biswas S, Ezer D, Gao M, Khattak AK, Box MS, Charoensawan V, Cortijo S, *et al.* Phytochromes function as thermosensors in Arabidopsis. *Science*, 354(6314):886–889, 2016.

[79] Nohales MA, Liu W, Duffy T, Nozue K, Sawa M, Pruneda-Paz JL, Maloof JN, Jacobsen SE, and Kay SA. Multi-level Modulation of Light Signaling by GIGANTEA Regulates Both the Output and Pace of the Circadian Clock. *Developmental Cell*, 49(6):840–851, 2019.

[80] Somers DE, Schultz TF, Milnamow M, and Kay SA. ZEITLUPE Encodes a Novel Clock-Associated PAS Protein from Arabidopsis. *Cell*, 101(3):319–329, 2000.

[81] Nelson DC, Lasswell J, Rogg LE, Cohen MA, and Bartel B. FKF1, a clock-controlled gene that regulates the transition to flowering in Arabidopsis. *Cell*, 101(3):331–340, 2000.

[82] Schultz TF, Kiyosue T, Yanovsky M, Wada M, and Kay SA. A Role for LKP2 in the Circadian Clock of Arabidopsis. *The Plant Cell*, 13(12):2659–2670, 2001.

[83] Kim J, Geng R, Gallenstein RA, and Somers DE. The F-box protein ZEITLUPE controls stability and nucleocytoplasmic partitioning of GIGANTEA. *Development*, 140(19):4060–4069, 2013.

[84] Kiba T, Henriques R, Sakakibara H, and Chua NH. Targeted degradation of PSEUDO-RESPONSE REGULATOR5 by an SCF-ZTL complex regulates clock function and photomorphogenesis in Arabidopsis thaliana. *The Plant Cell*, 19(8):2516–2530, 2007.

[85] Michael TP, Salomé PA, Yu HJ, Spencer TR, Sharp EL, McPeek MA, Alonso JM, Ecker JR, and McClung CR. Enhanced fitness conferred by naturally occurring variation in the circadian clock. *Science*, 302(5647):1049–53, 2003.

[86] Legris M, Klose C, Burgie ES, Rojas CC, Neme M, Hiltbrunner A, Wigge PA, Schäfer E, Vierstra RD, and Casal JJ. Phytochrome B integrates light and temperature signals in Arabidopsis. *Science*, 354(6314):897–900, 2016.

[87] Boikoglou E, Ma Z, von Korff M, Davis AM, Nagy F, and Davis SJ. Environmental memory from a circadian oscillator: the Arabidopsis thaliana clock differentially integrates perception of photic vs. thermal entrainment. *Genetics*, 189(2):655–64, 2011.

[88] Salomé PA and McClung CR. PSEUDO-RESPONSE REGULATOR 7 and 9 are partially redundant genes essential for the temperature responsiveness of the Arabidopsis circadian clock. *The Plant Cell*, 17(3):791–803, 2005.

[89] Marshall CM, Tartaglio V, Duarte M, and Harmon FG. The Arabidopsis sickle Mutant Exhibits Altered Circadian Clock Responses to Cool Temperatures and Temperature-Dependent Alternative Splicing. *The Plant Cell*, 28(10):2560–2575, 2016.

[90] Cha JY, Kim J, Kim TS, Zeng Q, Wang L, Lee SY, Kim WY, and Somers DE. GIGANTEA is a co-chaperone which facilitates maturation of ZEITLUPE in the Arabidopsis circadian clock. *Nature Communications*, 8(1):3, 2017.

[91] Mwimba M, Karapetyan S, Liu L, Marqués J, McGinnis EM, Buchler NE, and Dong X. Daily humidity oscillation regulates the circadian clock to influence plant physiology. *Nature Communications*, 9(1):4290, 2018.

[92] Haydon MJ, Mielczarek O, Robertson FC, Hubbard KE, and Webb AAR. Photosynthetic entrainment of the Arabidopsis thaliana circadian clock. *Nature*, 502(7473):689–92, 2013.

[93] Frank A, Matiolli CC, Viana AJ, Hearn TJ, Kusakina J, Belbin FE, Wells Newman D, Yochikawa A, Cano-Ramirez DL, Chembath A, *et al.* Circadian Entrainment in Arabidopsis by the Sugar-Responsive Transcription Factor bZIP63. *Current Biology*, 28(16):2597–2606, 2018.

[94] Litthauer S, Chan KX, and Jones MA. 3'-Phosphoadenosine 5'-Phosphate Accumulation Delays the Circadian System. *Plant Physiology*, 176(4):3120–3135, 2018.

[95] Salomé PA, Oliva M, Weigel D, and Krämer U. Circadian clock adjustment to plant iron status depends on chloroplast and phytochrome function. *The EMBO Journal*, 32(4):511–23, 2013.

[96] Gutierrez RA, Stokes TL, Thum K, Xu X, Obertello M, Katari MS, Tanurdzic M, Dean A, Nero DC, McClung CR, *et al.* Systems approach identifies an organic nitrogen-responsive gene network that is regulated by the master clock control gene CCA1. *Proceedings of the National Academy of Sciences*, 105(12):4939–4944, 2008.

[97] Shor E, Paik I, Kangisser S, Green R, and Huq E. PHYTOCHROME INTERACTING FACTORS mediate metabolic control of the circadian system in Arabidopsis. *New Phytologist*, 215(1):217–228, 2017.

[98] Covington MF and Harmer SL. The circadian clock regulates auxin signaling and responses in Arabidopsis. *PLoS Biology*, 5(8):e222, 2007.

[99] Hanano S, Domagalska MA, Nagy F, and Davis SJ. Multiple phytohormones influence distinct parameters of the plant circadian clock. *Genes to Cells*, 11(12):1381–1392, 2006.

[100] Haydon MJ, Mielczarek O, Frank A, Román Á, and Webb AA. Sucrose and ethylene signaling interact to modulate the circadian clock. *Plant Physiology*, 175(2):947–958, 2017.

[101] Johnson C, Knight M, Kondo T, Masson P, Sedbrook J, Haley A, and Trewavas A. Circadian oscillations of cytosolic and chloroplastic free calcium in plants. *Science*, 269(5232):1863–1865, 1995.

[102] Martí Ruiz MC, Hubbard KE, Gardner MJ, Jung HJ, Aubry S, Hotta CT, Mohd-Noh NI, Robertson FC, Hearn TJ, Tsai YC, *et al.* Circadian oscillations of cytosolic free calcium regulate the Arabidopsis circadian clock. *Nature Plants*, 4(9):690–698, 2018.

[103] Dodd AN, Gardner MJ, Hotta CT, Hubbard KE, Dalchau N, Love J, Assie JM, Robertson FC, Jakobsen MK, Gonçalves J, *et al.* The Arabidopsis circadian clock incorporates a cADPR-based feedback loop. *Science*, 318(5857):1789–92, 2007.

[104] Hearn TJ, Marti Ruiz MC, Abdul-Awal SM, Wimalasekera R, Stanton CR, Haydon MJ, Theodoulou FL, Hannah MA, and Webb AAR. BIG Regulates Dynamic Adjustment of Circadian Period in Arabidopsis thaliana. *Plant Physiology*, 178(1):358–371, 2018.

[105] Lee HJ, Ha JH, Kim SG, Choi HK, Kim ZH, Han YJ, Kim JI, Oh Y, Fragoso V, Shin K, *et al.* Stem-piped light activates phytochrome B to trigger light responses in Arabidopsis thaliana roots. *Science Signaling*, 9(452):ra106, 2016.

[106] Andrés-Colás N, Perea-García A, Puig S, and Peñarrubia L. Deregulated copper transport affects Arabidopsis development especially in the absence of environmental cycles. *Plant Physiology*, 153(1):170–184, 2010.

[107] Rennie S, Adamson J, Anderson R, Andrews C, Bater J, Bayfield N, Beaton K, Beaumont D, Benham S, Bowmaker V, *et al.* UK Environmental Change Network (ECN) meteorology data: 1991-2015, 2017.

[108] Song YH, Kubota A, Kwon MS, Covington MF, Lee N, Taagen ER, Laboy Cintrón D, Hwang DY, Akiyama R, Hodge SK, *et al.* Molecular basis of flowering under natural long-day conditions in Arabidopsis. *Nature Plants*, 4(10):824–835, 2018.

[109] Nagano AJ, Kawagoe T, Sugisaka J, Honjo MN, Iwayama K, and Kudoh H. Annual transcriptome dynamics in natural environments reveals plant seasonal adaptation. *Nature Plants*, 5(1):74–83, 2019.

[110] Thain SC, Hall A, and Millar AJ. Functional independence of circadian clocks that regulate plant gene expression. *Current Biology*, 10(16):951–956, 2000.

[111] Bordage S, Sullivan S, Laird J, Millar AJ, and Nimmo HG. Organ specificity in the plant circadian system is explained by different light inputs to the shoot and root clocks. *New Phytologist*, 212(1):136–49, 2016.

[112] Dawson GB and Fisher RG. Diurnal and seasonal ground temperature variations at Wairakei. *New Zealand Journal of Geology and Geophysics*, 7(1):144–154, 1964.

[113] Parton WJ and Logan JA. A model for diurnal variation in soil and air temperature. *Agricultural Meteorology*, 23:205–216, 1981.

[114] Harper RE, Dayan P, Albert JT, and Stanewsky R. Sensory Conflict Disrupts Activity of the Drosophila Circadian Network. *Cell Reports*, 17(7):1711–1718, 2016.

[115] Hennessey TL and Field CB. Evidence of Multiple Circadian Oscillators in Bean Plants. *Journal of Biological Rhythms*, 7(2):105–113, 1992.

[116] Sai J and Johnson CH. Different circadian oscillators control Ca(2+) fluxes and lhcb gene expression. *Proceedings of the National Academy of Sciences of the United States of America*, 96(20):11659–63, 1999.

[117] Thain SC, Murtas G, Lynn JR, McGrath RB, and Millar AJ. The circadian clock that controls gene expression in Arabidopsis is tissue specific. *Plant Physiology*, 130(1):102–110, 2002.

[118] Xu X, Hotta CT, Dodd AN, Love J, Sharrock R, Lee YW, Xie Q, Johnson CH, and Webb AA. Distinct Light and Clock Modulation of Cytosolic Free Ca 2+ Oscillations and Rhythmic CHLOROPHYLL A/B BINDING PROTEIN2 Promoter Activity in Arabidopsis. *The Plant Cell*, 19(11):3474–3490, 2007.

[119] Endo M. Tissue-specific circadian clocks in plants. *Current Opinion in Plant Biology*, 29:44–49, 2016.

[120] Yakir E, Hassidim M, Melamed-Book N, Hilman D, Kron I, and Green RM. Cell autonomous and cell-type specific circadian rhythms in Arabidopsis. *The Plant Journal*, 68(3):520–531, 2011.

[121] Muranaka T and Oyama T. Heterogeneity of cellular circadian clocks in intact plants and its correction under light-dark cycles. *Science Advances*, 2(7):e1600500–1600500, 2016.

[122] Okada M, Muranaka T, Ito S, and Oyama T. Synchrony of plant cellular circadian clocks with heterogeneous properties under light/dark cycles. *Scientific Reports*, 7(1):317, 2017.

[123] Shimizu H, Katayama K, Koto T, Torii K, Araki T, and Endo M. Decentralized circadian clocks process thermal and photoperiodic cues in specific tissues. *Nature Plants*, 1(11):15163, 2015.

[124] Shimizu H, Araki T, and Endo M. Photoperiod sensitivity of the Arabidopsis circadian clock is tissue-specific. *Plant Signaling & Behavior*, 10(6):e1010933, 2015.

[125] Endo M, Shimizu H, Nohales MA, Araki T, and Kay SA. Tissue-specific clocks in Arabidopsis show asymmetric coupling. *Nature*, 515:419–422, 2014.

[126] Shimizu H, Torii K, Araki T, and Endo M. Importance of epidermal clocks for regulation of hypocotyl elongation through PIF4 and IAA29. *Plant Signaling & Behavior*, 11(2):e1143999, 2016.

[127] Meireles-Filho ACA, Bardet AF, Yáñez-Cuna JO, Stampfel G, and Stark A. cis-regulatory requirements for tissue-specific programs of the circadian clock. *Current Biology*, 24(1):1–10, 2014.

[128] Millar AJ, Carre IA, Strayer CA, Chua NH, Kay SA, Riechmann JL, and Mas P. Circadian clock mutants in Arabidopsis identified by luciferase imaging. *Science*, 267(5201):1161–1163, 1995.

[129] James AB, Monreal JA, Nimmo GA, Kelly CL, Herzyk P, Jenkins GI, and Nimmo HG. The circadian clock in Arabidopsis roots is a simplified slave version of the clock in shoots. *Science*, 322(5909):1832–5, 2008.

[130] Para A, Farré EM, Imaizumi T, Pruneda-Paz JL, Harmon FG, and Kay SA. PRR3 Is a vascular regulator of TOC1 stability in the Arabidopsis circadian clock. *The Plant Cell*, 19(11):3462–73, 2007.

[131] Koo J, Kim Y, Kim J, Yeom M, Lee IC, and Nam HG. A GUS/Luciferase Fusion Reporter for Plant Gene Trapping and for Assay of Promoter Activity with Luciferin-Dependent Control of the Reporter Protein Stability. *Plant and Cell Physiology*, 48(8):1121–1131, 2007.

[132] Edwards J, Martin AP, Andriunas F, Offler CE, Patrick JW, and McCurdy DW. GIGANTEA is a component of a regulatory pathway determining wall ingrowth deposition in phloem parenchyma transfer cells of Arabidopsis thaliana. *The Plant Journal*, 63(4):651–661, 2010.

[133] Lee HG and Seo PJ. Dependence and independence of the root clock on the shoot clock in Arabidopsis. *Genes & Genomics*, 40(10):1063–1068, 2018.

[134] Marrocco K, Thomann A, Parmentier Y, Genschik P, and Criqui MC. The APC/C E3 ligase remains active in most post-mitotic Arabidopsis cells and is required for proper vasculature development and organization. *Development*, 136(9):1475–1485, 2009.

[135] Sheldon CC, Hills MJ, Lister C, Dean C, Dennis ES, and Peacock WJ. Resetting of FLOWERING LOCUS C expression after epigenetic repression by vernalization. *Proceedings of the National Academy of Sciences of the United States of America*, 105(6):2214–2219, 2008.

[136] Fujiwara S, Wang L, Han L, Suh SS, Salomé PA, McClung CR, and Somers DE. Post-translational regulation of the Arabidopsis circadian clock through selective proteolysis and phosphorylation of pseudo-response regulator proteins. *Journal of Biological Chemistry*, 283(34):23073–23083, 2008.

[137] Michael TP, Salome PA, and McClung CR. Two Arabidopsis circadian oscillators can be distinguished by differential temperature sensitivity. *Proceedings of the National Academy of Sciences of the United States of America*, 100(11):6878–83, 2003.

[138] Brown SA and Azzi A. Peripheral Circadian Oscillators in Mammals. In A Kramer and M Merrow, editors, *Circadian Clocks*, pages 45–66. Springer Berlin Heidelberg, 2013.

[139] Wenden B, Toner DLK, Hodge SK, Grima R, and Millar AJ. Spontaneous spatiotemporal waves of gene expression from biological clocks in the leaf. *Proceedings of the National Academy of Sciences of the United States of America*, 109(17):6757–6762, 2012.

[140] Fukuda H, Nakamichi N, Hisatsune M, Murase H, and Mizuno T. Synchronization of Plant Circadian Oscillators with a Phase Delay Effect of the Vein Network. *Physical Review Letters*, 99(9):098102, 2007.

[141] Fukuda H, Ukai K, and Oyama T. Self-arrangement of cellular circadian rhythms through phase-resetting in plant roots. *Physical Review E*, 86(4):041917, 2012.

[142] Takahashi N, Hirata Y, Aihara K, and Mas P. A Hierarchical Multi-oscillator Network Orchestrates the Arabidopsis Circadian System. *Cell*, 163(1):148–159, 2015.

[143] Nimmo HG. Entrainment of Arabidopsis roots to the light:dark cycle by light piping. *Plant, Cell & Environment*, 41(8):1742–1748, 2018.

[144] Kuramoto Y. Self-entrainment of a population of coupled non-linear oscillators. In *International Symposium on Mathematical Problems in Theoretical Physics*, pages 420–422. Springer-Verlag, Berlin/Heidelberg, 1975.

[145] Rascher U, Hütt MT, Siebke K, Osmond B, Beck F, and Lüttge U. Spatiotemporal variation of metabolism in a plant circadian rhythm: the biological clock as an assembly of coupled individual oscillators. *Proceedings of the National Academy of Sciences of the United States of America*, 98(20):11801–5, 2001.

[146] Ukai K, Inai K, Nakamichi N, Ashida H, Yokota A, Hendrawan Y, Murase H, and Fukuda H. Traveling Waves of Circadian Gene Expression in Lettuce. *Environment Control in Biology*, 50(3):237–246, 2012.

[147] Ukai K, Murase H, and Fukuda H. Spatiotemporal dynamics of circadian clock in lettuce. *IFAC Proceedings Volumes*, 46(4):214–217, 2013.

[148] Schmal C, Myung J, Herzel H, and Bordyugov G. Moran's I quantifies spatio-temporal pattern formation in neural imaging data. *Bioinformatics*, 33(19):3072–3079, 2017.

[149] Bloemendal S and Kück U. Cell-to-cell communication in plants, animals, and fungi: a comparative review. *Naturwissenschaften*, 100(1):3–19, 2013.

[150] Sparks E, Wachsman G, and Benfey PN. Spatiotemporal signalling in plant development. *Nature Reviews Genetics*, 14(9):631–644, 2013.

[151] Thieme CJ, Rojas-Triana M, Stecyk E, Schudoma C, Zhang W, Yang L, Miñambres M, Walther D, Schulze WX, Paz-Ares J, *et al.* Endogenous Arabidopsis messenger RNAs transported to distant tissues. *Nature Plants*, 1(4):15025, 2015.

[152] Eveland AL and Jackson DP. Sugars, signalling, and plant development. *Journal of Experimental Botany*, 63(9):3367–3377, 2012.

[153] Choi WG, Miller G, Wallace I, Harper J, Mittler R, and Gilroy S. Orchestrating rapid long-distance signaling in plants with Ca 2+ , ROS and electrical signals. *Plant Journal*, 90(4):698–707, 2017.

[154] Sanchez SE and Kay SA. The Plant Circadian Clock: From a Simple Timekeeper to a Complex Developmental Manager. *Cold Spring Harbor Perspectives in Biology*, 8(12):a027748, 2016.

[155] Vatén A, Dettmer J, Wu S, Stierhof YD, Miyashima S, Yadav S, Roberts C, Campilho A, Bulone V, Lichtenberger R, *et al.* Callose Biosynthesis Regulates Symplastic Trafficking during Root Development. *Developmental Cell*, 21(6):1144–1155, 2011.

[156] Mandoli DF and Briggs WR. Fiber-optic plant tissues: spectral dependence in dark-grown and green tissues. *Photochemistry and Photobiology*, 39(3):419–424, 1984.

[157] Sun Q, Yoda K, Suzuki M, and Suzuki H. Vascular tissue in the stem and roots of woody plants can conduct light. *Journal of Experimental Botany*, 54(387):1627–1635, 2003.

[158] Sun Q, Yoda K, and Suzuki H. Internal axial light conduction in the stems and roots of herbaceous plants. *Journal of Experimental Botany*, 56(409):191–203, 2005.

[159] Oyama T, Shimura Y, and Okada K. The Arabidopsis HY5 gene encodes a bZIP protein that regulates stimulus-induced development of root and hypocotyl. *Genes & Development*, 11(22):2983–95, 1997.

[160] Li G, Siddiqui H, Teng Y, Lin R, Wan XyY, Li J, Lau OSS, Ouyang X, Dai M, Wan J, *et al.* Coordinated transcriptional regulation underlying the circadian clock in Arabidopsis. *Nature Cell Biology*, 13(5):616–622, 2011.

[161] Andronis C, Barak S, Knowles SM, Sugano S, and Tobin EM. The Clock Protein CCA1 and the bZIP Transcription Factor HY5 Physically Interact to Regulate Gene Expression in Arabidopsis. *Molecular Plant*, 1(1):58–67, 2008.

[162] Hajdu A, Dobos O, Domijan M, Bálint B, Nagy I, Nagy F, and Kozma-Bognár L. ELONGATED HYPOCOTYL 5 mediates blue light signalling to the Arabidopsis circadian clock. *The Plant Journal*, 96(6):1242–1254, 2018.

[163] Libault M, Pingault L, Zogli P, and Schiefelbein J. Plant Systems Biology at the Single-Cell Level. *Trends in Plant Science*, 22(11):949–960, 2017.

[164] Duncan S and Rosa S. Gaining insight into plant gene transcription using smFISH. *Transcription*, 9(3):166–170, 2018.

[165] Lemoine R, La Camera S, Atanassova R, Dédaldéchamp F, Allario T, Pourtau N, Bonnemain JL, Laloi M, Coutos-Thévenot P, Maurousset L, *et al.* Source-to-sink transport of sugar and regulation by environmental factors. *Frontiers in Plant Science*, 4(JUL):272, 2013.

[166] Palágyi A, Terecskei K, Adám E, Kevei E, Kircher S, Mérai Z, Schäfer E, Nagy F, and Kozma-Bognár L. Functional analysis of amino-terminal domains of the photoreceptor phytochrome B. *Plant Physiology*, 153(4):1834–45, 2010.

[167] Locke JCW, Kozma-Bognár L, Gould PD, Fehér B, Kevei E, Nagy F, Turner MS, Hall A, and Millar AJ. Experimental validation of a predicted feedback loop in the multi-oscillator clock of Arabidopsis thaliana. *Molecular Systems Biology*, 2:59, 2006.

[168] Clough SJ and Bent AF. Floral dip: a simplified method for Agrobacterium-mediated transformation of Arabidopsis thaliana. *The Plant Journal*, 16(6):735–43, 1998.

[169] Siligato R, Wang X, Yadav SR, Lehesranta S, Ma G, Ursache R, Sevilem I, Zhang J, Gorte M, Prasad K, *et al.* Multisite gateway-compatible cell type-specific gene-inducible system for plants. *Plant Physiology*, 170(2):627–641, 2016.

[170] Conn SJ, Hocking B, Dayod M, Xu B, Athman A, Henderson S, Aukett L, Conn V, Shearer MK, Fuentes S, *et al.* Protocol: optimising hydroponic growth systems for nutritional and physiological analysis of Arabidopsis thaliana and other plants. *Plant Methods*, 9(1):4, 2013.

[171] Ingram P, Dettmer J, Helariutta Y, and Malamy JE. Arabidopsis Lateral Root Development 3 is essential for early phloem development and function, and hence for normal root system development. *The Plant Journal*, 68(3):455–467, 2011.

[172] Gu L, Fuentes JD, Garstang M, da Silva JT, Heitz R, Sigler J, and Shugart HH. Cloud modulation of surface solar irradiance at a pasture site in southern Brazil. *Agricultural and Forest Meteorology*, 106(2):117–129, 2001.

[173] Martins BMC, Tooke AK, Thomas P, and Locke JCW. Cell size control driven by the circadian clock and environment in cyanobacteria. *Proceedings of the National Academy of Sciences of the United States of America*, 115(48):11415–11424, 2018.

[174] Zielinski T, Moore AM, Troup E, Halliday KJ, and Millar AJ. Strengths and limitations of period estimation methods for circadian data. *PLoS ONE*, 9(5):e96462, 2014.

[175] Johnson M and Frasier S. Nonlinear least squares analysis. *Methods Enzymology*, 117:301–342, 1985.

[176] Straume M, Frasier-Cadoret SG, and Johnson ML. Least-Squares Analysis of Fluorescence Data. In *Topics in Fluorescence Spectroscopy*, pages 177–240. Kluwer Academic Publishers, Boston, 2002.

[177] Bresenham JE. Algorithm for computer control of a digital plotter. *IBM Systems Journal*, 4(1):25–30, 1965.

[178] Wetzler A. Bresenham optimized for Matlab, 2010.

[179] Daubechies I. The wavelet transform, time-frequency localization and signal analysis. *IEEE Transactions on Information Theory*, 36(5):961–1005, 1990.

[180] Torrence C, Compo GP, Torrence C, and Compo GP. A Practical Guide to Wavelet Analysis. *Bulletin of the American Meteorological Society*, 79(1):61–78, 1998.

[181] Soroldoni D, Jörg DJ, Morelli LG, Richmond DL, Schindelin J, Jülicher F, and Oates AC. A Doppler effect in embryonic pattern formation. *Science*, 345(6193), 2014.

[182] Webb AB, Lengyel IM, Jörg DJ, Valentin G, Jülicher F, Morelli LG, and Oates AC. Persistence, period and precision of autonomous cellular oscillators from the zebrafish segmentation clock. *eLife*, 5:e08438, 2016.

[183] Kuramoto Y. *Chemical Oscillations, Waves, and Turbulence*, volume 19 of *Springer Series in Synergetics*. Springer Berlin Heidelberg, Berlin, Heidelberg, 1984. ISBN 978-3-642-69691-6.

[184] Park DH, Somers DE, Kim YS, Choy YH, Lim HK, Soh MS, Kim HJ, Kay SA, and Nam HG. Control of circadian rhythms and photoperiodic flowering by the Arabidopsis GIGANTEA gene. *Science*, 285(5433):1579–1582, 1999.

[185] Ito S, Matsushika A, Yamada H, Sato S, Kato T, Tabata S, Yamashino T, and Mizuno T. Characterization of the APRR9 pseudo-response regulator belonging to the APRR1/TOC1 quintet in Arabidopsis thaliana. *Plant & Cell Physiology*, 44(11):1237–45, 2003.

[186] Bordyugov G, Abraham U, Granada A, Rose P, Imkeller K, Kramer A, and Herzel H. Tuning the phase of circadian entrainment. *Journal of the Royal Society, Interface*, 12(108):20150282, 2015.

[187] Granada AE, Bordyugov G, Kramer A, and Herzel H. Human chronotypes from a theoretical perspective. *PLoS ONE*, 8(3):e59464, 2013.

[188] Schmal C, Herzog ED, and Herzel H. Measuring Relative Coupling Strength in Circadian Systems. *Journal of Biological Rhythms*, 33(1):84–97, 2018.

[189] Aschoff J and Pohl H. Phase relations between a circadian rhythm and its zeitgeber within the range of entrainment. *Die Naturwissenschaften*, 65(2):80–4, 1978.

[190] Dodd AN, Dalchau N, Gardner MJ, Baek SJ, and Webb AAR. The circadian clock has transient plasticity of period and is required for timing of nocturnal processes in Arabidopsis. *New Phytologist*, 201(1):168–179, 2014.

[191] Sakaguchi H. Cooperative Phenomena in Coupled Oscillator Systems under External Fields. *Progress of Theoretical Physics*, 79(1):39–46, 1988.

[192] Gonze D, Bernard S, Waltermann C, Kramer A, Herzel H, Albrecht U, Okamura H, Harmar A, Piggins H, Reubi J, *et al.* Spontaneous synchronization of coupled circadian oscillators. *Biophysical Journal*, 89(1):120–9, 2005.

[193] Seki N, Tanigaki Y, Yoshida A, and Fukuda H. Spatiotemporal Analysis of Localized Circadian Arrhythmias in Plant Roots. *Environmental Control in Biology*, 56(3):93–97, 2018.

[194] Zhong HH, Painter JE, Salomé PA, Straume M, and McClung CR. Imbibition, but not release from stratification, sets the circadian clock in Arabidopsis seedlings. *The Plant Cell*, 10(12):2005–17, 1998.

[195] Salomé PA, Xie Q, McClung CR, Hangarter RP, and McClung CR. Circadian timekeeping during early Arabidopsis development. *Plant Physiology*, 147(3):1110–25, 2008.

[196] Yamaguchi S, Isejima H, Matsuo T, Okura R, Yagita K, Kobayashi M, and Okamura H. Synchronization of cellular clocks in the suprachiasmatic nucleus. *Science*, 302(5649):1408–12, 2003.

[197] Welsh DK, Takahashi JS, and Kay SA. Suprachiasmatic Nucleus: Cell Autonomy and Network Properties. *Annual Review of Physiology*, 72(1):551–577, 2010.

[198] Fukuda H, Tokuda I, Hashimoto S, Hayasaka N, and Hayashi S. Quantitative Analysis of Phase Wave of Gene Expression in the Mammalian Central Circadian Clock Network. *PLoS ONE*, 6(8):e23568, 2011.

[199] Myung J, Hong S, DeWoskin D, De Schutter E, Forger DB, and Takumi T. GABA-mediated repulsive coupling between circadian clock neurons in the SCN encodes seasonal time. *Proceedings of the National Academy of Sciences of the United States of America*, 112(29):3920–3929, 2015.

[200] DeWoskin D, Myung J, Belle MD, Piggins HD, Takumi T, and Forger DB. Distinct roles for GABA across multiple timescales in mammalian circadian timekeeping. *Proceedings of the National Academy of Sciences of the United States of America*, 112(29):3911–3919, 2015.

[201] Hall A, Bastow RM, Davis SJ, Hanano S, McWatters HG, Hibberd V, Doyle MR, Sung S, Halliday KJ, Amasino RM, *et al.* The TIME FOR COFFEE gene maintains the amplitude and timing of Arabidopsis circadian clocks. *The Plant Cell*, 15(11):2719–29, 2003.

[202] Kikis EA, Khanna R, and Quail PH. ELF4 is a phytochrome-regulated component of a negative-feedback loop involving the central oscillator components CCA1 and LHY. *The Plant Journal*, 44(2):300–313, 2005.

[203] Dalchau N, Baek SJ, Briggs HM, Robertson FC, Dodd AN, Gardner MJ, Stancombe MA, Haydon MJ, Stan GB, Gonçalves JM, *et al.* The circadian oscillator gene GIGANTEA mediates a long-term response of the Arabidopsis thaliana circadian clock to sucrose. *Proceedings of the National Academy of Sciences of the United States of America*, 108(12):5104–9, 2011.

[204] Whitelam GC and Devlin PF. Roles of different phytochromes in Arabidopsis photomorphogenesis. *Plant, Cell and Environment*, 20(6):752–758, 1997.

[205] Sharrock RA and Quail PH. Novel phytochrome sequences in Arabidopsis thaliana: structure, evolution, and differential expression of a plant regulatory photoreceptor family. *Genes & Development*, 3(11):1745–57, 1989.

[206] Onai K and Ishiura M. PHYTOCLOCK 1 encoding a novel GARP protein essential for the Arabidopsis circadian clock. *Genes to Cells*, 10(10):963–972, 2005.

[207] Webb AAR, Seki M, Satake A, and Caldana C. Continuous dynamic adjustment of the plant circadian oscillator. *Nature Communications*, 10(1):550, 2019.

[208] Yamazaki S, Numano R, Abe M, Hida A, Takahashi RI, Ueda M, Block GD, Sakaki Y, Menaker M, and Tei H. Resetting central and peripheral circadian oscillators in transgenic rats. *Science*, 288(5466):682–685, 2000.

[209] Arble DM, Ramsey KM, Bass J, and Turek FW. Circadian disruption and metabolic disease: Findings from animal models. *Best Practice and Research: Clinical Endocrinology and Metabolism*, 24(5):785–800, 2010.

[210] Evans JA and Davidson AJ. Health consequences of circadian disruption in humans and animal models. In *Progress in Molecular Biology and Translational Science*, volume 119, pages 283–323. Elsevier B.V., 2013. ISBN 9780123969712.

[211] van der Vinne V, Swoap SJ, Vajtay TJ, and Weaver DR. Desynchrony between brain and peripheral clocks caused by CK1δ/e disruption in GABA neurons does not lead to adverse metabolic outcomes. *Proceedings of the National Academy of Sciences of the United States of America*, 115(10):E2437–E2446, 2018.

[212] Aschoff J. Exogenous and Endogenous Components in Circadian Rhythms. *Cold Spring Harbor Symposia on Quantitative Biology*, 25:11–28, 1960.

[213] Seluzicki A, Burko Y, and Chory J. Dancing in the dark: Darkness as a signal in plants. *Plant Cell and Environment*, 40(11):2487–2501, 2017.

[214] Riou-Khamlichi C, Menges M, Healy JM, and Murray JA. Sugar control of the plant cell cycle: differential regulation of Arabidopsis D-type cyclin gene expression. *Molecular and cellular biology*, 20(13):4513–21, 2000.

[215] Ahrens C. *Meteorology today: An introduction to weather, climate, and the environment.* Thomson/Brooks/Cole, Pacific Grove, California, 2003.

[216] Dixon LE, Hodge SK, van Ooijen G, Troein C, Akman OE, and Millar AJ. Light and circadian regulation of clock components aids flexible responses to environmental signals. *New Phytologist*, 203(2):568–577, 2014.

[217] Flis A, Fernández AP, Zielinski T, Mengin V, Sulpice R, and Others. Defining the robust behaviour of the plant clock gene circuit with absolute RNA timeseries and open infrastructure. *Open Biology*, 5(10):764–776, 2015.

[218] Farré EM, Harmer SL, Harmon FG, Yanovsky MJ, and Kay SA. Overlapping and Distinct Roles of PRR7 and PRR9 in the Arabidopsis Circadian Clock. *Current Biology*, 15(1):47–54, 2005.

[219] Nagel DH, Doherty CJ, Pruneda-Paz JL, Schmitz RJ, Ecker JR, and Kay SA. Genome-wide identification of CCA1 targets uncovers an expanded clock network in Arabidopsis. *Proceedings of the National Academy of Sciences of the United States of America*, 112(34):4802–4810, 2015.

[220] Dodd AN, Kusakina J, Hall A, Gould PD, and Hanaoka M. The circadian regulation of photosynthesis. *Photosynthesis Research*, 119(1-2):181–190, 2014.

[221] Abrahamson EE and Moore RY. Suprachiasmatic nucleus in the mouse: Retinal innervation, intrinsic organization and efferent projections. *Brain Research*, 916(1):172–191, 2001.

[222] Hong JH, Jeong B, Min CH, and Lee KJ. Circadian waves of cytosolic calcium concentration and long-range network connections in rat suprachiasmatic nucleus. *European Journal of Neuroscience*, 35(9):1417–1425, 2012.

[223] Rellán-Álvarez R, Lobet G, Lindner H, Pradier PL, Sebastian J, Yee MC, Geng Y, Trontin C, LaRue T, Schrager-Lavelle A, *et al.* GLO-Roots: an imaging platform enabling multidimensional characterization of soil-grown root systems. *eLife*, 4, 2015.

[224] Rand DA, Shulgin BV, Salazar D, and Millar AJ. Design principles underlying circadian clocks. *Journal of the Royal Society Interface*, 1(1):119–130, 2004.

[225] Akman OE, Rand DA, Brown PE, and Millar AJ. Robustness from flexibility in the fungal circadian clock. *BMC Systems Biology*, 4(1):88, 2010.

[226] Faure S, Turner AS, Gruszka D, Christodoulou V, Davis SJ, von Korff M, and Laurie DA. Mutation at the circadian clock gene EARLY MATURITY 8 adapts domesticated barley (Hordeum vulgare) to short growing seasons. *Proceedings of the National Academy of Sciences of the United States of America*, 109(21):8328–33, 2012.

[227] Müller NA, Wijnen CL, Srinivasan A, Ryngajllo M, Ofner I, Lin T, Ranjan A, West D, Maloof JN, Sinha NR, *et al.* Domestication selected for deceleration of the circadian clock in cultivated tomato. *Nature Genetics*, 48(1):89–93, 2016.